Charles University in Prague
Faculty of Physical Education and Sport

Study programme:
Biomechanics

Mgr. David Vondrášek

Morphological and mechanical properties of fibrous tissue localized in congenital talipes equinovarus

Morfologické a mechanické vlastnosti fibrózní tkáně lokalizované v kongenitální talipes equinovarus

Dissertation Thesis

Supervisor: Ing. Mgr. Daniel Hadraba, Ph.D.
Supervisor specialist: Ing. František Lopot, Ph.D.

Prague, 2024

Author's declaration:

I hereby declare that this dissertation thesis is my independent original work and that I have cited all used literature, information and sources. This thesis or subsections of the thesis have not been used and presented to achieve another or similar academic title. This thesis is permitted to be used for study purposes and should be freely available to students.

In Prague, 04.01.2024

Signature

Acknowledgement:

I acknowledge Ing. Mgr. Daniel Hadraba, Ph.D. and Ing. František Lopot, Ph.D., for their valuable guidance, advice and intellectual support during the doctoral study and the dissertation thesis preparation.

I acknowledge the Institute of Physiology and its microscopy core facility and its people, who provided me with research equipment, collaboration and financial support for conducting the research. I acknowledge the Ministry of Health of the Czech Republic, Department Program for Research and Development (grant No. 17 31564A), the Ministry of Health of the Czech Republic, Department Program for Research and Development (grant No. NU22-10-00072), MEYS CR (Large RI Project LM2018129 and LM2023050 Czech-BioImaging) and ERDF (project No. CZ.02.1.01/0.0/0.0/18_046/ 0016045). I acknowledge the collaboration with University Hospital Bulovka and its Department of Orthopaedics for providing the tissue for the research. I also acknowledge the Core Facility of Nanobiotechnology of CIISB, Instruct-CZ Centre, which provided essential equipment support for Atomic Force Microscopy. I acknowledge the support from the Faculty of Physical Education and Sport and the Cooperatio Program, research area Sport Sciences – Biomedical & Rehabilitation Medicine.

Preface

The aim of the doctoral thesis is to present the reader with the research of clubfoot deformity, specifically the relapsed clubfoot, and establish clubfoot fibrotic tissue in the biomechanical context. The thesis is organized in a book format, and each chapter is dedicated to a coherent topic. The topic of each chapter is consequently specified for the relapsed clubfoot and the researched fibrotic tissue. The final chapter discusses and concludes on the conducted research described in the thesis and specifies the limitations of the research and possibilities for future research.

Chapter I is an introductory chapter and specifies the initial clinical sample. The chapter introduces the clubfoot deformity. Macro-morphology, phenotype and aetiology of clubfoot are briefly described. The clubfoot is established in the context of fibroproliferative disorders. A conservative approach to treatment is described for clubfoot with specifications about the severity classification of the deformity. In severe cases of relapsed clubfoot, surgery is adopted as an approach to treatment, and the identified fibrotic tissue is the studied material presented in the thesis research.

Chapter II is dedicated to the researched sample material and the related sample preparation techniques. The chapter navigates the sample preparation techniques and presents several limitations of the preparation of the sample in terms of altering mechanical properties. The chapter introduces an overview of the sample manipulation techniques, including fixation, sectioning, labelling, ablation, and (de)hydration. The chapter includes a brief visual overview of the sample manipulation, which includes temperature, transport and measured modalities, and provides a number of samples used in each analysis. The chapter specifies the selected sample preparation techniques for relapsed clubfoot tissue and provides reasoning for the selected techniques. The relapsed clubfoot sample preparation includes a description of identifying the identical tissue structures for correlative microscopy.

Chapter III is a methodological section dedicated to the morphological characterization of the relapsed clubfoot tissue and includes the results and a conclusion on the morphological characterization. The chapter advances the description of the clubfoot fibrotic tissue, its morphology and visualization.

The chapter describes the visualization techniques used in visualizing the relapsed clubfoot tissue. The visualization techniques are compatible with the mechanical testing of the tissue without introducing artefacts. Each visualization technique for characterizing the relapsed clubfoot tissue's morphology is followed by the results of the specific modality used. The chapter also identifies a relationship between clubfoot morphology and the mechanical properties of fibrotic tissue.

Chapter IV is a methodological chapter dedicated to the problems of viscoelastic materials and establishes the clubfoot fibrotic tissue in the context of biomechanics. The chapter includes the results of the biomechanical characterization of the relapsed clubfoot tissue. Atomic force microscopy (AFM) is the biomechanical test of choice for characterizing the mechanical properties of the relapsed clubfoot tissue. The reasoning for selecting the AFM is clarified by the physical size of the samples, which are small for conventional tensile testing. The chapter expands on the crucial sample preparation previously described in Chapter II, as improper sample preparation can influence the result of the mechanical characterization. The section is followed by the limitations and effects of the AFM theoretical models and compares the relapsed clubfoot tissue to other tissue measured with AFM. The chapter finishes with the results of the AFM indentation of the tissue.

Chapter V brings the measured morphological data from Chapter III and data on the mechanical properties from Chapter IV together in multimodal analysis. The chapter presents the data processing automation and summarizes the morphological and mechanical characterization. The relapsed clubfoot fibrotic tissue of the medial side is compared with the connective tissue of the lateral side clubfoot in terms of mechanical properties, collagen and adipose tissue content, and fibre orientation. The chapter is a highlight of the methodological importance of correlative microscopy in evaluating the relapsed clubfoot tissue.

Chapter VI focused on the limitations of the study, and the results are discussed in terms of the methodology and statistics. The chapter concludes on the results presented in the thesis. The chapter is followed by the list of publications that resulted from the biomechanics research.

Content

Chapter I

1. Clubfoot – The Fibroproliferative Disorder

Talipes equinovarus congenitus, *i.e.* clubfoot, is an orthopaedic deformity of lower limbs, an idiopathic congenital defect primarily characterized by malformations in the area of talus, calcaneus and the tissue surrounding these bones (Kyzer & Stark, 1995; Siapkara & Duncan, 2007; Ošťádal et al., 2017; Novotny et al., 2022). The phenotype of the clubfoot deformity is mainly characterized by a club-like appearance of one foot or both feet; hence, the term clubfoot is used (Figure 1)(Kyzer & Stark, 1995; Pandey & Pandey, 2003; Anand & Sala, 2008; Cooke et al., 2008; Bridgens & Kiely, 2010; Ošťádal et al., 2017). The club-like appearance is described by anatomical nomenclature with the following terms: plantar flexion, adduction, supination of the foot or feet, and a combination of medial rotation, flexion and inversion of the hindfoot, also known as varus. Additionally, the deformity is recognized to affect other areas of lower limbs besides the foot, for instance, torsional deformity of the tibia, shortening of the affected lower limb, or atrophy of calf muscles, though some of these can develop as secondary symptoms of the clubfoot deformity (Pandey & Pandey, 2003; Fulton et al., 2015).

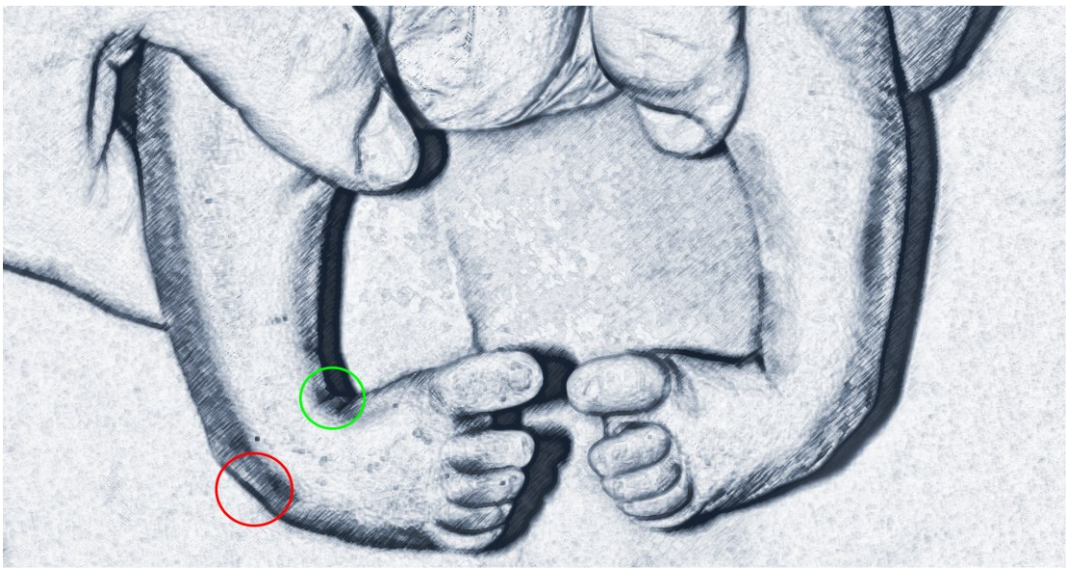

Figure 1. Illustrative image of clubfoot deformity. Medial side (Green) and lateral side (Red) of the deformity, where biopsies are obtained during the surgery of relapsed clubfoot.

1.1 Development of Clubfoot

According to Ponseti, 2002, clubfoot develops during the fetal stage of ontogenesis in the third month of intrauterine development. Both feet are in equinovarus during ontogenesis and assume a pronated position of the foot at birth. However, during pathological ontogenesis of the clubfoot, a foot or feet remain arrested in the equinovarus after birth and require medical correction into physiological position (Anand & Sala, 2008). Clubfoot occurs in approximately 1 birth out of 1000 live births (Cooke et al., 2008; Kadhum et al., 2019), although the incidence can vary between different populations (Mkandawire & Kaunda, 2004; Wallander et al., 2006; Mathias et al., 2010; Ošťádal et al., 2017; Dibello et al., 2022). The deformity can develop as unilateral or bilateral with a ratio of 1:1. Boys are affected with either unilateral or bilateral clubfoot up to three times more than girls (Mkandawire & Kaunda, 2004; Wallander et al., 2006; Mathias et al., 2010). Untreated clubfoot deformity hinders physiological mobility of the foot and ankle joint (Owen et al., 2018). Some corrective methods have been proposed, such as the Ponseti casting method (Ponseti, 2002) or the French functional physical therapy method (Dimeglio & Canavese, 2012).

1.2 Treatment of the Deformity

The Ponseti casting method treats clubfoot in a series of gentle force manipulations of the foot, with each manipulation set followed by plaster casting to secure the foot in the new position. Casts are changed every 14 days, and the foot may reach the physiological position within 6 weeks (Figure 2). A percutaneous tenotomy of the Achilles tendon can be performed to release the tension preventing the foot from reaching the physiological position. The patient wears the last plaster cast for up to 4 weeks. Patients are required to wear orthosis after casting to maintain the physiological position of the foot until about the age of four (Ponseti, 2002).

The French functional physical therapy method treats clubfoot in a series of gentle force manipulations of the foot on a daily basis while stimulating the muscles around the foot. The correction is maintained with adhesive tapes that immobilize the foot. The treatment is applied during the first 4 months of the newborn child. During the third month of the treatment, the foot

normalization is assessed. If the correction produces insufficient results in normalizing the foot position, the surgical release is performed (Dimeglio & Canavese, 2012).

Regardless of the correction method of the clubfoot, orthopaedic practitioners and surgeons always assess the severity of clubfoot before they correct the deformity. The severity of the clubfoot cases varies, ranging from mild to severe, based on the score assigned to the deformity according to the classification systems. Two classification systems can be applied to assess the severity of the clubfoot: the Pirani score or the Dimeglio score (Goriainov et al., 2010; Cosma & Vasilescu, 2015).

Figure 2. Illustration of the Ponseti casting method. The figure depicts a gradual correction of the position of the deformed foot over several weeks.

The Pirani classification system examines the clubfoot at two locations of the foot – midfoot and hindfoot. At each location, three observation parameters are examined. The three parameters at midfoot are the curvature of the lateral border, medial crease and talar head reducibility. The three parameters at the hindfoot are the posterior crease, empty heel and rigid equinus. Each observed parameter is scored 0 for no abnormality, 0.5 for moderate abnormality and 1 for severe abnormality. The total Pirani score ranges from 0.0 to 6.0 (Goriainov et al., 2010; Cosma & Vasilescu, 2015).

The Dimeglio classification system is a four-grade system that evaluates the force required for correcting the clubfoot into a physiological position. The orthopaedic practitioner applies force until the stiff foot resists the deformation and measures an angle from a sagittal, frontal and horizontal plane. The angle is measured for four parameters in the Dimeglio classification system (Figure 3): equinus deviation in the sagittal plane, varus deviation in the frontal plane, de-rotation of the calcaneal-forefoot block and forefoot adduction in the horizontal plane. The ranges of the measured angles are scored as follows: 0 (-20°), 1 (-20° to 0°), 2 (0° to 20°), 3 (20° to 45°), 4 (45° to 90°). In addition, the orthopaedic practitioner scores four possible deformity characteristics with one point each. The four deformity characteristics are posterior crease, medial crease, cavus and fibrous musculature. The total score of the Dimeglio classification system ranges from 0 to 20 points (Cosma & Vasilescu, 2015).

In our research, orthopaedic practitioners from the Department of Orthopaedics at Hospital Bulovka used the Dimeglio classification system when correcting the foot position using the Ponseti method. Patients evaluated as grade III and IV, *i.e.* severe and very severe, experienced relapses and had to undergo corrective surgery (Table 1).

Grade	Type	Frequency, %	Score
I	Benign	-, -	[0, 5]
II	Moderate	21, 10	[5, 10]
III	Severe	52, 56	[10, 15]
IV	Very severe	27, 34	[15, 20]

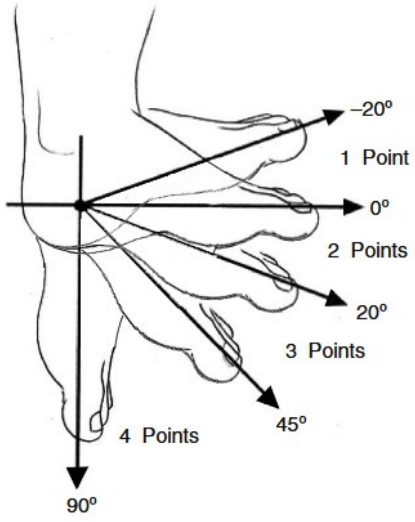

Equinus (Sagital plane)

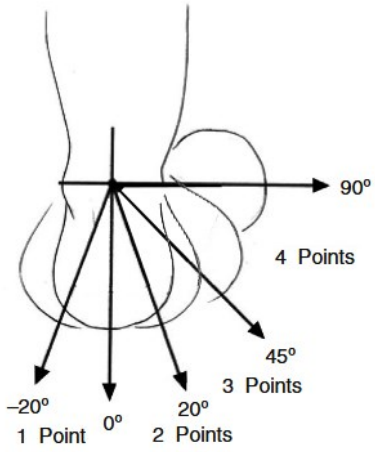

Varus deviation (Frontal plane)

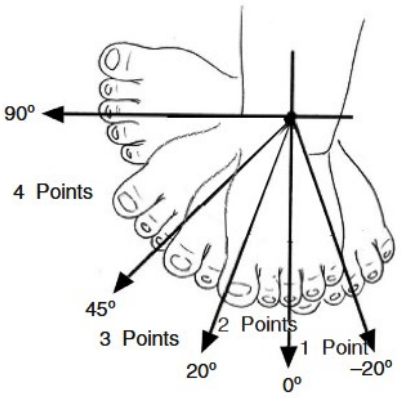

De-rotation of calcaneo-forefoot block (Horizontal plane)

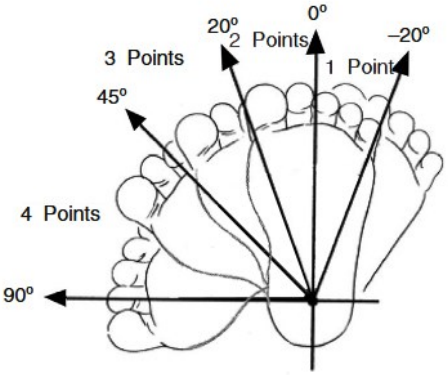

Forefoot adduction (Horizontal plane)

Additional characteristics scored 0, 0.5 or 1:

- Posterior crease
- Medial crease
- Cavus
- Fibrous musculature

Figure 3. The Dimeglio classification, adopted from Fernandes et al., 2016. The frequency of cases of different severity is expressed with data from Chotel et al., 2011.

1.3 Clubfoot Relapse and Fibrosis

Corrective treatments and the severity assessment of clubfoot deformity by orthopaedic practitioners and surgeons aim to correct the deformed foot. The available corrective methods often provide positive results, and the initial treatment is successful. However, in some cases of clubfoot, the position of the foot relapses back to the clubfoot position. The severity of the relapses varies, as well as the area of the foot that fails to retain the corrected position, and more severe cases of clubfoot are more likely to relapse. It has been suggested that the cause of clubfoot relapse is the same as the initial causal mechanism behind the development of clubfoot. However, the exact causal mechanisms for clubfoot and its relapses remain unknown (Ponseti, 2002).

Some potential causal mechanisms of clubfoot and its relapses have been proposed (Siapkara & Duncan, 2007). Among the proposed causal mechanisms are both genetic (Lin, 2020; Quiggle et al., 2022) and environmental factors. Among environmental factors, there are multiple aetiological candidates, including hypoxia (Novotny et al., 2020, 2022), neuromuscular factors (Handelsman & Badalamente, 2008); and fibrosis – an excessive collagen synthesis (Kerling et al., 2018), which is important from a biomechanical standpoint (Nelson & Bissell, 2006; Wells, 2013; Matera et al., 2021). However, the mechanical effect of fibrosis is different from mechanical factors such as the position of fetus in the uterus, which was considered among the first aetiological clubfoot theories that found little support as clubfoot was not present in cases such as twins, large babies and hydramnios, where the uterus was constraining the fetal development (Anand & Sala, 2008).

Orthopaedic practitioners observe fibrosis both in clubfoot and its relapses (Ponseti, 2002). The majority of clubfoot characterizations attempt to classify the resistance to correction methods. Resistance to correction is characterized by terms such as stiff, rigid or contracted (Pandey & Pandey, 2003; Poon et al., 2009; Kerling et al., 2018; Pavone et al., 2018; Quiggle et al., 2022) that are vaguely referring to the viscoelastic properties of the clubfoot tissue. Several studies suggest that the underlying factor for the tissue's rigidity is within its extracellular matrix (ECM) composition (Ošťádal et al., 2017; Eckhardt et al., 2019; Knitlova et al., 2020, 2021; Novotny et al., 2020, 2022). Clubfoot cases, especially those

that experience relapses, are showing clear signs of fibrosis. Fibrosis can be observed in the medial and posterior side of the clubfoot, the tarsal ligaments, the deep fascia, the Achilles and the posterior tibial tendon (Ponseti, 2002; Sano et al., 1998). Specifically, the medial side of the clubfoot between the medial malleolus, sustentaculum tali, and the navicular bone contains a bulk of fibrotic tissue (Sano et al., 1998; Eckhardt et al., 2019; Knitlova et al., 2020). Fibrosis contributes to altering the structure of the tissue and its ECM and is the characteristic process in fibroproliferative disorders, such as Dupuytren's contracture (Li et al., 2001; Poon et al., 2009; Kerling et al., 2018) and Peyronie's Disease (Patel et al., 2020) as well as for clubfoot (Eckhardt et al., 2019). The pathological accumulation of collagen might even be a key element in the aetiology of clubfoot and is likely one of the main factors contributing to relapses of clubfoot (Ponseti, 2002; Kerling et al., 2018; Eckhardt et al., 2019).

1.3.1 Surgery of Relapsed Clubfoot

According to the collaborative hospital Bulovka, failure of casting using the Ponseti method leaves limited treatment possibilities for the patients whose foot or feet relapsed into the club-like phenotype or for the patients who neglected the conservative treatment of the Ponseti method. Continuous lack of treatment leaves affected children walking on the sides of their feet instead of the soles. The changes in force distribution during gait lead to permanent morphological changes, so invasive treatment can prevent mobility impairment and return the ability of the plantigrade locomotion to individuals with the idiopathic congenital deformity (Ošt'ádal et al., 2015; Ošťádal et al., 2017).

Orthopaedic practitioners treated several young patients with the Ponseti method, but after the failure of the casting therapy, surgery on the relapsed clubfoot was performed to normalize the foot. The severity of the patients' clubfoot was classified according to Dimeglio classification as grade III or IV. Thirteen randomly selected patients operated for the relapsed clubfoot were included in this study. The selected biopsies were from nine males and four females with a mean age of 51 months (SD = 29 months). The anonymized patient information is stated in Table 1.

Two types of biopsies were dissected during surgery. The first type represents the fibrotic tissue, and the biopsy was dissected from the contracted tissue, specifically from the region of the medial malleolus, sustentaculum tali, and the navicular bone (length = 9.79 ± 5.29 mm [mean ± standard deviation (SD)], width = 5.42 ± 2.29 mm [mean ± SD]). The second type represents a control sample, and the biopsy was extracted from the lateral surface of the calcaneocuboid joint (n = 13, length = 6.16 ± 2.72 mm [mean ± SD], width = 4.11 ± 1.97 mm [mean ± SD]). The approximate location of the biopsy extraction site is depicted in Figure 1.

Orthopaedic practitioners subjectively classified the tissue and the extracted biopsy as stiff and contracted. Our research group further investigated the biopsies. The group investigated the biopsies in several characteristics, comparing the biopsy of the medial side with the biopsy of the lateral side. Lateral side biopsy functioned as a control group.

The lateral side is not a proper control because the samples do not originate from a medial side of healthy participants of the same age group with the same diet or similar physical history. Attempts to obtain a sufficient number of proper controls would be unethical and unrealistic. Therefore, the lateral side biopsy functions as a relative comparison for the medial side biopsy since both tissues come from the affected limb, and orthopaedic surgeons refer to both sides of the clubfoot when concluding on the characteristics of the relapsed clubfoot tissue.

The investigated characteristics of the relapsed clubfoot were protein composition (Ošt'ádal et al., 2015; Eckhardt et al., 2019; Novotny et al., 2022), vasculature (Novotny et al., 2020), fibrosis modulation and inhibition (Knitlova et al., 2020), crosslinks (Knitlova et al., 2021), tissue morphology and biomechanics. Our research group investigated the tissue, and early findings support the presence of fibrosis but also the possible presence of hypoxia. From a biomechanical standpoint, the most relevant findings are the difference in protein composition, increased collagen type I content and collagen crosslinking in the tissue from the medial side clubfoot (Ošt'ádal et al., 2015; Eckhardt et al., 2019; Knitlova et al., 2021; Novotny et al., 2022). The task of characterizing the tissue in the morphological and biomechanical context is the central part of the thesis.

1.3.2 Ethics Committee Approval

All procedures were performed in accordance with the ethical standards of the 1964 Declaration of Helsinki. Institutional approval for our study was obtained from the Ethics Committee of the Institute of Physiology of the Czech Academy of Sciences (project No. 17 31564A, 14 June 2016). The parents or legal guardians of all the patients provided written, informed consent to participate.

Table 1. Detailed data of 13 patients with idiopathic congenital clubfoot.

Patient No.	Gender	Dimeglio clubfoot classification	Patient's age at the time of surgery (months)	Ponseti treatment (Number of plasters)	Foot (left/right)	Previous surgeries	Clubfoot family anamnesis
1	Male	III	38	10	Left	Tenotomy of Achilles tendon	0
2	Male	IV	68	6	Right	Tenotomy of Achilles tendon	0
3	Male	III	84	5	Right	Tenotomy of Achilles tendon	0
4	Female	III	16	5	Left	Tenotomy of Achilles tendon	0
5	Male	III	124	5	Right	Tenotomy of Achilles tendon	0
6	Male	IV	31.5	unknown	Left	None	0
7	Male	III	44	10	Left	Tenotomy of Achilles tendon	0
8	Male	III	53.5	5	Right, Left	None	Mother
9	Female	IV	39.5	6	Right	Tenotomy of Achilles tendon	0
10	Female	IV	21.5	10	Right	Tenotomy of Achilles tendon + re-tenotomy	0
11	Male	III	66	15	unknown	unknown	0
12	Female	III	32	5	Right	Tenotomy of Achilles tendon	0
13	Male	III	48	5	unknown	unknown	Father

Chapter II

2. Preparations of Clubfoot Tissue

In order to characterize the morphology and mechanical properties of the tissue biopsy, sample preservation, visualization and mechanical testing are required. Biomechanical characterization of the tissue does not permit specific sample preparation procedures of fixation, staining and other sample preparation methods, which could alter the mechanical response of the tissue. The chapter will investigate the possible alternation of the tissue and present the least-altering approach chosen to characterize the tissue in a biomechanical context.

2.1 Overview of the Sample Manipulation

In this study, the devices used to prepare and analyse the sample included a cryostat for cutting the samples (Institute of Physiology, CAS, Prague) and an optical microscope for morphological analysis (Bioimaging Facility, Institute of Physiology, CAS, Prague). The microscope site is referred to as the primary microscopy site throughout the text. Additional devices included an atomic force microscope with an optical microscope for micromechanical and morphological analysis (Nanobiotechnology Core Facility, CEITEC, Brno). The microscope site is referred to as the secondary microscopy site throughout the text. The samples were maintained under cooled conditions during transport between the facilities. The sample preparation and the data acquisition for multimodal analysis were completed in five days after removing the samples from −80 °C storage, and the prepared sections went through rehydration twice (Figure 4).

On the first day, the samples were prepared at cryostat. The sample sections were dehydrated by adhering to the microscope slide during cryostat preparation. The sample sections were stored at +4 °C. On the second day, the sections were rehydrated for the morphological analysis conducted at the primary microscopy site (Chapter III). After the morphological analysis, the sections were dehydrated and stored at +4 °C. The sections were transported to the secondary microscopy site using dry ice. The sections were rehydrated before acquiring the morphological (Chapter III) and micromechanical properties (Chapter IV) at the secondary

microscopy site during the third, fourth and fifth days. The data acquisition was performed at the identical locations of the sections to those acquired at the morphological analysis of the primary microscopy site.

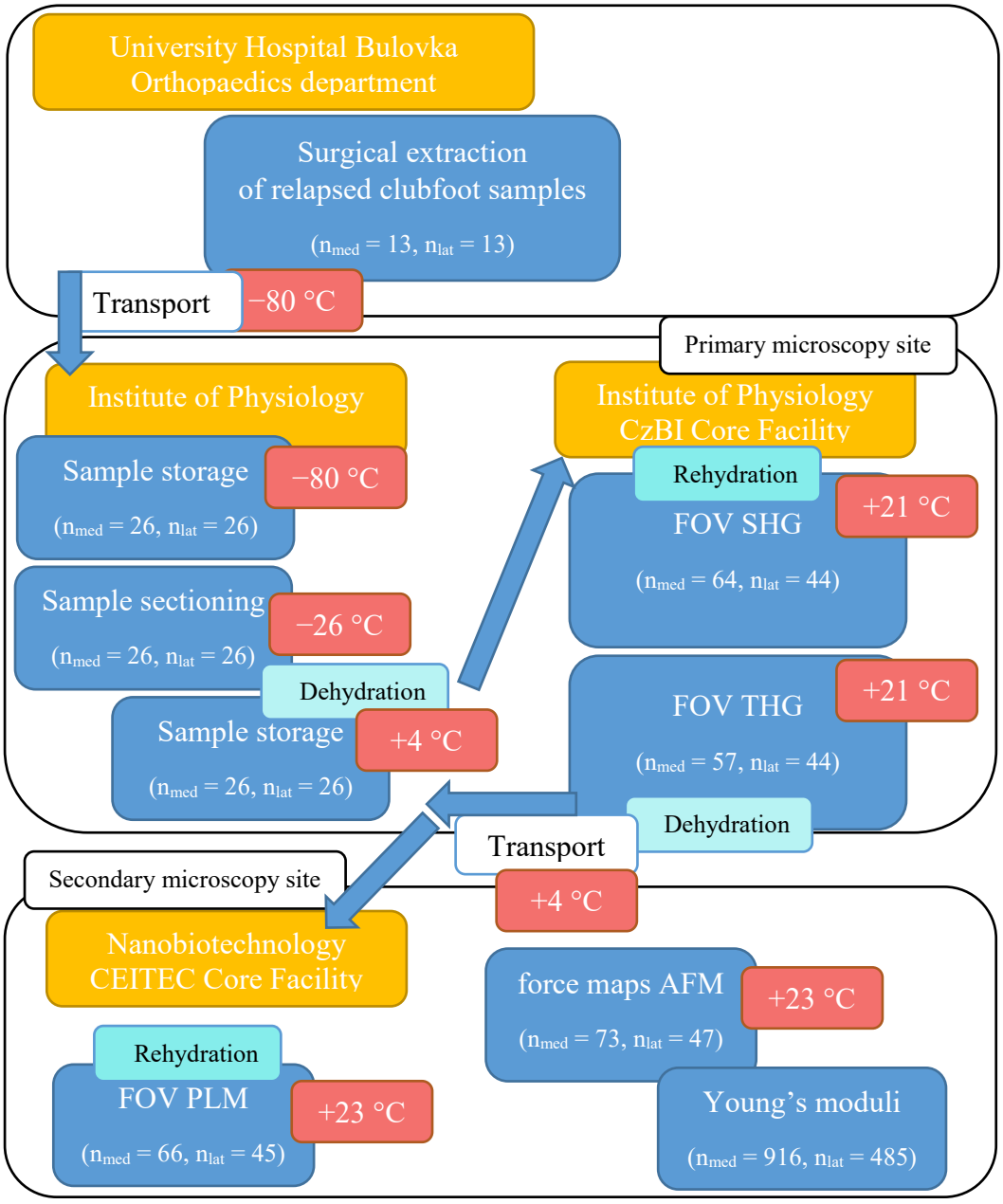

Figure 4. Overview of the sample manipulation. The figure shows sample manipulation and a number of tissue samples used in data analysis for the medial (n_{med}) and lateral (n_{lat}) sides of the relapsed clubfoot. Fields of view (FOV) of second harmonic generation (SHG), third harmonic generation (THG) and polarization microscopy (PLM) are discussed in Chapter III. Force maps acquired with atomic force microscopy (AFM) are discussed in Chapter IV.

2.2 Fixation of the Clubfoot Biopsy

Naturally, the tissue biopsy decays over time and some form of prevention from the tissue degradation is required (Taqi et al., 2018; Layton et al., 2019). The tissue processing method that preserves the micro-architecture and structural integrity of the tissue and cells is known as tissue fixation (Layton et al., 2019). Tissue fixation methodology aims to stop the decay processes such as autolysis (Taqi et al., 2018) and infectious agents (Layton et al., 2019). Two approaches of tissue fixation are commonly used – chemical fixation and heat fixation (Sosinsky et al., 2008; Layton et al., 2019) or their combination (Sosinsky et al., 2008). Each approach to tissue fixation is a potential source of artefacts – structural anomalies in tissue structure and composition created during tissue handling, including the fixation (Taqi et al., 2018). Only some examples will be made to demonstrate the possible effects of the fixation that relate to an alternation of the biomechanical properties of the biological tissue. Because of these alternations, fixation by freezing was applied to the relapsed clubfoot samples.

2.2.1 Chemical fixation

Chemical fixatives preserve the tissue in one of three possibilities: coagulation, cross-linking and covalent bonding. When proteins coagulate, they become insoluble in water (Layton et al., 2019). In a native state of the tissue, proteins are organized in higher structural orders, such as tertiary structure. The native tertiary structure is water soluble, *i.e.* free water molecules surround exposed hydrophilic areas and form hydrogen bonds together, while hydrophobic areas tend to interact with each other as they are repulsed from water and the surface of the protein's tertiary structure. Hydrophilic and hydrophobic interactions in water stabilize the protein structure (Willingham, 1999; Layton et al., 2019). The application of alcohol fixes the tissue by removing free water from the tissue, *i.e.* the tissue is dehydrated. The protein coagulation occurs when the concentration reaches around 50 % for ethanol and 80 % for methanol. Consequently, hydrogen bonds are diminished, while hydrophobic areas of the protein become exposed at the protein surface, leading to denaturation, a disruption of the protein's tertiary structure, and coagulation of proteins (Layton et al., 2019). Both changes

in the protein structure and the tissue's dehydration alternate the mechanical response of biological tissue (Wilke et al., 1996; Azril et al., 2023).

Other chemical fixatives, such as formaldehyde or glutaraldehyde, mediate covalent bonding and cross-linking between side chains of peptides and proteins (Layton et al., 2019; Musilkova et al., 2019; Adamiak & Sionkowska, 2020), in naked and free DNA, and also in unsaturated lipids (Layton et al., 2019). The formaldehyde fixation also mediates the formation of hydroxymethyl groups, leading to denaturation and rendering the macromolecules insoluble. The advantage of formaldehyde fixation is in preserving peptide-protein bonds and cellular organelles. With the addition of calcium, lipids are preserved as well (Layton et al., 2019). Cross-links formation is a time-dependent process, and the longer time the proteins like collagen are exposed to the cross-linking media, such as formaldehyde, glutaraldehyde and genipin, the more cross-links between individual collagen molecules are formed (Sundararaghavan et al., 2008; Layton et al., 2019). Cross-links support the preservation of tissue by stabilizing the tissue during fixation (Layton et al., 2019); however, they also affect the mechanical properties of tissue, stiffening the collagen network (Sundararaghavan et al., 2008; Richoz et al., 2013) and some cross-linkers increase an autofluorescence signal (Jastrzebska et al., 2003), which poses problem for morphological characterization of the tissue as well. Therefore, chemically fixed tissue is not representative of *in vivo* mechanical properties and other means of preserving the tissue were chosen for morphological and mechanical characterization of the clubfoot tissue.

2.2.2 Physical Fixation using Temperature Change

An alternative method of fixation to chemical fixatives is the application of temperature change to alter the properties of free water in the tissue together with inducing changes to the tissue structures (Sosinsky et al., 2008; Taqi et al., 2018; Layton et al., 2019). Fixation through temperature change can be as simple as heating, microwave heating or freezing the tissue sample (Layton et al., 2019). As surgeons proceed to extract biopsies during surgery, their primary focus is preserving the patient's health and not preserving the biopsy. Therefore, it is convenient to preserve the samples rapidly.

Out of the fixations through temperature change, freezing the tissue samples offers a rapid intra-operative fixation of biological samples (Steu et al., 2008). However, the freezing method can induce artefacts in the sample. The most common artefact of the freezing method is ice crystal formation. Ice crystals are formed when the temperature declines slowly and gradually, leaving enough time for the ice crystals to expand, eventually leading to structural damage to the tissue (Steu et al., 2008; Taqi et al., 2018). One way to prevent the ice crystal formation is the addition of cryoprotective agents. Cryoprotectants limit the ice crystal formation but may lead to other artefacts, *e.g.* cryoprotectant aggregation and toxicity (Bachmann & Schmitt, 1971; Sosinsky et al., 2008).

Another way of preventing the deformation of the tissue by ice crystals is to increase the freezing rate so there is no time for ice crystal formation. This can be achieved by adding the biopsy into liquid nitrogen or carbon dioxide dry ice (Steu et al., 2008; Taqi et al., 2018), both having low temperatures of −196 °C (Pogrel et al., 1990) and −78.5 °C (Górecki et al., 2016), respectively. Rapid freezing immobilizes all cellular and intracellular content almost instantly (Sosinsky et al., 2008). However, it is unsuitable for all tissue types as extremely soft tissue, *e.g.* brain, spleen and lymph node, becomes brittle (Steu et al., 2008). Rapid freezing is used to preserve fresh tissue prior to cryostat sectioning (Taqi et al., 2018),

The biopsies of relapsed clubfoot were preserved by freezing method immediately after the surgical extraction. The tissue was placed into a coolant with dry ice for transport in order to prevent the decay and formation of the ice crystals. Once the biopsies were transported, they were stored at −80 °C before further processing.

2.3 Clubfoot Sample Preparation for Optical Microscopy and AFM

Sample preparation methodology offers many approaches to visualize the relapsed clubfoot tissue with an optical microscope. However, the aim of the thesis is to characterize not only the tissue morphology but also the mechanical properties of the tissue. As such, the sample preparation methods for visualizing are limited to those that do not alter mechanical properties.

The preparation methodology considers the optical properties of the clubfoot tissue, both general and molecule specific, and considers limits of the micro-indentation by AFM.

2.3.1 Accessing Deep Layers of the Tissue

The first problem to consider when planning the sample preparation for the morphological characterization of the tissue is that the majority of biological samples are opaque on the macroscopic level (Schega et al., 2020), and the light that enters the sample is quickly absorbed or scattered (Welch et al., 1989; Pellicer & Bravo, 2011). Several biological molecules, such as lipids, various fibrillar proteins and other proteins, and also water, contribute significantly to light attenuation (Pellicer & Bravo, 2011). If some of these molecular components were removed from the tissue without significant disruption to the tissue morphology, light would penetrate deep into the sample, and the architecture of the whole clubfoot sample would be resolved. This reduction of the opacity of the biological tissue is achieved by clearing methods. Clearing methods either involve the removal of lipid molecules of the biological tissue using a clearing solution or involve replacing water with clearing media of a higher refractive index, which dehydrates the tissue. A combination of lipid removal and impregnation of the tissue with clearing media is also possible. Both clearing media and structures of interest maintain similar refractive indices, and the sample becomes transparent (Schega et al., 2020). However, the clearing methods present an apparent problem for testing mechanical properties as both lipids and water have an important role in the mechanical properties of the tissue. Additionally, the clearing method does not open access to the characterization of biomechanical properties of deep layers, as AFM is limited only to the surface or near-surface layers of the tissue. Therefore, a different methodological approach was selected for overcoming the opacity of the relapsed clubfoot biopsies.

A straightforward method for identifying deep structures within the biopsy, both its morphology and biomechanics, is tissue sectioning. A whole organ or a biopsy can be sectioned into thin slices, each containing a single focal plane of cells and tissue to be visualized. Consequently, a whole organ can be reconstructed during image data analysis (Braak & Braak, 1991). The thin slices

of the tissue often offer little contrast, and samples require staining with contrasting agents or fluorescent labels (Kasten, 2002; Lee et al., 2020; Balaur et al., 2021). A robust method for producing thin sections while maintaining tissue integrity is cryostat sectioning.

Cryostat sectioning is complementary to heat fixation, specifically freezing (Taqi et al., 2018). Therefore, we have selected cryostat sectioning to process the frozen biopsies of the relapsed clubfoot tissue for consequent imaging with light microscopy and biomechanical tests with atomic force microscopy. Biopsies are typically embedded into an Optimal Cutting Temperature (OCT) compound and positioned into the desired orientation before freezing (Pearse & Gardner, 1972; Cui et al., 2007). It is unclear how OCT affects local micromechanical properties and consequent AFM measurements. In order to preserve *in situ* mechanical properties, the biopsies were placed into cube-shaped moulds and immersed in phosphate-buffered saline (PBS).

From the perspective of biomechanical analysis, tissue sectioning presents a potential source of disruption of the tissue structures (Aitken et al., 1995; Taqi et al., 2018). Collagen fibres are anisotropic, and the directionality of the applied load yields different biomechanical responses (Wenger et al., 2007; McKee et al., 2011). Therefore, sectioning requires caution so that individual fibres are not perpendicular to the direction of the cut. We identified the collagen fibre orientation in the biopsies and aligned the tissue inside the mould parallel with the cutting axis of the cryostat. The moulds were placed into Leica CM1850 UV cryostat (Leica Biosystems Nussloch, GmbH, Germany), where the tissue embedded in PBS formed a frozen block at −26 °C. The operating temperature range of the cryostat is tissue-specific and ranges between −20 °C to −30 °C (Pearse & Gardner, 1972). We empirically determined the cutting temperature empirically, as the tissue was being torn outside of −25 °C to −27 °C.

Aligned frozen blocks were cut into tissue sections with a thickness of approximately 120µm. Sections from the upper layers of the biopsies were discarded as they were presumably damaged during surgical extraction. The discarding of upper layers was also motivated by a requirement for atomic force microscopy, as the technique requires minimal surface roughness due to the technical limit of the motion range of the indenter, *i.e.* the cantilever. The vertical operating motion range of the cantilever is only 15 µm. The AFM

indentation also requires the sample to be stationary, and the typical immobilization medium used to adhere the sample to a microscope slide or petri dish is glue (Morriss et al., 2008; Shirmohammadi et al., 2011). In order to avoid the usage of glue to fix the sample to the substrate and potentially modify the mechanical properties of the tissue with glue penetration, we utilized the phenomena of heat fixation. When frozen sections are pressed against a warm microscope slide, the temperature difference leads to the sections' attachment to the glass, partially fixing the sample to the glass substrate by heat and dehydration (Layton et al., 2019). Consequently, the adhered cryostat sections were dehydrated for approximately 24 hours, guaranteeing an intact adhesion to the microscope slide. Samples were rehydrated before the visualization by optical microscope and before the AFM measurement.

Cryostat sections are sufficiently thin for the light to pass through; however, not all the light is absorbed by biological tissue in the same magnitude (Pellicer & Bravo, 2011; Guosong et al., 2017). Terrestrial biological organisms had to evolve in the close presence of light radiation (Johnsen, 2001; Guosong et al., 2017) and cope with the mutagenic effects of ultraviolet (UV) light radiation (Sage et al., 2012), highly bioactive free oxygen radical (Lim et al., 2022) and utilize visible light for their biochemical processes (Edwards & Silva, 2001). As a result, the biological tissue extensively absorbs UV and visible light, but the light absorption capability decreases with the higher wavelengths. The absorption and scattering of light are tissue-dependent (Sandell & Zhu, 2011). However, the decrease in light absorption and scattering capability generally creates an optical window in a small range of near-infrared (NIR) light spectra. The optical window ranges from 600 to 1300 nm (Pellicer & Bravo, 2011; Guosong et al., 2017). Tuning the excitation laser to the frequency of NIR light allows for deeper tissue penetration (Welch et al., 1989). The NIR light is also used together with the molecule-specific optical properties to visualize connective tissue (Cicchi et al., 2013; Hadraba et al., 2017; Williams et al., 2020) or adipose tissue (Débarre et al., 2006; Weigelin et al., 2016). We utilized the non-linear effect of a high-power pulsed NIR laser with the relapsed clubfoot tissue to visualize the collagen fibres and adipose structures under the optical microscope.

2.3.2 Identifying Structures of the Tissue

The second problem to consider when planning the sample preparation for the morphological characterization of the tissue is that most mammalian biological samples lack colour and contrast, making structures of interest nearly indistinguishable. The tissue from clubfoot biopsy offers little contrast in transmitted light, and specific structures elude visualization (Figure 5). In order to visualize specific structures with either visible or NIR light, the sample is often stained with contrasting agents or fluorescent labels (Kasten, 2002; Lee et al., 2020; Balaur et al., 2021).

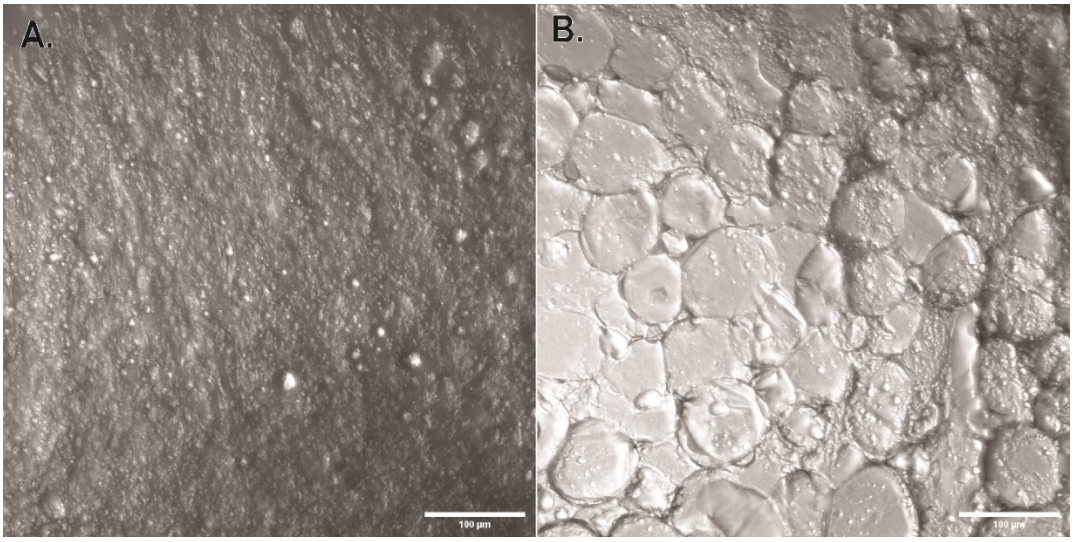

Figure 5. Brightfield image of connective tissue (A) and adipose tissue (B) of relapsed clubfoot. The image was acquired with NIR light transmitted through the sample.

The common method is to stain samples with a suitable dye. Dye staining faces two main challenges: transporting the dye to the target site and bonding the dye to the target (Dapson, 2005). One of the basic staining methods for enhancing contrast in tissue sections is the application of hematoxylin and eosin. Hematoxylin stains nuclei violet, while eosin stains the cytoplasm together with fibres and various proteins of the tissue in shades of pink, orange and red (Horobin, 2002; Kasten, 2002; Bancroft & Layton, 2019). Eosin is a suitable dye to stain connective tissue and identify primarily elastin but also collagen (Goldstein, 1969). Eosin is soluble in water or alcohol and diffuses into the tissue from the water or alcohol solution. The binding process to the target site is based on a strong affinity through electrostatic charges of anionic groups, a dipole

induction through van der Waals forces, and covalent bonds with amines (Horobin, 2002; Stochert, 2002; Dapson, 2005). Therefore, eosin staining is non-specific, and the resulting colour variation of eosin staining depends on the local variations in the density of stained structures, mainly proteins (Stochert, 2002; Bancroft & Layton, 2019).

Alternatively, specific fluorescent labels, based on the antigen-antibody interactions, are applied to the samples to achieve greater specificity of the staining to identify collagen (Zhu et al., 1995). Similar to immune reaction, the principles of antigen-antibody interaction is utilized in immunohistochemistry to stain specific target (Coons et al., 1941; Sanderson et al., 2019). An antibody carries a fluorescent label and can be attached directly to the target location – direct immunofluorescence (Coons et al., 1941; Burry, 2011) – or indirectly by marking target locations with a primary antibody, which itself acts as an antigen for a secondary antibody carrying the fluorescent label – indirect immunofluorescence (Weller & Coons, 1954; Burry, 2011). Applying a secondary antibody increases the binding specificity as the primary antibody carries an antigen of another animal species different from the investigated species. However, both direct and indirect immunofluorescence can produce errors in binding the antigen labels to an undesired antigen, introducing the uncertainty of proper label binding in antigen-antibody interactions (Saper, 2009; Burry, 2011).

Both staining methods alternate the native structures of the sample and introduce artifacts to the sample's morphology and mechanical properties. Fortunately, exogenous labels and chemical fixatives can be entirely omitted with a possible label-free approach. Biological samples can be excited by visible and NIR light radiation in the same manner as fluorescence labels to produce an endogenous autofluorescence without the addition of any fluorescent labels (Kingsley et al., 2001). Endogenous autofluorescence with a distinct contrast essentially fulfils the function of a specific label. In connective tissue, elastin fibres offer good contrast when imaged by two-photon microscopes.(Sutcliffe et al., 2017; Li et al., 2020). The intensity of the autofluorescence signal depends on the freshness of the sample (ElMasry et al., 2015), and the intensity decreases with the storage time (Croce et al., 2005). It is unclear how long-term storage of the clubfoot biopsies, *i.e.* several months, affects the autofluorescence. Of the thirteen patients, only one biopsy specimen had

a distinct autofluorescence signal of elastic fibres. Moreover, only the lateral side biopsy showed signs of elastin autofluorescence, while the same autofluorescence signal was barely detectable in the medial side biopsy (Figure 6). The experimental design did not allow immediate imaging of the biopsies under the two-photon microscope after surgery, and samples remained stored for an extended period at −80 °C before imaging.

Even with the lack of specific endogenous autofluorescence, clubfoot samples can be visualized in a label-free manner using unique optical properties specific to certain molecules, particularly collagen type I of connective tissue (Cicchi et al., 2013; Hadraba et al., 2017; Williams et al., 2020) and lipid-water interface of adipose tissue (Weigelin et al., 2016). The label-free visualization techniques are described in detail in the next chapter. The visualization of the collagen and adipose tissue is compatible with NIR light; therefore, it was possible to address the morphology of the relapsed clubfoot tissue without any added labels in a label-free manner. In summary, the samples were prepared in a way that avoids modifying the sample with any additives, such as fixatives or added fluorescence labels, which guarantees that no exogenous molecule will modify the micromechanical environment of the sample, making the sample suitable for both morphological and biomechanical investigation.

2.3.3 Identifying Position of the Structures using Coordinate system

Another problem of identifying tissue structures arises in correlative microscopy and multimodal analysis. The characterization of the tissue in multimodal analysis is often achieved by correlative microscopy, where various analytical and imaging devices are used to acquire data (Caplan et al., 2011). The relapsed clubfoot sections were imaged under two microscopes located at different microscopy facilities (primary and secondary microscopy sites).

The course and fine position identifiers were used to localize the same position in the sample for imaging between the primary and secondary microscopy sites. The course position identifier was created by marking each microscope slide with an asymmetrical red cross to indicate the zero XY position. The XY positions of the sample imaged at the primary microscopy site were found with respect to the zero at the secondary microscopy site.

The fine position identifier was made by ablating a rectangular mark in the sample (Figure 6). The ablation was done at the primary microscopy site with the upright optical microscope Bruker Ultima (Bruker Corporation, Billerica, USA) using a 1040 nm fixed output of Chameleon Discovery TPC pulsed laser (Coherent, Santa Clara, USA). The laser power of approximately 1.5 W was focused on the sample with objective CFI75 Apo 25XC W 1300 (1.1 NA) at each scanned focal plane during optical sectioning. The ablated rectangular mark helped to precisely localize the XY position in the sample at the secondary microscopy site. The ablated rectangular mark was also indispensable in the precise registration of images acquired with different modalities.

2.3.4 Rehydration of the Tissue

The characterization of the tissue in correlative microscopy and multimodal analysis requires the samples to be preserved for data acquisition and transport between the microscopy facilities, which are located at different locations (Caplan et al., 2011). The sample preparation is affected by the requirements of all the microscopes. Regarding the morphological and mechanical characterization of the clubfoot tissue, the AFM mechanical test required the samples to be adhered to the substrate (Kasas et al., 1997). The decision was made to avoid using glue for adhesion, and instead, the adhesion to the substrate was achieved by heat and dehydration. Several issues arise as both morphological characterization and mechanical testing of biological tissue are highly sensitive to the hydration level. First, the hydration level is closely linked to the ion concentration of the solution in which the tissue resides during the experiment. The (de)hydration induces osmotic pressure on the tissue structures, and the tissue shrinks or swells, altering both the morphology and mechanical properties of the tissue (Grant et al., 2009; Feher, 2017). Second, the tissue undergoing dehydration will transition from less stiff and fluid-like behaviour to more stiff and solid-like behaviour (Grant et al., 2008, 2009; Lefèvre et al., 2013; Munder et al., 2016). The (de)hydration of the tissue can make as much as three orders of magnitude difference between elastic modulus measurement between dry

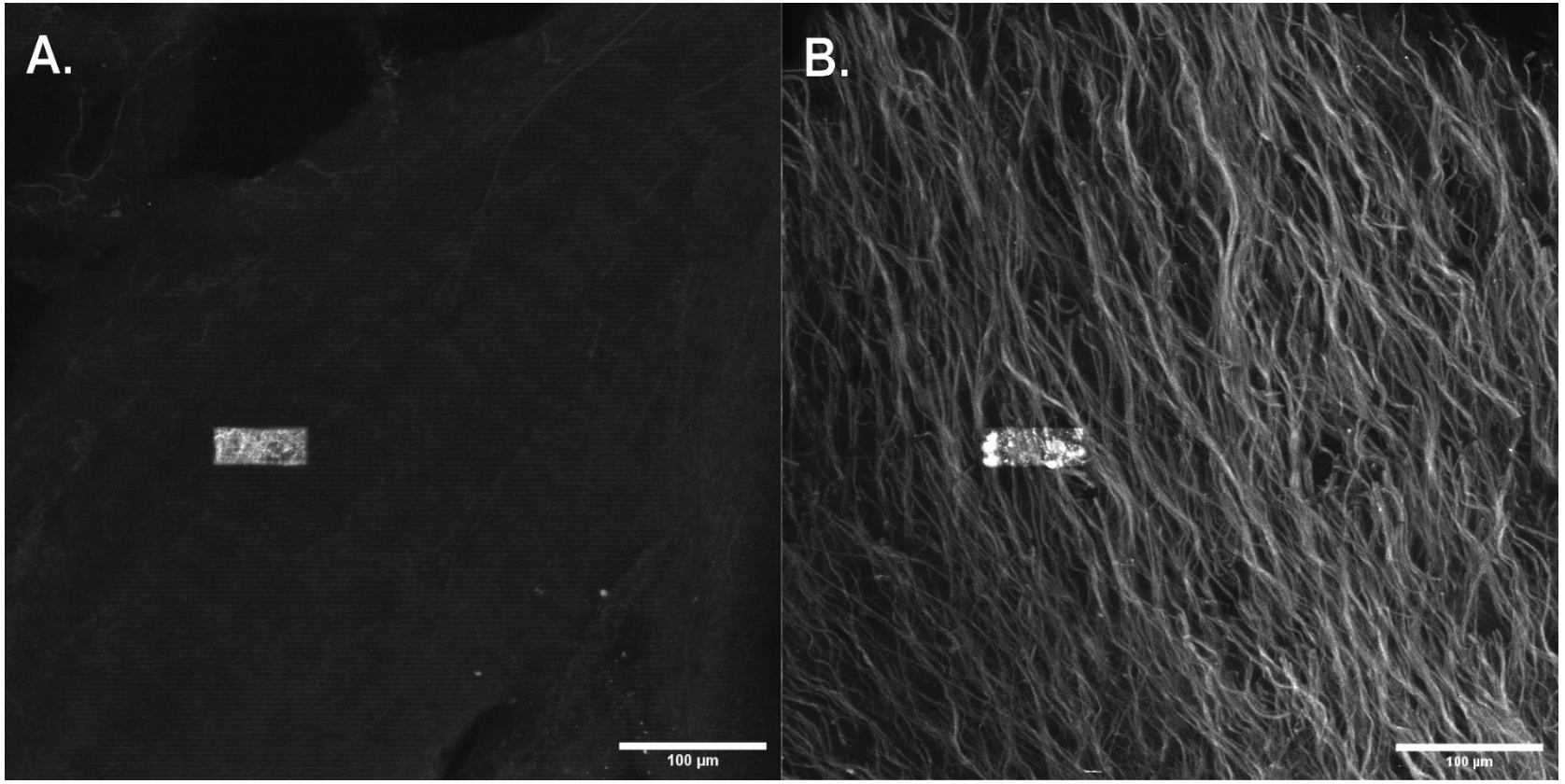

Figure 6. Autofluorescence signal excited by 810 nm femtosecond pulsed laser and detected in the visible region of the electromagnetic spectra (SP680 and BP595/50, Chroma, Vermont, USA). Medial side biopsy (A) shows sporadically fibrillar structures of low signal intensity. Lateral side biopsy (B) shows clear fibrillar structures, most likely elastic fibres. Rectangular signal in both images is autofluorescence released by ablation of the spot for co-registration of the images for multimodal analysis.

and hydrated tissue (Grant et al., 2008; Lefèvre et al., 2013). The change in mechanical properties identical to the hydration level happens by lowering the pH of the solution that defuses into the tissue (Grant et al., 2009; Munder et al., 2016). In order to achieve reproducible measurements of the mechanical properties of biological samples, the samples have to be in mechanical equilibrium in terms of osmotic pressure and pH of the solution. Hydration time for probing the mechanical properties of the surface is relatively quick and acquired Young's modulus is similar between different hydration times ranging from 3 to 60 minutes (Lefèvre et al., 2013).

In addition to the rehydration time from the literature, the rehydration time was established empirically by detecting the reflection of a 488 nm laser from the surface of the tissue (Figure 7). The reflection was detected under

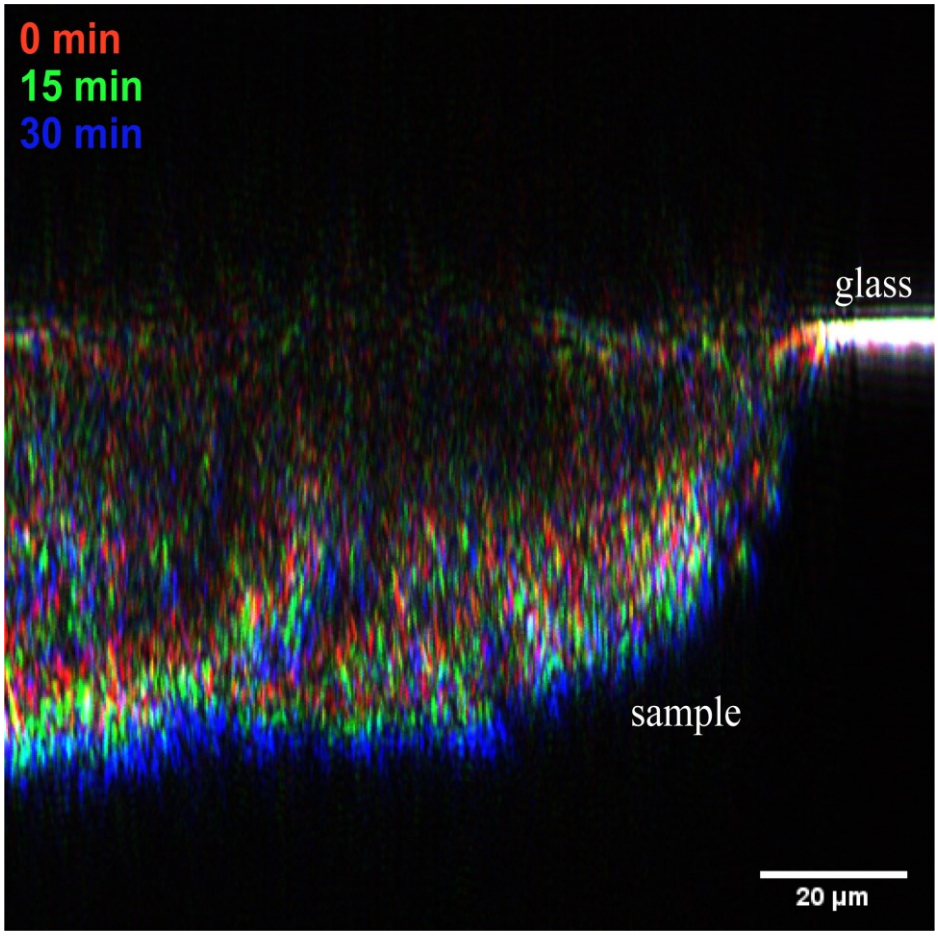

Figure 7. Volume change with hydration of the sample scanned in longitudinal plane (XZ). The reflection of the 488 nm laser from the relapsed clubfoot tissue surface is depicted for three time intervals. The sample changes its volume as water enters the sample. Glass reflection is used as a control of position.

the upright microscope Leica SPE using the Z-galvo stage, and XZ scans were collected over the span of 60 minutes. The rehydration process was stabilized after approximately 30 minutes. PBS was used to maintain the ion concentration of the sample to prevent shrinking and swelling of the sample. In the following experiments, all rehydrated samples were considered sufficiently hydrated after 30 minutes and were left hydrated for the duration of the experiment.

Chapter III

3. Visualization of Clubfoot Tissue

Clubfoot tissue from relapsed clubfoot biopsies is a composite material and consists of multiple functionally different tissue types. *In situ*, the tissue contains four tissue subtypes, particularly connective fibrotic tissue, providing structural integrity and cell signalling scaffold (Knitlova et al., 2021); blood vessels providing nutrition and thermoregulation (Merrill et al., 2011; Ošťádal et al., 2017; Novotny et al., 2020, 2022); neural bodies that provide innervation (Handelsman & Badalamente, 2008); and adipose tissue (Duce et al., 2013) providing nutrition storage, thermoregulation and endocrine signalling (Anderson, 1999; Walker et al., 2007). Each of the four tissue subtypes was reported to have pathological morphology or increased allocation of the tissue compared to controls (Handelsman & Badalamente, 2008; Merrill et al., 2011; Duce et al., 2013; Novotny et al., 2020; Knitlova et al., 2021).

The clubfoot has an apparent macroscopic morphology; however, the tissue's morphology is not immediately apparent. Several approaches exist to visualize the pathology using the same methods used in visualizing healthy tissue, such as electron microscopy, magnetic resonance imaging (MRI), light microscopy using immunohistochemistry or fluorescent labels, and label-free optical microscopy. The visualization of the morphology of the biopsies is not a straightforward process, and appropriate steps must be taken with both the biopsy sample preparation and the imaging itself. Electron microscopy can be used only on metal-coated samples and has nanoscale resolution (Malick et al., 1975; Sano et al., 1998). MRI is suitable for visualizing intact living patients and is resolution limited to millimetres (Hays et al., 2010; McDonald et al., 2017).

For imaging of tissue micromorphology, light microscopy is the closest approximation of *in situ* conditions (Hiraoka et al., 1990). We used NIR light to visualize the connective tissue and the adipose tissue of relapsed clubfoot biopsies in a label-free manner.

3.1 Label-Free Microscopy of Collagen

Label-free visualization methods can be used to visualize the collagen of fibrotic tissue (Ranjit et al., 2016). ECM of fibrotic tissue is abundant with collagen (Strupler et al., 2007). The collagen molecule is essential in the mechanical response of the tissue (Wells, 2013) and has anisotropic optical properties that allow the molecule and its hierarchical organization in the architecture of the tissue to be visualized in a label-free manner (Brasselet et al., 2010; Cicchi et al., 2013; Jan et al., 2015; Hadraba et al., 2017; Williams et al., 2020).

The visualization of collagen in fibrotic tissue is accomplished by generating a second harmonic (SHG) signal using NIR light. SHG signal is generated if the molecule has a non-centrosymmetric structure and structural organization at the focal volume. Collagen molecules meet both criteria for generating the SHG signal (Cicchi et al., 2013; Hadraba et al., 2017; Williams et al., 2020). The collagen fibres are also birefringent, which is an optical property required for generating extraordinary waves of light in polarization light microscopy (PLM)(Brasselet et al., 2010; Jan et al., 2015).

3.1.1 Second Harmonic Generation

The SHG signal is highly specific for collagen visualization. When the sample is stained with fluorescent labels for collagen type I molecules, the SHG signal co-localizes with the fluorescence of the labels (Strupler et al., 2007). The physical origins of the fluorescence label signal and SHG signal are different. Unlike fluorescent labels, which require a specific antigen (typically an amino acid sequence) of collagen for binding, an SHG signal requires a whole 3D structure of the molecule, together with the specific orientation of the molecule towards the incident light at the focal volume. SHG microscopy reveals both morphological and functional relations of collagen and its higher hierarchical organizations, such as fibrils and fibres. The SHG signal is sensitive to both the density of collagen and collagen orientation and distribution. Both information can be analysed quantitatively (Cicchi et al., 2013; Hadraba et al., 2017).

Out of the collagen types, only types I and II generate SHG signal (Cicchi et al., 2013). Other collagen types, such as type IV, would require staining

for visualization (Strupler et al., 2007). Since collagen type I, together with collagen type II and III, represent up to 90 % of all collagen types composition in a body, it is possible to use SHG microscopy for indications of disease state, disease progression and remodelling of collagen without the need for any additional labelling (Cicchi et al., 2013). Furthermore, SHG microscopy is based on multiphoton microscopy, where utilization of pulsed NIR laser light is highly favourable (Williams et al., 2005). As such, the SHG allows for depth imaging of collagen within the tissue biopsy (Welch et al., 1989). Therefore, visualizing the collagen of fibrotic tissue is possible without altering the mechanical properties of the tissue, making the SHG microscopy a suitable technique for multimodal analysis of the tissue and maintaining essentially the same condition of the tissue for other analytical instruments, such as atomic force microscopy.

Clubfoot deformity and its relapses have been identified to have fibrotic elements present in affected regions of the extremity (Sano et al., 1998; Ponseti, 2002; Eckhardt et al., 2019; Knitlova et al., 2020), thus an increase of collagen type I is expected in the relapsed clubfoot tissue. A hypothesis was postulated: the medial side of the affected limb is highly contracted, appears stiff, and fibrosis is present, which should result in an increase of the collagen type I content, unlike the lateral side of the affected limb. A comparison between the medial and lateral sides is made regarding collagen type I content. What is the difference in the quantity of collagen fibres in relapsed clubfoot tissue between the medial and lateral sides?

In order to identify the content of collagen in the relapsed clubfoot tissue, the 120μm sections of relapsed clubfoot biopsies were taken from cryostat to the upright optical microscope Bruker Ultima (Bruker Corporation, Billerica, USA), where the tissue was rehydrated for 30 minutes. Type I collagen was identified in the clubfoot tissue using an SHG signal (Figure 8) generated with Chameleon Discovery TPC pulsed laser (Coherent, Santa Clara, USA) tuned to 810 nm. The SHG signal was collected with high numerical aperture objective CFI75 Apo 25XC W 1300 (1.1 NA), passing through optical fibre into a detector housing with 2-inch filters (SP680, Chroma, Vermont, USA; and BP405/10, Edmund Optics, Barrington, USA). The SHG signal was converted into an image using non-descanned GaAsP photomultiplier tubes (type H11706-40, Hamamatsu, Japan). The voxel size was 0.51 x 0.51 x 3 μm^3.

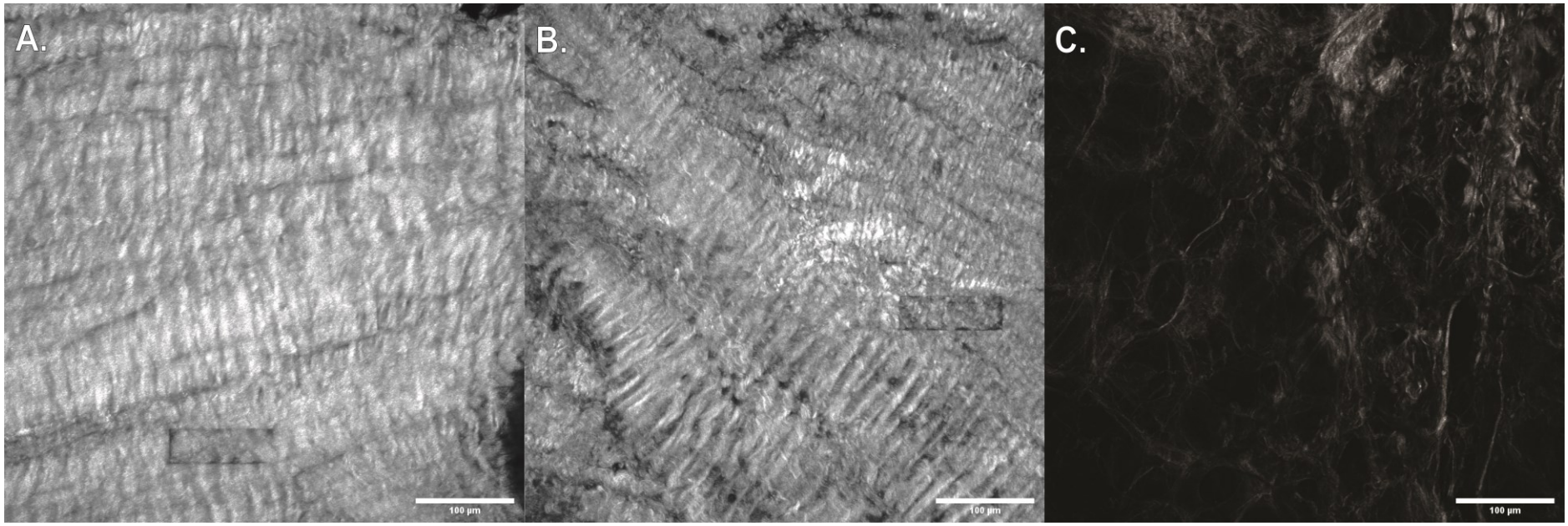

Figure 8. SHG signal of collagen fibres of fibrotic tissue in medial side biopsy (A) and lateral side biopsy (B). SHG signal of collagen in adipose tissue in lateral side biopsy (C). Rectangular signal in both images is left by ablation of the spot for co-registration of the images for multimodal analysis.

The morphology of collagen within cryostat sections was assessed in terms of the quality, cut damage and tissue type (Figure 8). The SHG images of collagen fibres with no apparent signs of damage and morphologically resembling connective tissue were used for further evaluation of the collagen content. The collagen of the adipose tissue was excluded from the evaluation (Figure 8, C).

The SHG z-stack images were first processed by filtering the noise from the SHG signal. The filtered images were projected using the maximum intensity projection. The collagen content was evaluated for the percentage of collagen within the field of view (FOV) for both the medial and lateral sides of relapsed clubfoot. The evaluation included 64 FOV from the medial side and 44 FOV from the lateral side of 10 individuals. The data were tested for normality by Shapiro-Wilk's parametric hypothesis test of composite normality in Matlab R2018b (MathWorks, Inc., Massachusetts, USA). Statistical differences between the medial and lateral side FOV were evaluated by the two-sample t-test in Matlab R2018b.

Statistical analysis of SHG images indicates a significant difference in the collagen amount between the medial and lateral sides of the relapsed clubfoot ($p = 0.035$). The results are stated as means ± SD. The medial side tissue contains a greater amount of the SHG signal per FOV ($\mu_{med} = 37.18 \pm 6.54$ [%]) than the lateral side tissue ($\mu_{lat} = 34.27 \pm 7.56$ [%], Figure 9). The result is in compliance with the expected result that fibrosis is present, leading to an increase of the collagen type I content in the medial contracted side and not in the lateral side of the affected limb of the relapsed clubfoot tissue.

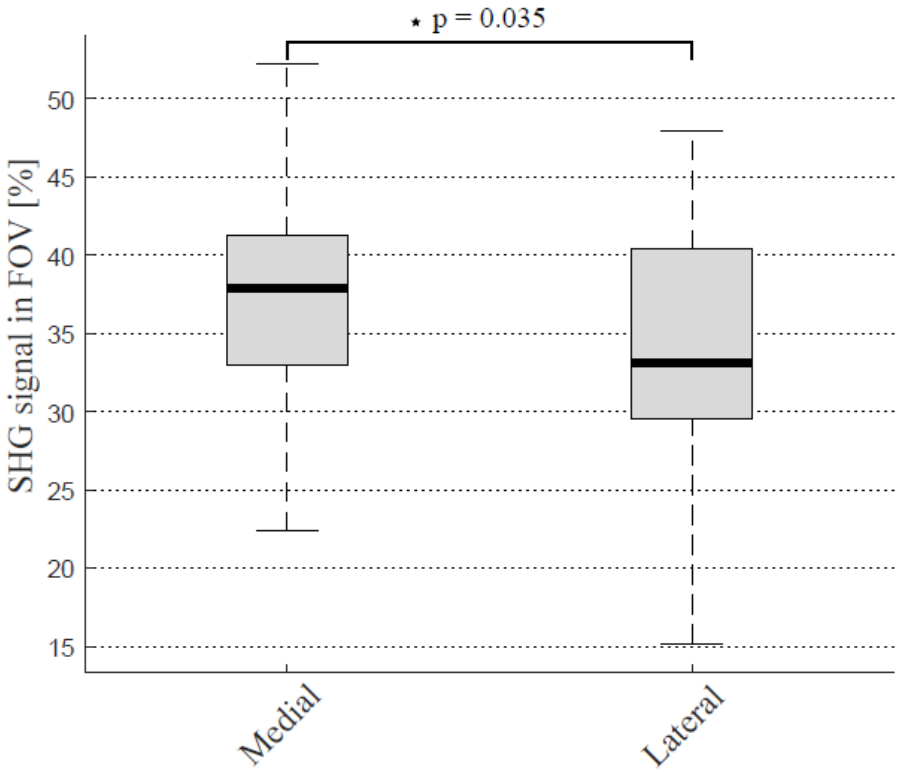

Figure 9. SHG signal representing the percentage of collagen content in FOV of medial and lateral relapsed clubfoot tissue.

3.1.2 Top-down Projection for AFM indentation

Besides evaluating the amount of collagen within the tissue, the SHG signal is an excellent indicator for localizing positions for AFM mechanical tests. There are two requirements for the positions in the tissue sections. One requirement is related to the quality of the collagen. The collagen fibres respond differently to mechanical tests based on their orientation to the indenter due to their anisotropy (van der Rijt et al., 2006; Strasser et al., 2007); therefore, it is crucial to avoid indenting loose fibres that result from cutting the sample into sections. The second requirement concerns the 15 µm vertical range limit of AFM cantilever indentation. For the second requirement, the SHG z-stack images were processed as a top-down projection (TDP) (Figure 10). The TDP is used in the multimodal analysis to indicate the surface roughness of each section and quality for AFM mechanical testing. The TDP images were used in the multimodal analysis.

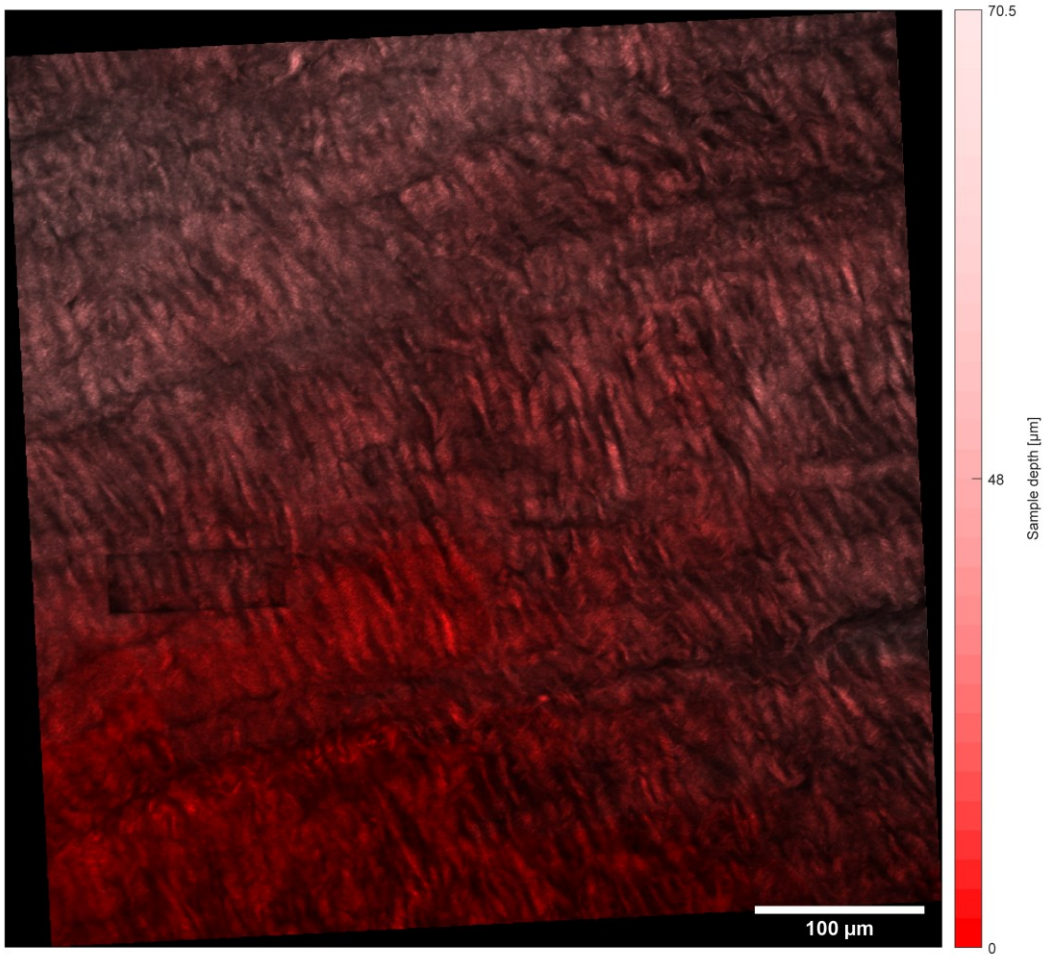

Figure 10. Top-down projection (TDP) of relapsed clubfoot tissue. The image appears rotated compared to the original acquisition, but the image actually underwent geometrical transformation according to the deformation induced by rehydration. The geometrical transformation is depicted in the deformation of the shape of an ablation rectangle.

3.1.3 Polarization Light Microscopy

Other means of visualizing collagen without staining come from the collagen's birefringence using PLM. Birefringence is another anisotropic optical property of collagen, which alters the polarization state of the incident light (Jan et al., 2015). Under bright-field illumination, the non-polarized light propagates through the sample as an ordinary wave (Simon & Gottschalk, 2007). Using a polarization filter in the illumination path of the microscope system, only the incident light with a polarization direction parallel to the main axis of the filter will reach the sample (Vidal, 2010). The electromagnetic field of the polarized

ordinary wave interacts with the birefringent sample, giving rise to an extraordinary wave. The extraordinary wave has a polarization direction perpendicular to the polarization direction of the ordinary wave (Simon & Gottschalk, 2007). When a second polarization filter, *i.e.* an analyser, is placed in the detection path of the microscope system with a polarization axis perpendicular to the polarization axis of the polarizer of the illumination path, the ordinary wave of light is rejected. Only extraordinary wave propagates to the detection unit (Vidal, 2010). The intensity of the extraordinary wave depends on the relative orientation between the sample and the crossed polarization axes of the polarization filters. When the sample is rotated, or the crossed polarization axes of the polarization filters are rotated, the intensity of the detected signal will change, with each iteration of the rotation visualizing a different orientation of the collagen fibres (Vidal, 2010; Jan et al., 2015). The PLM isolates the visualization of collagen only within a composite tissue. Therefore, the collagen within heterogeneous material can be precisely localized (Arun Gopinathan et al., 2015; Jan et al., 2015).

The application of both label-free techniques is frequently used to investigate collagen networks of biological tissue since the SHG and PLM signals of collagen carry information about the number of molecules, the fibre orientation (Stoller et al., 2002; Williams et al., 2005; Vidal, 2010), and molecular angular distribution (Brasselet et al., 2010). The techniques are suitable for both fixed and fresh samples (Williams et al., 2005; Vidal, 2010; Hutson et al., 2019), but fixation may change the morphology of the specimen, including the SHG signal or birefringence signal (Hutson et al., 2019).

Additionally, an important morphological feature of collagen fibres related to the mechanical properties of the tissue can be recognized in the SHG and birefringence signal. This morphological feature manifests in a load-free tissue as a periodic waveform pattern of collagen fibres, *i.e.* crimps or crimp pattern. It is believed that the crimps allow the fibrils to resist large tensile deformations, and the crimps gradually disappear as the fibres are straightened (Liu et al., 2014; Hamilton et al., 2021). The polarization sensitivity of both SHG and PLM opens the possibility of investigating the crimp pattern propagation and its dominant direction (Diamant et al., 1972; Hadraba et al., 2017; Hutson et al., 2019; Hamilton et al., 2021). The spatial period of crimp pattern propagation indicates the status of the tissue strain under applied stress (Hansen et al., 2002; Buckley et al., 2013)

and residual stress (Duclos & Michalek, 2017). A hypothesis was formed: since crimp pattern and orientation of fibres affect the resulting mechanical response of the tissue, does relapsed clubfoot tissue have a preferential directionality in the orientation of collagen fibres that could contribute to the rigid nature of the medial side of relapsed clubfoot tissue in comparison with the lateral side?

In order to test the hypothesis, the morphology of collagen fibres and crimp pattern must be visualized. Both SHG and PLM are label-free methods suitable for visualizing the collagen network morphology of fibrotic tissue and for the assessment of treatment effects on the morphology of the collagen network (Strupler et al., 2007; Arun Gopinathan et al., 2015), including the clubfoot deformity (Knitlova et al., 2020, 2021). The PLM was used to identify the positions at the secondary microscopy site. The dehydrated relapsed clubfoot sections were rehydrated in PBS for 30 minutes before the PLM image acquisition at an Olympus IX-81 microscope (LUCPlanFL N 20x objective, 0.45 NA; Olympus, Tokyo, Japan). The positions previously imaged by SHG at the primary microscopy site were localized at the secondary microscopy site according to the coordinate system (Chapter 2.3.3). The precise location of the FOV was identified according to the presence of the ablated rectangle in the bright-field imaging mode. Once the location was established, two polarizers with crossed polarization axes were inserted into the optical path. The two polarizers were sequentially rotated with a 10-degree step while the crossed axes were maintained. Ten images were acquired in the range from 0 to 90 degrees.

The sequence of polarization angles provided information about the local orientation of the collagen fibres at each pixel. Each polarization angle was assigned a colour (hue), and an overlay was reconstructed from the maximum intensity pixels (Figure 11). The polarization angles associated with the maximum intensity for each pixel were grouped and plotted in a histogram. The histogram was fitted with the von Mises probability density function (Gatto & Jammalamadaka, 2007) modified for a 90-degree interval. The fit provided the concentration parameter κ, which represents the orientation distribution of the collagen fibres. When $\kappa = 0$, the distribution of the collagen fibres is uniform.

Additionally, the PLM images were used to identify the crimp pattern and the orientation of the collagen fibres. First, the PLM images were transformed to the frequency domain using the 2D Fast Fourier Transform (FFT, Figure 12)

(Chaudhuri et al., 1987; Fung et al., 2010). The 2D FFT images were evaluated by central moments. The predominant orientation of the crimp pattern was determined by constructing the covariance matrix and calculating the eigenvectors of the matrix. The eigenvectors represent the semi-major and semi-minor axes of an ellipse, which are used to fit the covariance matrix and calculate the eccentricity ε of the ellipse. The eccentricity indicates the strength of the predominant orientation of the crimp pattern (Lo et al., 2012; Malacrida et al., 2017).

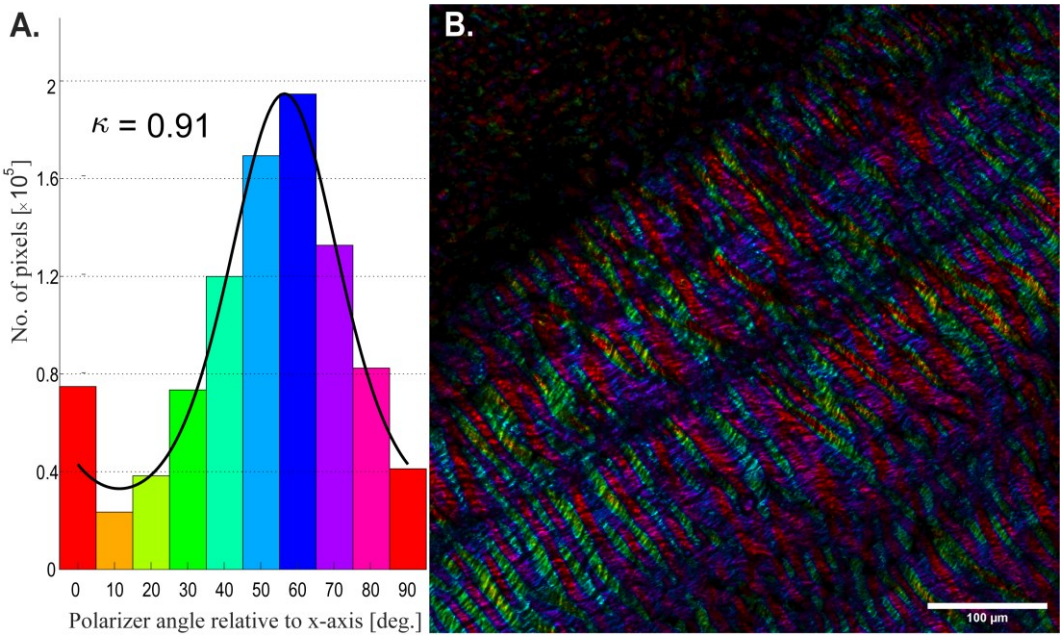

Figure 11. Distribution of individual polarization angles within a representative sample image (A). Polarization image of the medial side with HSV colour-code (B, each colour-angle pair represents the same colour-angle pair in A).

Statistical analysis of the concentration parameter κ and eccentricity ε was performed in Matlab R2018b (MathWorks, Inc., Massachusetts, USA). The data were tested for normality using Shapiro-Wilk's parametric hypothesis test of composite normality. Statistical differences were evaluated in Matlab R2018b using the two-sample t-test. The results are stated as means ± SD. No significant difference was observed between the medial and lateral side tissue when comparing the concentration parameter κ (μ_{med} = 1.84 ± 1.58, μ_{lat} = 1.60 ± 1.51, p = 0.27, Figure 8). In contrast, the relapsed clubfoot tissue of the medial side exhibited a more pronounced crimp pattern when compared with the lateral side tissue ($p < 0.001$). The FFT analysis of the crimp pattern shows an eccentricity

of 0.61 ± 0.16 [-] in the medial side tissue, while the tissue from the lateral side of the relapsed clubfoot exhibited an eccentricity of 0.48 ± 0.18 [-].

In conclusion, the analysis of the birefringence of the collagen fibres revealed that the crimp pattern of the fibres of the medial side tissue propagates at a higher frequency than the fibres of the lateral side tissue. The collagen crimp pattern was reported to function in force transduction in tendons during the initial elongation of the tendon. The functionality is observed as straightening of the crimps (Diamant et al., 1972; Hansen et al., 2002). The higher frequency of the crimp pattern propagation, i.e. more wavy fibres observed in the medial side tissue, could be a manifestation of released internal stresses after the surgical removal of the tissue from the body. The observed result suggests that greater tension is present in the medial side than in the lateral side tissue of the affected limb before the tissue is removed from the body, which corresponds to the deformity description of being contracted. However, the increased frequency of the crimp pattern could be related to clubfoot relapse or even to corrective treatment, as all the patients in the study had undergone the conservative, well-established Ponseti method of deformity correction before the surgical intervention.

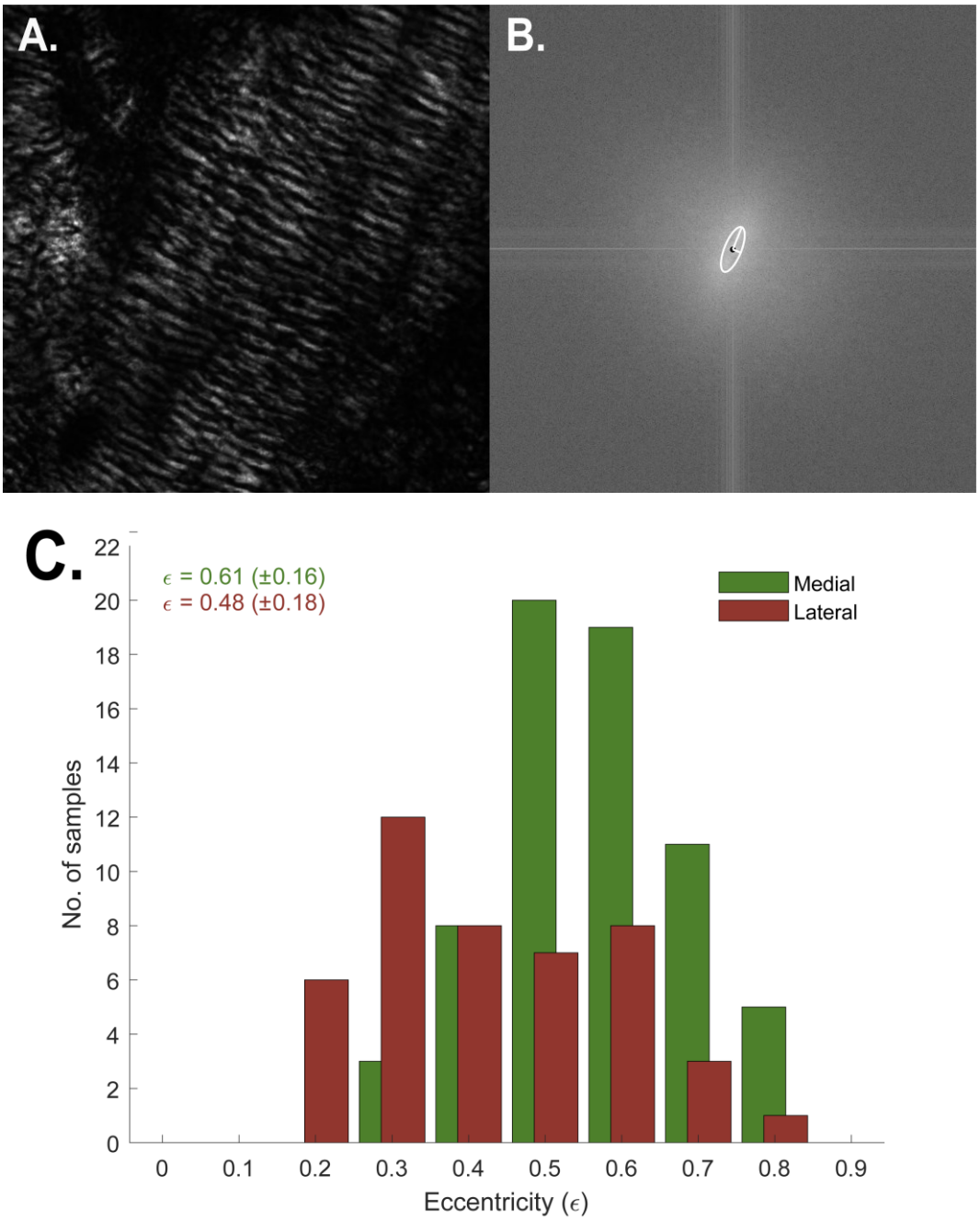

Figure 12. An overall directionality of collagen fibres of medial (green) and lateral (red) relapsed clubfoot tissue expressed as eccentricity ε (C). A single PLM image with one polarization angle (A) and its FFT image (B) is presented to illustrate the process of the analysis of crimp pattern propagation. When ε = 0, the collagen fibres are isotropic with no major orientation.

3.2 Label-Free Microscopy of Adipose Tissue

The biopsy from the surgery of relapsed clubfoot does not contain solely collagenous connective tissue but also adipose tissue, so it is meaningful to understand the role of the adjacent adipose tissue. The extremities affected with clubfoot deformity were reported to have a higher content of adipose tissue in comparison with an unaffected leg (Ippolito et al., 2009; Duce et al., 2013). It is highly probable that clubfoot biopsies contain adipose tissue, collagen and other extracellular matrix proteins. Adipose tissue has mechanical properties different from connective tissue and appears softer (Wenderott et al., 2020). Therefore, it is important to distinguish the adipose tissue from connective tissue. If the adipose tissue is measured together with the collagenous extracellular matrix, Young's modulus of the tissue would be lower overall, essentially contradicting the expected stiffening of the fibrotic tissue. A hypothesis was formed: relapsed clubfoot tissue biopsies from both medial and lateral side tissue contain adipose tissue adjacent to the fibrotic tissue. Is there any difference in the amount of adipose tissue between the medial and lateral side biopsies of the relapsed clubfoot tissue?

In order to answer the question, first, the adipose tissue has to be identified and quantified. The adipose tissue has a high lipid content (Weigelin et al., 2016). Lipids are a source of contrast for visualization in a label-free manner (Débarre et al., 2006; Weigelin et al., 2016) because of a higher refractive index compared to water (Schega et al., 2020). A transition between different refractive indices is observed at structural interfaces, such as the lipid-water interface, resulting in a label-free contrast with the application of pulsed laser. The laser's interaction with the structural interfaces results in a nonlinear coherent scattering process, termed third harmonic generation (THG). THG signal is generated from phase matching and interaction of waves in the sample with heterogeneous refractive indices, resulting in a signal with tripled energy compared to the incident light (Weigelin et al., 2016).

During the label-free investigation of the SHG signal from collagen type I at the primary microscopy site, the lipid-water interface was identified using THG microscopy (Figure 13). The tissue sections were under the same conditions as they were during the SHG imaging. The Chameleon Discovery TPC pulse laser (Coherent, Santa Clara, USA) was tuned to 1215 nm to visualize the adipose tissue

(THG), and the NIR light was focused through the CFI75 Apo 25XC W 1300 objective (1.1 NA). The generated THG signal was filtered with band-pass filter BP405/10 (Edmund Optics, Barrington, USA) and detected at the GaAsP detector. The voxel size for THG images was 0.51 x 0.51 x 3 μm^3, the same as the SHG images.

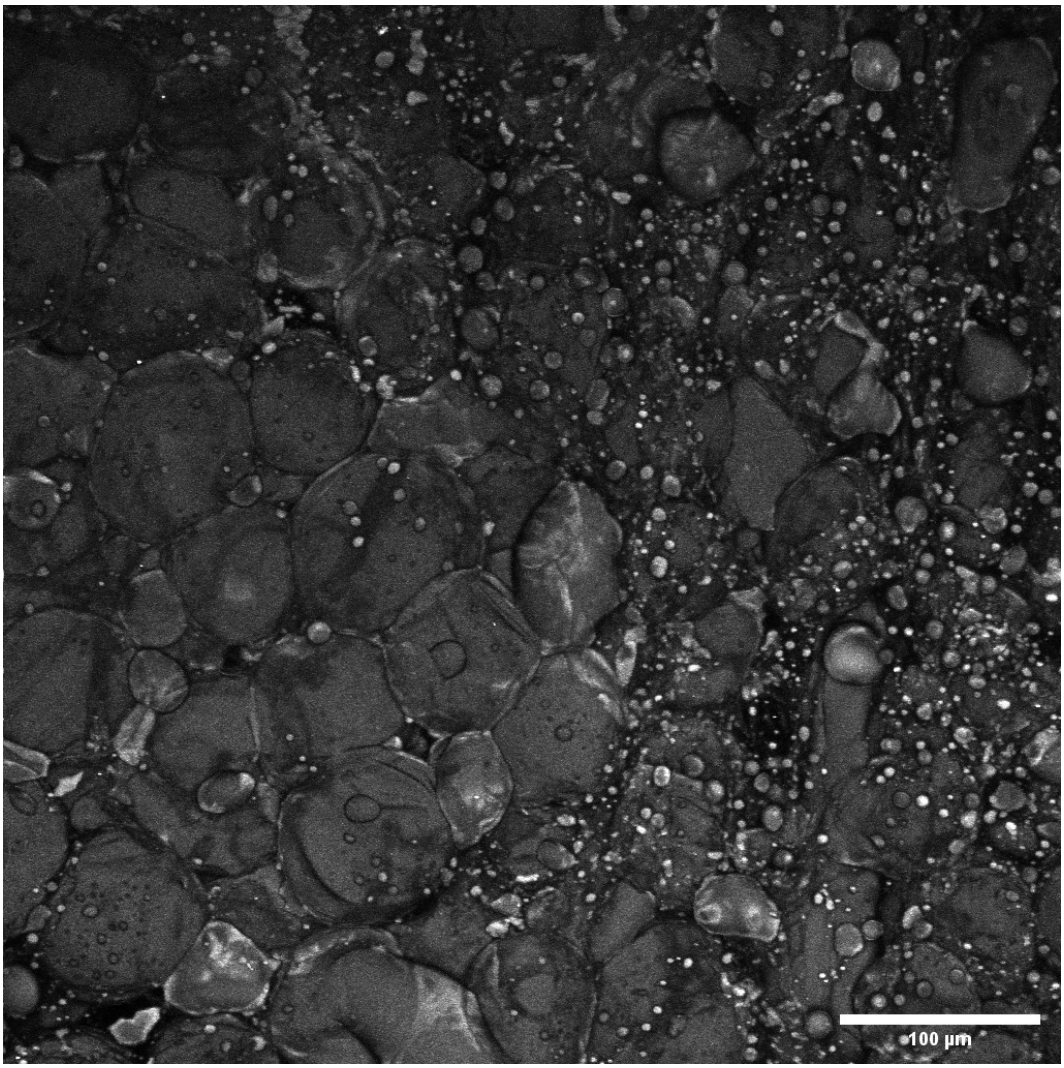

Figure 13. THG signal of adipose tissue. The THG signal on the left side of the image has a typical morphology of the adipose tissue. The FOV is the same as in Figure 8, C depicting SHG.

The medial and lateral side tissue were compared for the presence of adipose tissue using the THG signal. The background of THG z-stack images was filtered from the THG signal. The filtered THG signal was segmented for adipose features and was projected using the maximum projection. The percentage of FOV covered with THG signal was evaluated in the processed images (n_{medial} = 57 from 10 individuals, $n_{lateral}$ = 44 from 9 individuals). The normality of the data

and statistical differences were evaluated in Matlab R2018b (MathWorks, Inc., Massachusetts, USA). The statistical difference was evaluated with the Wilcoxon rank sum test (Figure 14).

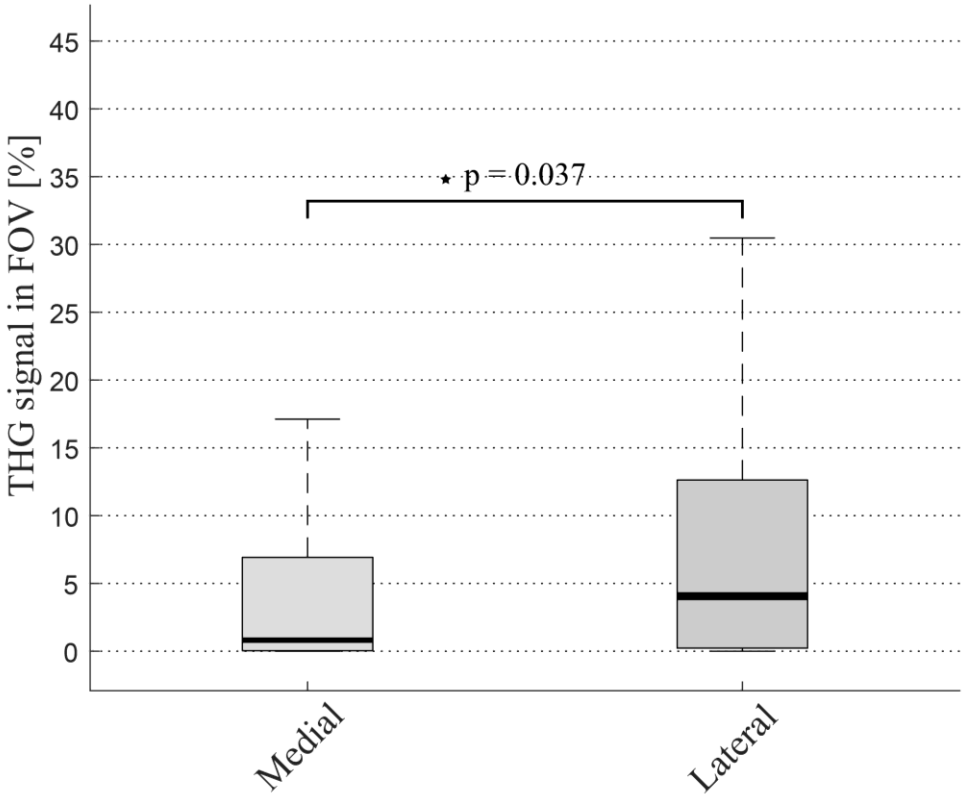

Figure 14. THG signal represents the percentage of adipose tissue content in the FOV of medial and lateral relapsed clubfoot tissue.

According to the Wilcoxon rank sum test, the THG signal coverage of FOV was found to be significantly different between the medial side and the lateral side biopsy sections of relapsed clubfoot (μ_{med} = 0.82 [%] (median; interquartile range (IQR) 6.89 [%]), μ_{lat} = 4.06 [%] (median; IQR 12.40 [%]), p = 0.037). Medial side tissue appears to contain a lower amount of THG signal per FOV overall compared to the lateral side tissue (Figure 14).

In summary, the lateral side of the clubfoot contains more adipose tissue. The adipose tissue is known to be less stiff (Wenderott et al., 2020) compared to the fibrous tissue (Grant et al., 2008) when responding to mechanical loading (Comley & Fleck, 2010). The softer nature of the adipose tissue could be why the lateral region of the relapsed clubfoot and the biopsy from the lateral side appear less stiff than the medial contracted side to the surgeons and orthopaedic practitioners. It is important to emphasize that the THG signal only approximates

the lipid content and is not an actual signal origination from lipids. For the scope of this study, the THG signal is a sufficient approximation of the adipose tissue. The THG signal is suitable for locating the regions without the adipose tissue for AFM mechanical testing. Additionally, the adipose tissue is accompanied by collagen (Comley & Fleck, 2010), and the presence of the THG signal among SHG signal reflects the composite nature of the tissue and highlights the interaction between adipose tissue and collagen tissue (SHG, Figure 8, C; THG, Figure 13). The level of adipose and collagen tissue interaction together with other proteins, e.g., GAGs, GP, have a significant impact on mechanical properties.

Chapter IV

4. Mechanical Properties of Clubfoot Tissue

When characterizing clubfoot deformity, the medial side of the affected foot, or feet, is characterized either as contracted or stiff and rigid across many publications describing clubfoot deformity (Ponseti, 2002; Pandey & Pandey, 2003; Poon et al., 2009; Kerling et al., 2018; Pavone et al., 2018; Quiggle et al., 2022). The collaborative orthopaedic practitioners also observe the same characterization in the relapsed clubfoot and the surgically extracted biopsy. The term stiffness used for characterizing the medial side clubfoot tissue is not well defined, nor is the force applied to the tissue. The observations of the orthopaedic practitioners are made during palpation of the affected foot or on the tissue after surgical excision. The tissue is obviously stiff to the medical professionals; however, the underlying reasons for the stiffness of the tissue are unclear. In this chapter, the stiffness used in clubfoot literature is explained in a broader context from the perspective of material sciences, followed by specifying the forces applied to the tissue used to characterize the biomechanical properties of the relapsed clubfoot tissue in the thesis. The biomechanical characterization was conducted using AFM.

4.1 Defining the Stiffness in Clubfoot Biopsies

The relapsed clubfoot tissue is a composite material. In the previous chapter, the tissue was shown to contain various tissue types that contribute to the overall macro-mechanical response of the tissue. The literature suggests that the underlying factor behind the rigidity of the tissue is linked to fibrosis. Fibrosis happens on the ECM level, where excess of collagen is observed (Eckhardt et al., 2019; Knitlova et al., 2020). The direct assumption would be that the increased amount of collagen through fibrosis is the source of the observed rigidity of the tissue. The material becomes more rigid as long as the amount of material increases and as a result, a greater force is required to deform the material (Namoco Jr., 2010). However, the material can also undergo changes in the internal organization resulting in an increased rigidity without an increase in size and geometry (Rader et al., 2002). In both instances, the material would be stiff and rigid. In biomedical field, the term stiffness is frequently used as a relative term for comparing

mechanical properties of the tissue based on the common sense with no regard for the engineering definition. The following section introduces the conventional biomechanical characterization that can be used in differentiating the increase of the amount of material, *i.e.* collagen, from the internal reorganization. The stiffness is defined in the broader context of geometry. The mechanical properties of clubfoot biopsies are introduced in the context of other biological tissue research in order to introduce a sense of scale for quantifying the biomechanical properties of the relapsed clubfoot tissue.

In classical mechanics and material sciences, rigidity or stiffness is a parameter that characterizes a relation between the resistance of the material and the force required to achieve a certain elongation of a sample or object with a specific geometry (Baumgart, 2000). Stiffness changes with the geometry and thus is sensitive to the variation in the amount of the extracellular matrix in the case of clubfoot. In the biomechanical investigation of tissue, the normalized sample geometry is unrealistic; therefore, Young's modulus is often used instead of stiffness. Unlike stiffness, Young's modulus is an intrinsic material property that is not dependent on the geometry of the tissue. The relation between the stiffness and Young's moduli is best described by the series of equations (Roark et al., 2002; Chen et al., 2010):

$$k = \frac{F}{\Delta L}\ , \qquad \sigma = \frac{F}{A}, \qquad \varepsilon = \frac{\Delta L}{L_0}, \qquad \sigma = E \times \varepsilon \tag{1},$$

where k is the stiffness, and F is the force required to achieve elongation ΔL of the material in the direction of applied force (Baumgart, 2000; Wells, 2013). The normalized force measurement to the area A, where force is exerted, or to the cross-section of the material A, is called stress σ (Roark et al., 2002). The normalized measure of elongation is strain (deformation) ε, which compares the elongation of the material ΔL to its original size L_0 (Baumgart, 2000; Roark et al., 2002). The last equation shows that stress and strain are generally linearly proportional to each other in homogeneous and isotropic materials, and the slope of the relation is Young's modulus of elasticity E. Young's modulus is a material property, and it is unique for each material (Roark et al., 2002; Zaitsev et al., 2017). The four equations show the relation between the stiffness and Young's modulus and can be written as:

$$k = E \times \frac{A}{L_0}$$

(2),

making it clear that Young's modulus, unlike stiffness, is an intrinsic property of the material and will be the same for a given material regardless of its geometry. The literal meaning of the equation is that stiffness is Young's modulus scaled by the ratio of the area (cross-section) and the initial length (Roark et al., 2002; Zaitsev et al., 2017).

In biological materials, the mechanical response to force is rarely purely elastic, but for instance, viscosity also contributes to the overall mechanical properties of the tissue. Due to the viscosity and composite nature of the soft biological tissue, the overall Young's modulus depends on the speed of the applied stress as well as the prior stress history and the type of loading. The composite nature of the soft biological tissue is exhibited in non-linear stress-strain relation composed of elastic, viscous, plastic and inelastic responses as multiple components of the tissue participate in the stress-strain response (Gralka & Kroy, 2015). Since the soft tissue contains a considerable amount of fluids, the viscous response, in particular, significantly impacts measured Young's modulus. Due to the effect of viscosity, the soft tissue responds not only as a solid-state material to the magnitude of applied forces in an elastic response but also exhibits a fluid-like behaviour by resisting the applied forces as the strain rate changes (Humphrey, 2003; Pal, 2014). If the tissue were purely elastic, the mechanical response is immediate, but the viscous component delays the response, and the speed rates increase or decrease the mechanical properties of the tissue (Nicolle et al., 2010; Wu et al., 2018). It is possible to assume that the biological tissue behaves as an elastic material in an initial linear region of the stress-strain relationship under the slow stress rate. The slow rate of stress results in an elastic response, where the contribution of the viscous component is minimal and mimics the purely elastic response (Carniel et al., 2013). For this linear region, Young's modulus is estimated in biological tissue (Dastjerdi & Mahloojifar, 2008; McKee et al., 2011). The characterization of the mechanical properties of the relapsed clubfoot tissue is conducted with the use of AFM, and Young's modulus is estimated for the initial elastic response under a quasi-static rate of AFM cantilever approach and retraction.

4.2 Mechanical Testing of Clubfoot Tissue by AFM

Mechanical measurements of biological tissue are sensitive to the type of mechanical test used (Baumgart, 2000; Grant et al., 2008; Chen et al., 2010; McKee et al., 2011; Wells, 2013). Each type of mechanical test applies forces with spatial and temporal variability to introduce stress or strain to the biological sample. Biological tissue is often anisotropic; therefore, the amount of the sample deformation depends on the directionality of applied force (Humphrey, 2003; Grant et al., 2008; Chen et al., 2010; McKee et al., 2011). Depending on the applied force, the biological sample is tested in tension, compression, shear (Wells, 2013), bending and torsion (Baumgart, 2000). Conventional mechanical tests investigate the macro-mechanical properties of the tissue, and the scale of measurement includes the biomechanical properties of multiple tissue components. In order to separate the individual components and achieve higher resolution of the biomechanical contribution of individual components, the biologists adopted AFM to measure local micromechanical properties of the tissue (Loparic et al., 2010; Akhtar et al., 2011; Grant & Twigg, 2013; Jorba et al., 2017). Since the relapsed clubfoot tissue is a composite material and the fibrous tissue is considered to be associated with the etiopathology of the tissue, the AFM is a suitable technique to determine Young's modulus of fibrous tissue of relapsed clubfoot.

An atomic force microscope is a force-scanning device initially developed to measure interatomic interactions, and a force-sensing cantilever equipped with a probe is the central detection piece of the microscope (Figure 15). The AFM technique was first presented in 1986 as a tool capable of studying interaction forces between a sharp tip and the surface of the sample (Binnig et al., 1986). The AFM technique was quickly adopted in biology to investigate biological structures at atomic resolution (Worcester et al., 1988). Later, the AFM technique was used for investigating various scales of biological structures, such as mechanisms of protein folding (Best et al., 2003), surface topography of molecules, including collagen type I (Bozec & Horton, 2005) and mechanical properties of individual molecules (Grant et al., 2009) and tissue (Lewis et al., 2008). The biological samples can be measured in liquid solutions, allowing for a better approximation

of physiological conditions (Worcester et al., 1988; Grant et al., 2008; Lefèvre et al., 2013).

The AFM can be operated as an indenter or a tensile device (Andriotis et al., 2018). The AFM operates in various scanning modes that rely either on the direct physical contact between the probe and the sample or on attractive/repulsive forces between the probe and the sample (Kasas et al., 1997; Santos & Castanho, 2004). A probe of a particular shape is mounted at the end of a cantilever (Kasas et al., 1997; Vinckier & Semenza, 1998). The cantilever is usually constructed as a single string or a triangle and is rigid in the X and Y axis while being relatively soft in the vertical Z axis (Kasas et al., 1997; Giessibl, 2003; Santos & Castanho, 2004). The length of the cantilevers should be as small as possible to avoid low-frequency resonance (Kasas et al., 1997).

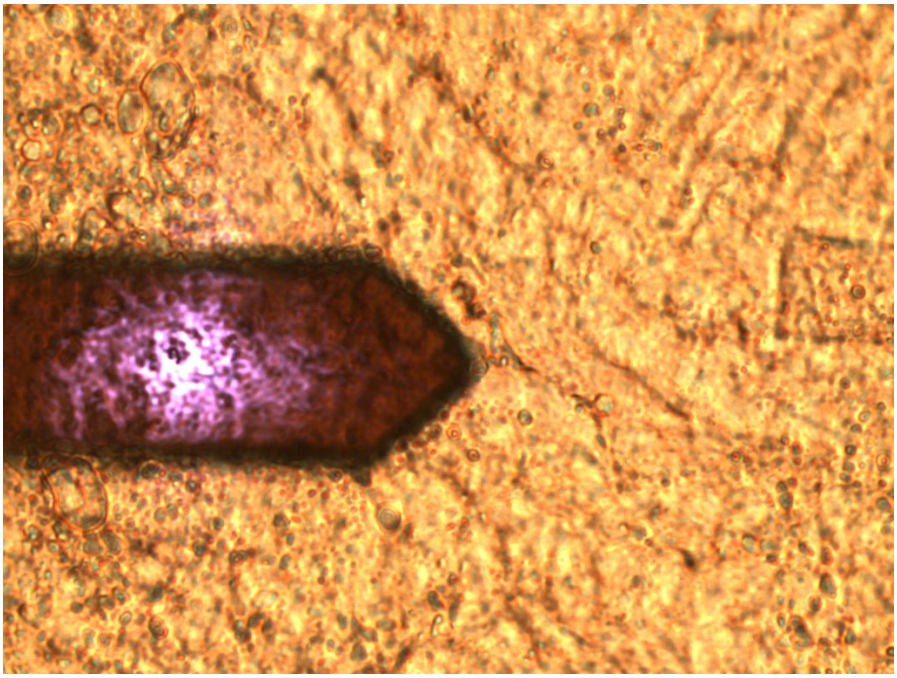

Figure 15. Cantilever imaged over relapsed clubfoot section. The ablated rectangular mark is visible in the field of view on the right side. The brightfield image was calibrated to the AFM tip position for later multimodal analysis.

The cantilever approaches the sample (or is being retracted from the sample), and the interaction between the probe and the sample causes the cantilever to bend. The bending of the cantilever, also known as the cantilever's deflection, is monitored by a laser, which points to the area on the cantilever located

opposite to the tip of the probe. Laser is then reflected onto a photodiode (Kasas et al., 1997; Giessibl, 2003; Santos & Castanho, 2004). The deflection of the cantilever is dependent on the resistance of the material being indented (or pulled in tension) and on the spring constant of the cantilever (Giessibl, 2003; Santos & Castanho, 2004), which can range from 0.01 to 100 N/m (Kasas et al., 1997; Santos & Castanho, 2004). The detected deflection of the cantilever is not immediately returned as a force [N], and cantilever deflection needs to be calibrated by either indenting a hard surface or by the thermal noise method. Once the deflection is converted to the force, the data from different measurements can be compared (Slattery et al., 2013).

The interaction forces between the probe and the sample are used to reconstruct the topography of samples (Kasas et al., 1997) and are also used in estimating the local mechanical properties of the sample, expressed as Young's modulus (Radmacher, 1997; Vinckier & Semenza, 1998; Heim et al., 2006; Matyka et al., 2007; Thomasy et al., 2014). Conventionally, the indentation force and the indentation depth are plotted in the force-distance curves (Figure 16). The force-distance curves are recorded during the approach and the retraction of the cantilever from the sample. The retraction force-distance curve carries information about adhesion forces (Kasas et al., 1997; Vinckier & Semenza, 1998). The theoretical model is used, and the force-distance curves are fitted to estimate the elastic modulus. The approach force-distance curve is used to estimate the elastic modulus of the sample without the effect of the adhesion (Vinckier & Semenza, 1998; Roduit et al., 2009).

The final result of the AFM measurement is also dependent on the indentation of the probe, which is limited by the force response from the sample and by the maximum vertical position of the probe (Kasas et al., 1997). The maximum range of the probe's indentation is 15 μm, so the surface needs to be smooth and levelled in the case of a biological sample with a rough surface (Kasas et al., 1997; Santos & Castanho, 2004). However, sample preparation is not standardized (Kasas et al., 1997), and several difficulties and obstacles related to sample preparation need to be overcome (Santos & Castanho, 2004). Fortunately, some AFM modes deal with obstacles like surface roughness (Santos & Castanho, 2004). Unlike contact mode, force mode

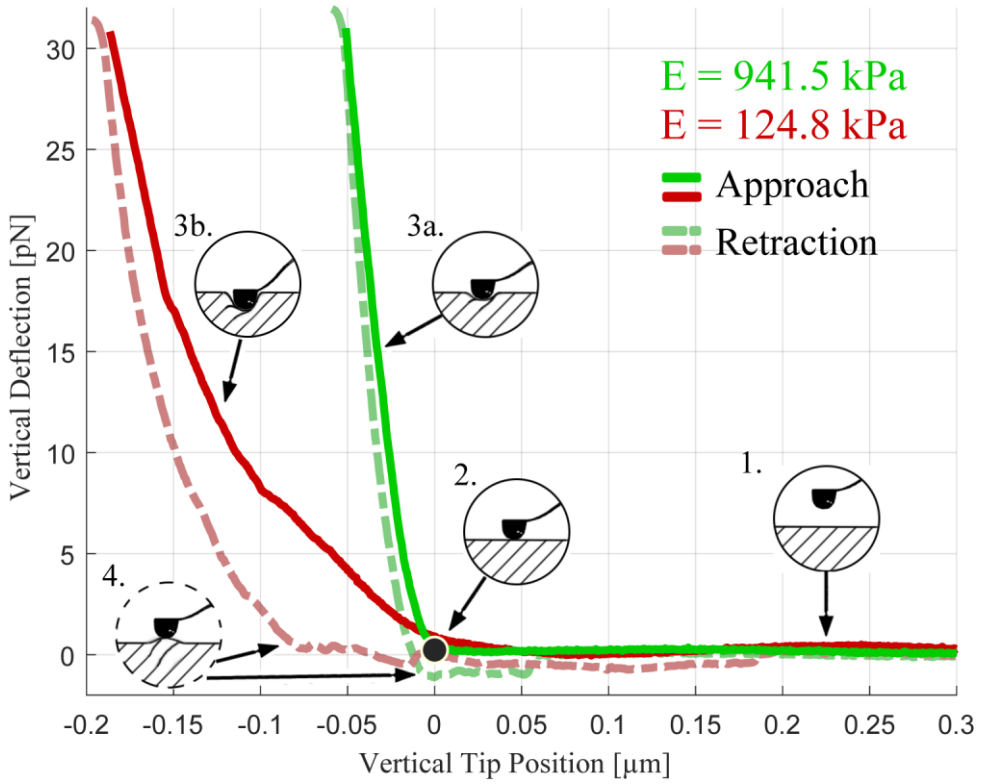

Figure 16. Force-distance curve. The force is represented by the vertical deflection of the probe, and the distance is represented by the vertical tip position from the sample. Both axes were zeroed to demonstrate the contact point (black dot). The full lines show the approach of the cantilever, and the dashed lines show the retraction of the cantilever. The position of the probe relative to the sample is depicted with numbers: 1. (no contact), 2. (contact), 3a. (stiff sample indentation), 3b. (compliant sample indentation), 4. (adhesion).

and tapping modes used in topography imaging provide a full range of the movement of the probe (15 µm). Therefore, samples do not need to be perfectly smooth, and samples with surface roughness within the range of the probe's movement are measurable (Kasas et al., 1997; Santos & Castanho, 2004; Matyka et al., 2007). The tapping mode seems to alter the sample the least (Santos & Castanho, 2004) and also increases the resolution when applied in liquids (Radmacher, 1997). Therefore, AFM is readily used for testing micromechanical properties of smoothed biological samples and can be paired with an inverted optical microscope (Kasas et al., 1997; Radmacher, 1997). The possibility of pairing the AFM with an optical microscope makes the AFM technique suitable for correlative microscopy and multimodal analysis of the relapsed clubfoot tissue, providing mechanical and morphological characterization. However, for proper

AFM measurements, several key steps need to be addressed, particularly the immobilization of the sample, the selection of the theoretical model, which leads to the selection of the shape of the probe, and last, the estimation of Young's modulus of the relapsed clubfoot tissue to select cantilever of similar stiffness.

4.2.1 Sample Immobilization for AFM

In order to use the AFM in the investigation of the mechanical properties of the clubfoot tissue, the tissue must be immobilized. The immobilization of the sample is important for both the topographical characterization and the biomechanical characterization of the tissue. The sample is conventionally glued or adhered to the substrate (Morgan et al., 2014). The glue can penetrate into the sample, increasing the stiffness of the sample (Chaurasia et al., 2012). Alternatively, the tissue can be clamped to the surface by applying glass with a punctuated hole in the middle over the sample and gluing the glass to the substrate. The punctuated glass holds the sample stationary, allowing the AFM probe to approach the sample through the hole in the glass (Morgan et al., 2014). However, when we applied the clamping method to the relapsed clubfoot tissue, the adhesive forces pulled the sample through the hole, rendering the measurement useless. Therefore, the immobilization of the sample was done by adhesion of the sample to the substrate through heat fixation, described in detail in Chapter 2.3.1.

4.2.2 Theoretical Model

Multiple theoretical models estimate the elastic modulus (Hermanowicz et al., 2014), for example, Hertz's or Sneddon's model (Vinckier & Semenza, 1998). Hertz's model describes the deformation of an elastic sphere against a rigid flat surface through an external load (Vinckier & Semenza, 1998; García, 2002; Heim et al., 2006), while Sneddon's model describes an infinitely hard indenter with a specific geometry deforming a flat substrate (Vinckier & Semenza, 1998). Some models consider adhesion forces with the spherical probe and are applicable to the retraction curve, such as Johnson-Kendall-Roberts's (JKR) model, which utilizes a parabolic approximation of the shape of the probe (Johnson et al., 1997) or Maugis's model, which uses precise dimensions of the spherical probe (Maugis,

1995). Therefore, selecting the theoretical model is just as critical as the selection of the probe for the proper AFM measurement.

The theoretical model that was decided to be used for fitting the force-distance curves from the measurement of relapsed clubfoot sections was the Hertzian-Sneddon model for the spherical indenter, which is available in JPK Data Processing software (JPK, Berlin, Germany):

$$F = \frac{\boldsymbol{E}}{1 - v^2}\left[\frac{a^2 + R^2}{2} ln \frac{R + a}{R - a} - aR\right] \quad (3),$$

$$\delta = \frac{a}{2} ln \frac{R + a}{R - a} \quad (4),$$

where F is the measured force, E is Young's modulus that represents the mechanical properties of the fibrous tissue of the relapsed clubfoot, v is the Poisson's ratio, a is the radius of the contact circle, R is the radius of the indentation sphere, and δ is the indentation depth (Neumann, 2008). In the equations 3 and 4, there are measured parameters, constants and calculated parameters. The measured parameters are the indentation force F, based on the cantilever calibration, and the indentation depth δ. Constant parameters are Poisson's ratio v and sphere probe radius R. The Poisson's ratio varies for different tissue types, and the value 0.5 is reported for incompressible biological samples (Liu et al., 2006). Dermis is reported to have Poisson's ratio in the range of 0.38 to 0.63 (Shah et al., 2017). In skeletal muscle, the measured Poisson's ratio was reported to be 0.28, 0.47 and 0.74 for different directions of applied stress (Takaza et al., 2013). Finally, the calculated parameter is Young's modulus, which describes the mechanical response of the relapsed clubfoot tissue.

4.2.3 AFM probe and Estimate of Elastic Modulus of Clubfoot Tissue

The AFM probe is carried at the tip of the cantilever. The available probes for AFM have various shapes and sizes. The size can be as small as a single atom at the tip of the probe. The shape of the probe tip determines the resolution of AFM.

In general, sharper tips are better for resolving the structures as the contact area is relatively small (Figure 17), making the sharp tips more suitable for topography measurement. Round tips, such as spherical tips, will include more structures during the indentation, thus functioning as a micro-indenter (Kasas et al., 1997; Stolz et al., 2004). The final image is a convolution of the tip's shape and the sample (Kasas et al., 1997).

While the tip shape is important in resolving the structures of the sample, the resolution is affected mainly by the softness of the sample and the loading force applied (Radmacher, 1997). Selecting a cantilever with a spring constant that is too high compared to the sample will result in barely any deflection while having a spring constant too low will result in almost no indentation in the sample (Thomas et al., 2013). Therefore, for accurate AFM measurements, the cantilever deflection must be significantly larger than the deformation of the probe and the sample (Giessibl, 2003). In addition, the probe parameters, such as tip radius, cone angle and force constant, must be known to calculate elastic modulus accurately (Vinckier & Semenza, 1998).

The biomechanical characterization of the relapsed clubfoot tissue does not require sharp tips, as the intention is to measure the mechanical properties of the tissue and not the mechanical properties of the individual collagen molecules and fibres. The size of individual molecules, namely tropocollagen, is around 287 nm (Bozec & Horton, 2005), while the size of the fibrils is around 1 µm and 10 µm for fibres (Cicchi et al., 2013). Therefore, the spherical shape probe with a micrometre size is optimal for characterizing biomechanical properties of fibrous tissue of relapsed clubfoot.

The optimal shape of the probe is known; however, it remains to determine the optimal stiffness of the cantilever, *i.e.* the spring constant. Biological tissue is considerably softer in comparison with engineering materials. When measured with AFM, the mechanical response of engineering materials is typically observed in hundreds of GPa, such as stainless steel with 259 GPa or titanium carbonitride with 510 GPa (Miller et al., 2012). In contrast, Young's modulus of biological tissue measured with AFM is considerably smaller, ranging from units of Pa to GPa (Weisenhorn et al., 1993; Radmacher, 1997; Vinckier & Semenza, 1998; Jorba et al., 2017; Wenderott et al., 2020). The range varies for a single type of tissue based on the probe used, as different structures contribute to the measured

biomechanical response (Stolz et al., 2004). In order to optimize the AFM measurement in the face of the large variability of biological samples, it is essential to estimate an approximate stiffness of relapsed clubfoot tissue. The cantilever used to measure the biological sample should have a similar stiffness to the biological sample (Gavara, 2017).

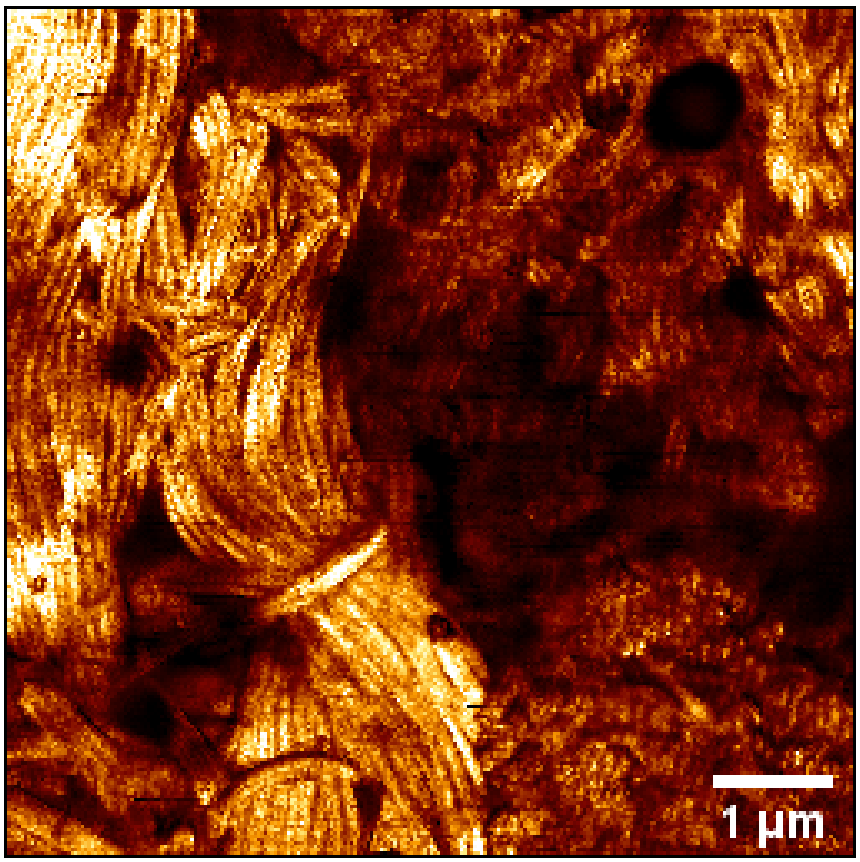

Figure 17. Topography AFM scan of relapsed clubfoot tissue. The image was acquired using a sharp pyramidal tip.

In order to create a sense of scale for understanding how the relapsed clubfoot biopsy fits in the range of various biological tissue types, several examples of Young's modulus measured by AFM are made. Rabbit lamellar bone exhibited Young's modulus of 26.6 GPa when measured in dry conditions (Donnelly et al., 2006). In liquid conditions, the bone, specifically bovine osteonal lamellae, exhibited lower values ranging from 0.7 to 0.9 GPa (Tao et al., 1992). When AFM was used to measure sheep Achilles tendons, which partake in the locomotion, with a cantilever of 17.5 N/m spring constant, the elastic modulus measured in dry air peaked in the 4.0 ± 2.3 GPa range. In contrast, the range measured was 290 ± 100 MPa with humidified airflow (Magerle et al., 2020). Tendons

participating in the eye movement were reported to have a smaller elastic modulus of 60.127 MPa. The cantilever used to measure the tendons had a spring constant of 0.02 N/m (Yoo et al., 2014). Another type of tissue associated with locomotion is cartilage. Porcine cartilage measured with a 13 N/m cantilever was reported to have an elastic modulus of 2.6 MPa (Stolz et al., 2004), and an elastic modulus of bovine cartilage measured with a 0.37 N/m cantilever ranged from 0.16 to 0.60 MPa (Weisenhorn et al., 1993).

Examples of measurement on tissue with AFM, which are not expected to withstand large force load associated with locomotion, would be the cornea, myocardium and lungs. Porcine cornea measured with a 4.01 N/m cantilever was reported to exhibit Young's modulus of 49 kPa (Seifert et al., 2014), while Young's modulus of the human cornea was measured in a range of 1.14 to 2.63 MPa, measured with 25 and 33 N/m cantilevers (Lombardo et al., 2012). Elastic moduli of both the myocardium and lungs of mice were measured in comparison with fibrotic changes observed in clubfoot tissue as well. The elastic modulus of an approximate native myocardium tissue was measured to be 109 kPa compared to 804 kPa for myocardial scar tissue (Hiesinger et al., 2012). Native lungs exhibited an elastic modulus of 1.96 kPa, while the elastic modulus of lungs with induced fibrosis was increased tenfold to 17.29 kPa, measured with 0.06 to 0.08 N/m cantilever (Brown et al., 2013).

The above examples provide a good sense of scale; however, a better approximation of an expected stiffness exists for clubfoot tissue. Some orthopaedic practitioners and surgeons described the presence of fibrous mass in the medial side of the clubfoot and relapsed clubfoot tissue as "disc-like". The term is used as the fibrous structure appears to be analogous to the annulus fibrosus of intervertebral discs (Hersh, 1967; Ošt'ádal et al., 2015). The Young's modulus of rabbit annulus fibrosus was measured with AFM (cantilever spring constant was 0.12 N/m) by Lewis et al., 2008, and varied by the region measured. The elastic modulus ranged from 0.63 to 1.08 MPa (Lewis et al., 2008).

A few conclusions important for the biomechanical characterization of relapsed clubfoot tissue can be made from the AFM measurement of the various types of biological tissue found in the literature. First, the tissue that withstands higher force loads generally exhibits higher values of Young's modulus. Furthermore, an interspecies variability exists in the biomechanical properties

of the tissue of the same functionality. This conclusion is more interesting for possible animal models of clubfoot deformity rather than the research performed in the thesis. In addition, the fibrotic tissue exhibits higher values of Young's modulus in comparison with native tissue or with approximation of the native tissue. Last, the AFM indentation of biological tissue is sensitive to measurement conditions, such as hydration level.

With the knowledge of the approximate elastic modulus range of fibrous tissue, the optimal spring constant of the cantilever suitable for soft collagenous tissue was selected to characterize the micromechanical properties of relapsed clubfoot tissue. A cantilever with a micrometre-sized probe suitable for soft collagenous tissue was used in the AFM measurement of relapsed clubfoot tissue (CONT-Silicon-SPM-Sensor, NanoAndMore GmbH, Wetzlar, Germany). The spherical probe, made from silicon dioxide, had a diameter of 6.62 µm. According to the manufacturer, the spring constant ranged from 0.02 to 0.77 N/m. The resonance frequency of the cantilever was 6 to 21 kHz. The thickness of the cantilever was 2.0 ± 1 µm, length was 450 ± 10 µm and width was 50 ± 7.5 µm. The sensitivity and the precise spring constant of the cantilever were calibrated using the thermal drift approach in PBS at 23 °C. The average spring constant was determined to be approximately 0.34 N/m.

4.2.4 Young's modulus of Relapsed Clubfoot Tissue

The fibrous tissue that was localized during the morphological analysis (Chapter 3.1.2) was identified under an inverted microscope Olympus IX-81 (LUCPlanFL N 20x objective, 0.45 NA; Olympus, Tokyo, Japan) according to the XY coordinate system established during the sample preparation (Chapter 2.3.3). The Olympus IX-81 was equipped with a JPK NanoWizard 3 AFM microscope setup (JPK, Berlin, Germany) for biomechanical characterization of the relapsed clubfoot tissue. The precise location for AFM indentation was identified according to the ablated rectangular mark (Chapter 2.3.3, Figure 6, Figure 15).

The AFM indentation was conducted in a force mode with a calibrated cantilever over an area of 20 µm x 20 µm with a resolution of 8 x 8 pixels according to the Nyquist sampling theorem. The sampling rate was 5 kHz. The indentation

speed was quasi-static (6 µm/s) in order to limit the manifestation of viscosity. The indentation depth was kept in a range of 0.662 µm and 0.105 µm, according to the Brinell Ball model (Darvell, 2018). Five positions of 20 µm x 20 µm were indented with the probe in each section of the relapsed clubfoot. Force-distance curves containing the approach and retraction of the cantilever were acquired at each pixel. The data were acquired for the medial and lateral sides of the relapsed clubfoot.

The curves were evaluated using JPK Data Processing software, version 6.1.74 (JPK, Berlin, Germany). The processing tools of the software were used to identify the contact point of the probe with the sample and the correct height for cantilever bending (vertical tip position). The approach force-distance curves were fitted with the Hertzian-Sneddon model with a Poisson ratio set to 0.5. Force-distance curves with an atypical baseline, low model accuracy or without a linear region were excluded from the evaluation. The values of Young's modulus were exported as TSV files and imported in Matlab R2018b (MathWorks, Inc., Natick, Massachusetts, USA) for further analysis.

The imported Young's moduli values were reconstructed as 8 x 8 maps in Matlab. Even though the maps were acquired over fibrous tissue, the possible presence of adipose tissue was not altogether excluded. In order to separate the Young's moduli of fibrous tissue comprising collagen from the Young's moduli of the residual adipose tissue, a threshold of 30 kPa was established based on the literature dealing with the AFM research of the adipose tissue (Wenderott et al., 2020). The threshold was used to filter the maps of Young's moduli. The resulting maps were split into four quadrants and evaluated for spatial dependence using 2D autocorrelation (Bramowicz et al., 2014). The below equation for 2D autocorrelation was translated into Matlab code:

$$\hat{R}(k,l) = \frac{1}{(n-|k|)(n-|l|)\sigma^2} \sum_{y=\max(1,1-l)}^{\min(n,n-l)} \sum_{x=\max(1,1-k)}^{\min(n,n-k)} (I(x,y)-\mu)(I(x+k,y+l)-\mu) \quad (5),$$

where n is the number of points in one dimension, x and y are the coordinates of the Young's moduli (x, y = 1 ... n), k and l are the coordinates' shifts (k, l = n+1 ... n-1), µ is the mean value of the Young's moduli in the AFM map,

and σ^2 is the variance of the Young's moduli in the AFM map. When Young's moduli were evaluated as independent, one average value per quadrant was used in statistical analysis. When Young's moduli were evaluated as dependent, a single average value per AFM map was used in statistical analysis.

Statistical analysis was conducted in Matlab. The data of Young's moduli were tested for normality by Shapiro-Wilk's parametric hypothesis test of composite normality. Statistical differences between Young's moduli of medial and lateral side tissue were evaluated using the Wilcoxon rank sum test at alpha level 0.01 ($p < 0.001$, Figure 18). The results are stated in the following format: median; interquartile range (IQR). A significant difference was observed between the elastic moduli of the medial side tissue (E_{med} = 186 kPa; 90 – 458 kPa) and the lateral side tissue (E_{lat} = 130 kPa; 62 – 350 kPa) of the relapsed clubfoot.
In summary, Young's moduli of collagenous tissue of the relapsed clubfoot are comparable to Young's moduli of cartilage and annulus fibrosus of intervertebral discs (Weisenhorn et al., 1993; Lewis et al., 2008). The tissue of the medial side, designated as fibrotic and stiff by orthopaedic practitioners, appears to be more rigid than the equivalent tissue from the lateral side of the relapsed clubfoot. While the assumption of excessive collagen production through fibrosis stands with the current data and is supported by SHG data, additional information is present in the AFM data. The AFM investigates micromechanical properties, and the difference between Young's moduli of the medial and the lateral side tissue suggests that structural change contributes to macro-mechanical stiffness observed by orthopaedic practitioners. However, this work only evaluated material properties expressed by Young's modulus. From the biomechanical perspective, Young's moduli oscillate at the same range of hundreds of kPa, and therefore, the clinical significance needs to be further investigated. It is highly possible that the increase in stiffness described by the orthopaedic practitioners is due to the local extensive growth, which would affect the parameters A and L_0 in equation 2.

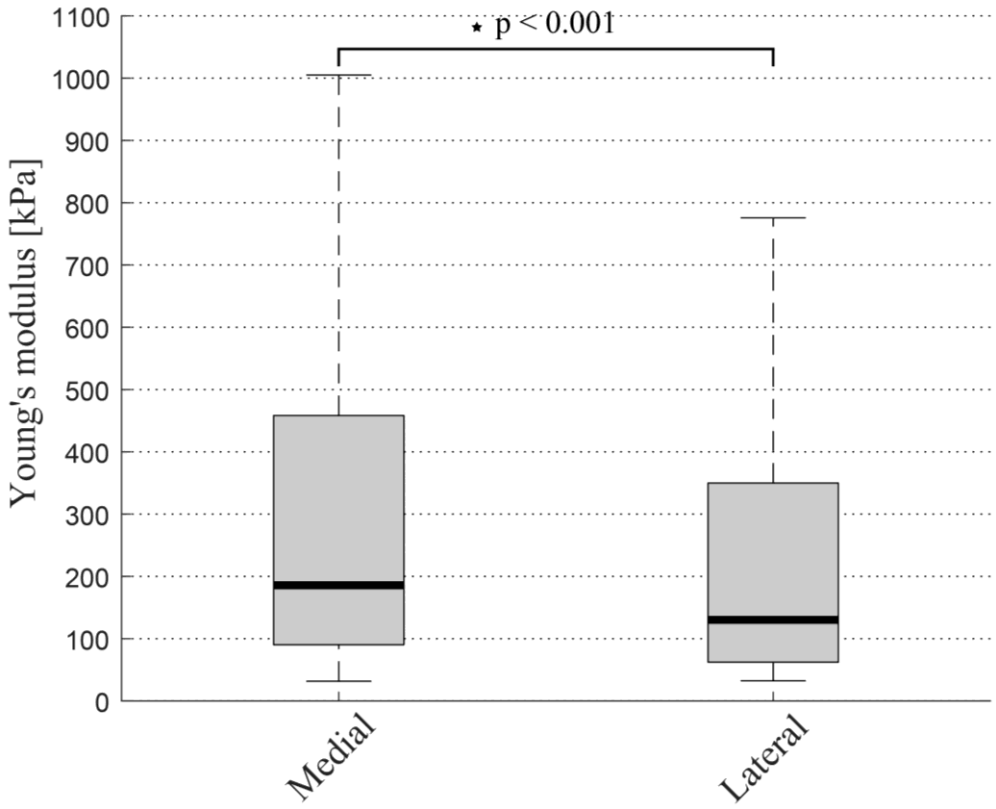

Figure 18. Mechanical properties of fibrous tissue from the medial and lateral sides of relapsed clubfoot tissue. The mechanical properties are represented by Young's moduli.

Chapter V

5. Multimodal Analysis of Relapsed Clubfoot

In the thesis, the relapsed clubfoot tissue was characterized morphologically and mechanically by different microscopy methods – optical microscopy and AFM. Each of the microscopy methods used has its advantages and limitations; however, the combination of the methods can reveal additional information. There are two approaches to combining the methods: one is through correlative microscopy, and the other is through multimodal microscopy. Generally, correlative microscopy combines methodological approaches of multiple microscopy devices to investigate a complex issue from different perspectives, with different scales and details (Caplan et al., 2011). An example of using correlative microscopy is the use of Bruker Ultima and Olympus IX-81 microscopes in the thesis. The workflow of correlative microscopy involves locating a specific target, e.g., the structure of a tissue or a cell type; identifying the target in a larger region; identifying unique information from different stains; and lastly, enhancing the information from a previous instrument at the secondary microscopy site (Caplan et al., 2011). The last step is usually a resolution enhancement through electron microscopy (Caplan et al., 2011); however, it can be done utilizing AFM (Odermatt et al., 2015).

Multimodal microscopy utilizes the same device but uses different modalities for visualizing different tissue structures, such as Coherent Raman Scattering to visualize molecular bonds and SHG to visualize non-centrosymmetric molecules (Yue et al., 2011). The example of multimodal microscopy in the thesis is the use of SHG and THG at Bruker Ultima microscope or AFM and PLM at Olympus IX-81 microscope.

Correlative microscopy and multimodal analysis were combined to identify additional information about the relapsed clubfoot tissue that individual modalities would not otherwise reveal. The workflow of combining the individual modalities is described in this chapter, followed by a summary and conclusion of the results.

5.1 Co-registration of the Individual Modalities

The clubfoot tissue was investigated both with different microscopes and with different modalities, all while maintaining the position information

of the first investigated FOV from the primary microscopy site. The workflow of the correlative microscopy for the clubfoot tissue was described in Chapter II, specifically Chapter 2.1, where the two microscopy sites are described in temporal succession, and Chapter 2.3.3, where the identification of the structure and position on the microscopy slide is described in detail. It was possible to identify the identical position at the secondary microscopy site with the use of the relative slide coordinate system and the ablation of the rectangular mark,

Matlab R2018b (MathWorks, Inc., Natick, Massachusetts, USA) was used to co-register individual modalities related to the collagen tissue (Figure 19, Figure 20). The modalities included a brightfield image calibrated to the position of the AFM probe (AFM image), PLM images, TDP image and Young's moduli maps. The images of the individual modalities had to be rotated, as the optical path between the AFM image and PLM images utilized different cameras, each of which had a slightly different rotation angle in the camera mounting.

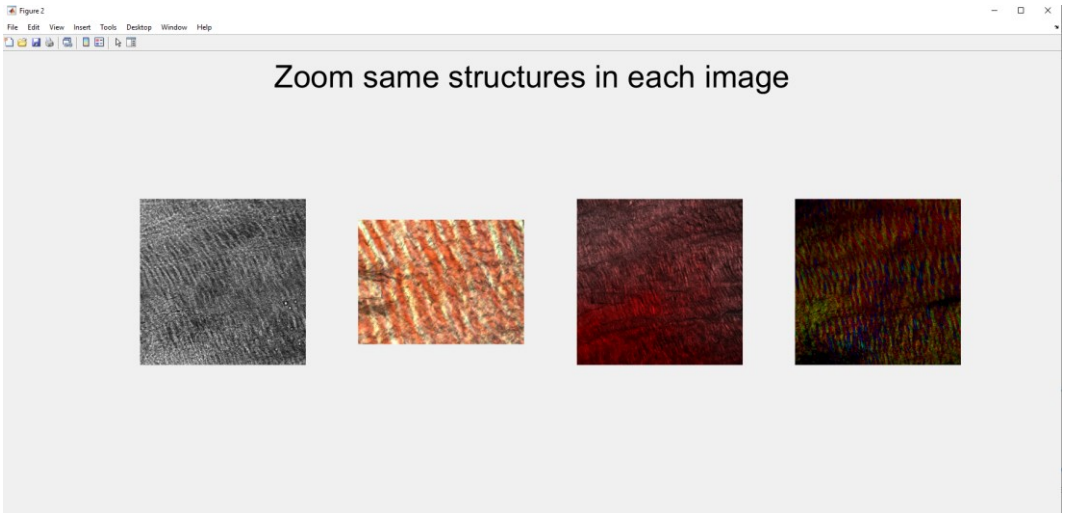

Figure 19. Matlab figure of scripted to overlay individual modalities. The first image is a PLM brightfield image (ordinary and extraordinary waves). The second image is the brightfield image from AFM. The third image is the SHG image. The fourth image is the PLM image (extraordinary waves).

In order to co-register the individual modalities, the individual images had to be transformed in accordance with the ablated rectangular mark. The template for the transformation was the AFM image since the calibrated data of the AFM probe allows for precise co-registration of the Young's moduli maps (Figure 20). Therefore, the first transformation was the rotation of the PLM images. Since

the PLM images never revealed the intact ablated rectangle, the brightfield image was used as a reference to rotate the PLM images (Figure 20). The PLM images were acquired in the same field of view as the brightfield image; therefore, the PLM images could be transformed in the same way as the brightfield image.

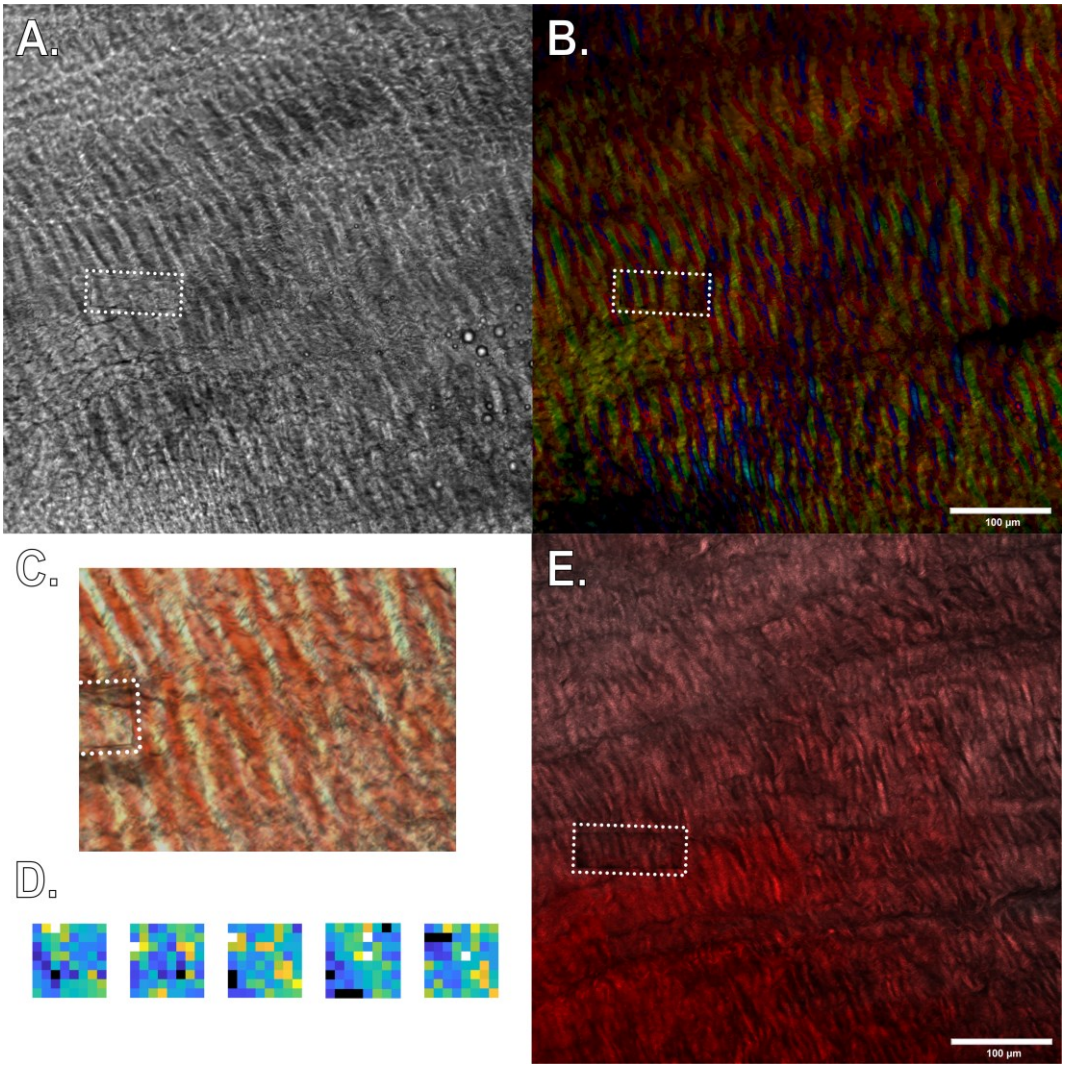

Figure 20. Individual modalities related to the collagen tissue. The brightfield image (A) from the PLM path was acquired without the cross-axes of the two polarization filters. The PLM image (B) is an HSV colour-coded image of individual extraordinary waves acquired at different angles of crossed polarization axes. The AFM image (C) was calibrated to the position of the AFM probe and, therefore, to individual Young's moduli maps (D). The TDP indicates surface roughness for AFM. The ablated rectangular mark is inside the white dotted rectangle.

The next step of co-registration of the modalities was the transformation of the TDP (Figure 20). However, the TDP modality was acquired at the primary microscopy site, and the effect of (re)hydration could modify the shape of the tissue. The shape of the ablated rectangle indicates the degree of change between the primary and secondary microscopy site; thus, the TDP image was transformed according to the shape of the ablated rectangle in the brightfield image (Figure 21). The final step involved the co-registration AFM image and Young's moduli maps (Figure 20, Figure 21). The AFM image was co-registered based on the two corner points of the ablated rectangle to the PLM image. Young's moduli maps were co-registered based on the AFM probe calibration data.

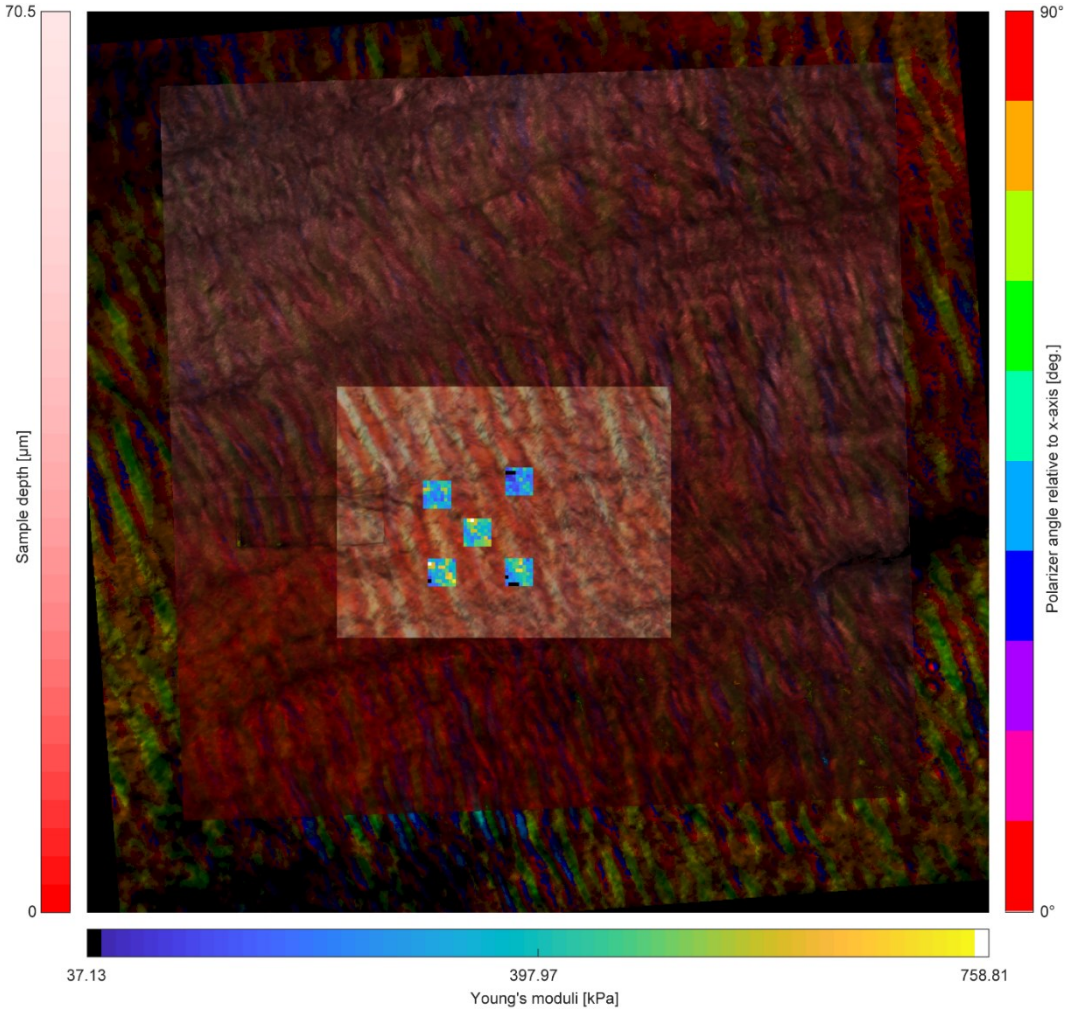

Figure 21. Overlay of different microscopy modalities providing different information about relapsed clubfoot tissue. The right side scale bar refers to the PLM image, the left side scale bar refers to the PLM image, and the bottom scale bar refers to the AFM maps.

The multimodal analysis revealed that the transformation of the TDP image was always performed. The image transformation indicates that (re)hydration modified the shape of the tissue. Furthermore, an attempt was made to evaluate the relation between the local polarization angle, which indicates local directionality, and the value of Young's modulus. The polarization angles for each AFM pixel were identified. Since there were multiple pixels with polarization angles for one AFM map pixel, the uniformity distribution analysis was performed with the Rayleigh test. In the case of non-uniform distribution, the AFM map pixel was paired with the predominant polarization angle of multiple pixels of the PLM image. In the case of uniform distribution, the NaN value was used. However, the majority of angles in the AFM pixels appeared uniformly distributed with no predominant orientation. Therefore, the relationship between local orientation and Young's modulus value was not evaluated.

5.2 Summary of Results

5.2.1 Collagen and Adipose Tissue in Relapsed Clubfoot

The measurements at the primary microscopy site (Bruker Ultima) targeted morphological features of collagen and adipose tissue. The results from the SHG modality in Chapter 3.1.1 show that the quantity of collagen fibres per field of view of relapsed clubfoot tissue is greater overall ($p = 0.035$) in medial side tissue compared to lateral side tissue (Figure 9). The results of THG modality in Chapter 3.2, Label-Free Microscopy of Adipose Tissue, suggest that there is a difference between medial and lateral side biopsies in the adipose tissue content ($p = 0.037$). When viewing the medial side tissue biopsies, there is a lower number of adipose structures generating THG signal compared to the lateral side tissue (Figure 14). The SHG signal, processed as TDP, described in detail in Chapter 3.1.2, was used in multimodal analysis. The TDP co-registration suggests that the tissue shape slightly changed between the primary and secondary microscopy sites due to (re)hydration (Figure 21).

5.2.2 Collagen Spatial Distribution in Relapsed Clubfoot

The measurements at the secondary microscopy site (Olympus IX-81 and JPK Nanowizard 3) targeted both morphological and mechanical characteristics of the tissue. The morphological analysis included a brightfield image from PLM path without the cross-polarized filters (BR image), a PLM image and a brightfield image from AFM path (AFM image). The mechanical characterization of the tissue included five maps of Young's moduli per a sample section.

The result from PLM modality was twofold: a local orientation distribution of collagen fibres expressed with κ and the predominant orientation of the regularity of the collagen fibres pattern expressed with eccentricity ε. The local orientation expressed by concentration parameter κ was not found to be significantly different between medial and lateral side tissue biopsies. The eccentricity ε, on the other hand, suggests that the medial side crimp pattern appears with greater frequency compared to the lateral side.

5.2.3 Mechanical Properties in Relapsed Clubfoot

The mechanical analysis described in chapter IV, with the results specified in Chapter 4.2.4, revealed a significant difference between overall Young's moduli between the medial and lateral side relapsed clubfoot tissue (Figure 18). The medial side tissue resisted the deformation caused by the AFM probe indentation more than the lateral side tissue.

Chapter VI

6. Discussion and Conclusion

The thesis presents relapsed clubfoot biopsies as composite material and focuses on its micro-morphological and micro-mechanical properties. The two tissue components under the micro-morphological scientific investigation were the adipose tissue and fibrillar collagen tissue. The identification of the adipose tissue within clubfoot was crucial for comparing the composition of the relapsed clubfoot tissue and for targeting the fibrillar collagen in micromechanical tissue characterization. The fibrillar collagen is targeted due to its significance in the elastic response of tissue (Robinson et al., 2004; Sherman et al., 2015). The significance of fibrillar collagen for the mechanical characterization of clubfoot is underlined by the literature, where fibrosis was observed (Sano et al., 1998; Ponseti, 2002), as fibrosis is a process of excessive collagen synthesis (Kerling et al., 2018) related to a general alternation of the mechanical properties of the tissue (Nelson & Bissell, 2006; Wells, 2013; Matera et al., 2021). However, no prior study investigated the micro-mechanical properties of the relapsed clubfoot tissue.

6.1 Rigidity of the Relapsed Clubfoot Tissue

The collaborative orthopaedic practitioners observed the rigidity and stiffness of the relapsed clubfoot tissue in the medial side of the deformed foot during surgical extraction (Ošťádal et al., 2017). The observed rigidity and stiffness are also frequently reported in the literature (Pandey & Pandey, 2003; Poon et al., 2009; Faldini et al., 2013; Kerling et al., 2018; Pavone et al., 2018). The increase in rigidity of the medial side of the relapsed clubfoot was hypothesized to originate from two phenomena based on the previously discovered fibrotic markers (Eckhardt et al., 2019; Novotny et al., 2022). The first phenomenon is related to a change in geometry and structure as the amount of material increases (Namoco Jr., 2010). The second phenomenon is characterized by a change in the structure and properties of the building material (Rader et al., 2002). Our study showed that the amount of collagenous material in the medial side is higher than in the control lateral side of relapsed clubfoot. Increased Young's modulus E is most likely the result of both the fibrosis and the changes

in the internal structure; cross-section A is linked to fibrosis as the volume of collagen increases in the tissue, and elongation L is the matter of shortening as the medial side is contracted. All these processes are happening altogether, making the relapsed clubfoot of the medial side appear stiff to orthopaedic practitioners.

6.1.1 Fibrosis and Mechanical Properties

The presence of fibrosis reported in the literature (Kerling et al., 2018; Eckhardt et al., 2019; Knitlova et al., 2021; Novotny et al., 2022) is supported by the results presented in the thesis. The SHG signal was presented as a representation of the quantitative and qualitative information about the collagen fibres in the relapsed clubfoot tissue. The SHG signal is more prevalent in the tissue from the medial side of the relapsed clubfoot in comparison with the equivalent tissue in the lateral side. Therefore, it is possible to argue that the fibrosis is present in the medial side of the relapsed clubfoot.

Additionally, the increased values of Young's moduli in medial side could arguably be attributed to the fibrosis as well, and the results would fall under the category of the first phenomenon – an increased amount of the material leads to greater tissue stiffness. However, the results are challenged by a macroscopic comparison of the medial and lateral sides of the tissue. The medial side biopsies from the surgeries are larger in general. Furthermore, the scope of the microscale investigation of the SHG signal was far greater than the scope of the AFM indentation. As such, the fibrosis and the increased amount of collagen fibres do not have to lead to increased stiffness of the medial side tissue alone, and the higher values could result from the higher number of cross-linkers, higher abundance of other proteins or different collagen fibre orientation. In other words, even though the increased amount of collagen fibres would eventually cause relatively higher tissue stiffness, the AFM results suggest a difference in the internal micro-structural organization between tissue from the lateral and medial sides of the relapsed clubfoot. Therefore, the second phenomenon, a change in the structure and properties of the building material, is likely present.

The internal micro-structural tissue organization change has been reported in the work of our collaborative team. These reported structural changes include

the increase in collagen cross-links in the medial side of the relapsed clubfoot tissue or alternations in the 3D structure of the tissue and its composition, such as different composition of the components of viscoelastic ground substance (Novotny et al., 2020; Knitlova et al., 2021; Novotny et al., 2022). The changes in the internal structural composition of the tissue can account for the moderate increase in Young's modulus in the medial side because the small region of several collagen fibres is loaded with the AFM probe of a large size of 6.62 μm. The AFM micro-indentation introduces a complex state of stress that includes the response of multiple components of the tissue's microenvironment besides the collagenous network. However, the AFM force spectroscopy with the large spherical probe is equivalent to an indentation test. The type of loading is rather complex but is far from the tension loading of relapsed clubfoot that exists in a preloaded state in vivo. Unfortunately, the size of the samples does not allow for replicating the type of load in vivo. Therefore, the AFM force spectroscopy is the best micromechanical comparison that reflects the local, basic tissue building blocks in the ECM, such as collagen, cross-links, elastin, fibronectin or glycosaminoglycans (GAGs).

6.1.2 Mechanical contribution of various components of connective tissue

Collagen accounts for about 65 % to 80 % of the total composition of the dry mass of typical healthy connective tissue, such as tendons (Kannus, 2000), and accounts for the majority of the mechanical response of the tissue (Ault & Hoffman, 1992a; Levillain et al., 2016). However, the fibrous connective tissue constitutes other components, and just as the clubfoot is a composite of various tissue types, the individual tissue types are also composite materials. The connective tissue consists of other components not included in the analysis, such as elastin, glycoproteins, proteoglycans and various growth factors (Halper & Kjaer, 2014). What is the function of these omitted components, and how do they contribute to the mechanical response of the tissue?

One of the omitted components, elastin, is similar to collagen. Elastin is a fibrillar protein adjacent to collagen fibrils, which typically occupies superficial layers of the tissue and supports the elastic recoil of collagen fibres (Levillain et al.,

2016). Elastin represents about 1 to 2 % of the total composition of the dry mass of connective tissue (Kannus, 2000). Since both elastic and collagen are in large quantities, the overall mechanical response of the tissue to mechanical loading is greatly determined by the inter-relations of the two fibrillar proteins and by variations in their content within the tissue (Levillain et al., 2016). Although collagen was the main target of the thesis, it is important to note that the mechanical properties measured here are also the convolution of the contributions of various components of the tissue and not just of the collagen fibres. Targeting collagen is beneficial for targeting fibrotic tissue, as the molecule is easily detectable by both SHG and PLM. Targeting collagen allows for AFM indentation of intact tissue locations without tears and, more importantly, helps with identifying the correct type of tissue. Collagen of different tissue types has different morphological features, as is demonstrated in Figure 8, where fibrotic connective tissue of relapsed clubfoot is shown alongside the collagen of adipose tissue.

The presence of elastic fibres is suggested in Figure 6; however, the autofluorescence of elastic fibres was not present in all the samples. The absence of the autofluorescence signal can be attributed to prolonged storage of the samples in frozen conditions, which we base on unrelated imaging of porcine blood vessels, of which part was imaged prior and part after one-year storage. However, the morphological data presented here suggest it is more likely that the elastic fibres were lost during the surgical extraction or the cryosectioning of the biopsies. Therefore, the elastic fibres are likely not present and do not contribute to the measured Young's modulus.

Another important group of components within the connective tissue, which were not targeted in the thesis, are glycoproteins, proteoglycans (PGs) and GAGs. These components are part of an amorphous gel-like ground substance surrounding the fibres (Minns et al., 1973; Ault & Hoffman, 1992b; Sharma & Maffulli, 2006), which also contains other molecules, such as fibronectin and Tenascic-C, that most likely take part in mechanical loading of the tissue (Kannus et al., 1998). These molecules account only for a small amount of dry mass of tissue; *e.g.*, the GAGs were reported to account for about 0.5 to 2.8 % of dry mass (Breen et al., 1972; Murienne et al., 2016). Despite the small amount, the ground substance is crucial in encouraging (re)hydration through negative ionic charges (Murienne et al., 2016). The level of hydration alters the viscose component of the viscoelastic

mechanical response of the tissue. However, while collagen and elastin moduli have been directly measured by isolating the individual fibrils from the tissue (Strasser et al., 2007; Koenders et al., 2009), measurement of the ground substance proves to be difficult due to the separation of the gel-like material from the fibrillar network (Ault & Hoffman, 1992a).

Some ground substance components have been targeted in biomechanical studies of tissue. For example, the GAGs and PGs are frequently evaluated indirectly by their removal through enzymatic treatment of the tissue (Minns et al., 1973; Schmidt et al., 1990; Lujan et al., 2007; Legerlotz et al., 2013; Murienne et al., 2016), but the results in the literature are inconsistent. Some results presented in the literature show no difference when the ground substance is enzymatically removed (Lujan et al., 2007). Other results show either an overall destabilization of the tissue (Minns et al., 1973) or an increase in stiffness of the tissue (Hoffman et al., 1977; Schmidt et al., 1990; Murienne et al., 2016). Several authors hypothesize that the removal of the ground substance component brings fibres in closer proximity, thus allowing greater friction between the fibres (Hoffman et al., 1977; Murienne et al., 2016). The GAGs appear to mediate the cross-linking between collagen fibres (Minns et al., 1973; Fessel & Snedeker, 2011) and slow down the extension of the collagen crimps, preventing sudden extension of collagen fibres under extension (Schmidt et al., 1990). These results are comparable with the AFM studies of collagen fibrils, where hydration levels greatly affected the resulting elastic modulus (Grant et al., 2008; Andriotis et al., 2018).

The work presented here did not specifically target any components of ground substance. Instead, the focus was placed on approximating the native tissue conditions and maintaining the hydration level. The aim was to use advanced microscopy techniques to identify the places containing the type I collagen in highly unprocessed samples and then to examine these places using the AFM probe at a very low speed. The low-speed approach guaranteed the minimum effect of viscosity and, therefore, minimized the effect of the hydration.

6.1.3 Mechanical test sensitivity

As stated in Chapter 6.1.1, the limitation of the AFM force spectroscopy is the nature of the applied load, i.e. compression. It is well known that the collagen

network functions mainly as a tensile element, while the majority of tissue's resistance to compressive load is attributed to the inter-fibrillar elements, such as GAGs (Ottani et al., 2001; Li et al., 2005; Eleswarapu et al., 2011). The tensile test is a standard for testing engineering materials. The sample is clamped at the ends, and load is applied in the direction of the major axis of the sample (Wells, 2013). The tensile test can be applied to a bulk of biological tissue using the same method used for stretching the engineering materials (Rosalia et al., 2023). Unlike engineering materials, biological materials are frequently very small and irregular, so clamping or volume normalization of the sample in a uniaxial tensile device would prove unsuccessful, as is the case of the samples of the relapsed clubfoot tissue. Therefore, the AFM test was the only method that could describe very small samples acquired from the surgery.

6.2 Statistical and clinical significance

Even though the biomechanical AFM test provided a significant result, the result does not necessarily have clinical significance. Statistical significance is determined by p-value under predefined alpha level, while clinical significance refers to a difference between the treatment and control groups, and the difference has a meaningful impact on medical practice (Friedman, 2005; Ranganathan et al., 2015). The biomechanical AFM test provided the statistically significant difference between the two groups, medial and lateral sides of the relapsed clubfoot, in the measured parameter, Young's modulus. From a biomechanical perspective, the clinical significance of the statistically different Young's moduli between the two groups can lie much further from biomechanical relevance. However, from a biological or cellular perspective, a difference in tens of kPa in Young's modulus can be related to an unusual cell behaviour that manifests, for example, in increased collagen production. Therefore, the possible impact and clinical significance of the different Young's moduli between the medial and lateral sides of the tissue needs to be further investigated.

Multiple parameters in this study had statistically significant differences between the two groups (SHG per FOV, THG per FOV, eccentricity ε, Young's modulus); however, the parameters also exhibited great variability. The variability suggests that there is a great heterogeneity between individuals. Inter-individual

heterogeneity is a common fact in biological studies, and in the case of our study, it was even more amplified by the uniqueness of the samples. The samples were removed from individuals of different ages and genders, but we did not observe any correlation between the parameters and the factors of age or gender.

The study also lacked a true control to the medial side of the relapsed clubfoot tissue. It is not possible to meet ethical standards and realistically obtain control samples from healthy patients of the same age group, diet or similar physical history (Hubbard & Soutas-Little, 1984; Couppé et al., 2014; Svensson et al., 2016; Ošťádal et al., 2017), so instead, the lateral side takes a role of control as an approximation of healthy tissue. Therefore, several considerations must be made when assessing the results of the thesis, such as the treatment history or the aetiology of the deformity. As for the treatment history, the surgical intervention was always preceded by the well-established Ponseti method for correcting the deformity. The treatment could introduce micro-damage, hypoxia (Novotny et al., 2022) and further remodelling (Egbo, 2021), which would have been introduced to both medial and lateral sides. As for the aetiology, fibrosis is a plausible causal mechanism; however, our samples represent only a small portion of the deformed foot, and the disc-like tissue could be a local symptom of the deformity, which is localized in the contracted medial side of the relapsed clubfoot. Contrary to the limitations, the lateral side remains the best available approximation to the true control. The lateral side tissue acts as a relative comparison to medial side tissue, comes from the limb affected by the same deformity, functions as an antagonist from the biomechanical perspective and orthopaedic practitioners refer to both medial and lateral side when concluding on the characteristics of the relapsed clubfoot tissue.

6.3 Conclusion

The thesis presents a quantitative comparison of the morphological and micro-mechanical properties of the connective tissue extracted from the relapsed clubfoot deformity. In light of the presented data, the medial side appears as stiff and rigid due to both collagen synthesis through fibrosis and an internal reorganization of the tissue. The medial side has a higher Young's modulus and contains more collagen and less adipose tissue compared

to the analogous tissue of the lateral side. Additionally, the collagen fibres in the medial side propagate at a higher frequency of the crimp pattern, which indicates tension release that is absent in the lateral side. The results of the thesis are presented in several papers, attached at the end of the thesis.

List of Publications

The research presented in the thesis was published in international journals. Four publications were published on the topic of relapsed clubfoot deformity with biological relevance. Two additional publications were published, and their topic was methodologically relevant to the presented research work.

Microstructural Analysis of Collagenous Structures in Relapsed Clubfoot Tissue

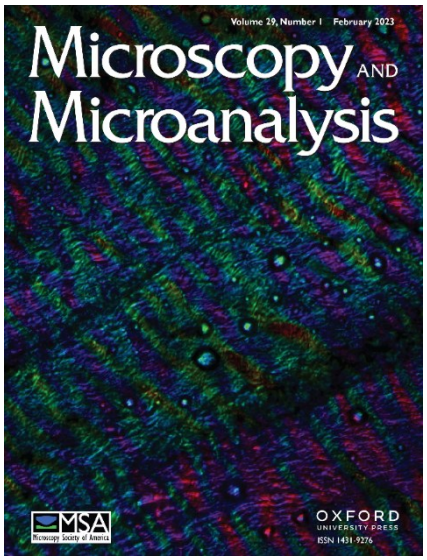

David Vondrášek, Daniel Hadraba, Jan Přibyl, Adam Eckhardt, Martin Ošťádal, František Lopot, Karel Jelen, Martina Doubková, Jarmila Knitlová, Tomáš Novotný, Jiří Janáček

Microscopy and Microanalysis, Volume 29, Issue 1, February 2023, Pages 265–272
DOI: https://doi.org/10.1093/micmic/ozac012

Published: 20 December 2022

Abstract: Talipes equinovarus congenitus (clubfoot) is frequently defined as a stiff, contracted deformity, but few studies have described the tissue from the point of view of the extracellular matrix, and none have quantified its mechanical properties. Several researchers have observed that clubfoot exhibits signs of fibrosis in the medial side of the deformity that are absent in the lateral side. Our study aims to quantify the differences between the medial and lateral side tissue obtained from relapsed clubfoot during surgery in terms of the morphological and mechanical properties of the tissue. Combining methods of optical and atomic force microscopy, our study revealed that the medial side has a higher Young's modulus, contains more collagen and less adipose tissue and that the collagen fibers propagate at a higher frequency of the crimp pattern after surgical dissection of the tissue. Our study offers a multi-correlative approach that thoroughly investigates the relapsed clubfoot tissue.

The possible role of hypoxia in the affected tissue of relapsed clubfoot

Tomas Novotny, Adam Eckhardt, Martina Doubkova, Jarmila Knitlova, David Vondrasek, Eliska Vanaskova, Martin Ostadal, Jiri Uhlik, Lucie Bacakova, Jana Musilkova

Scientific Reports, Volume 12, Article number: 4462 (2022)
DOI: https://doi.org/10.1038/s41598-022-08519-z

Published: 15 March 2022

Abstract: Our aim was to study the expression of hypoxia-related proteins as a possible regulatory pathway in the contracted side tissue of relapsed clubfoot. We compared the expression of hypoxia-related proteins in the tissue of the contracted (medial) side of relapsed clubfoot, and in the tissue of the non-contracted (lateral) side of relapsed clubfoot. Tissue samples from ten patients were analyzed by immunohistochemistry and image analysis, Real-time PCR and Mass Spectrometry to evaluate the differences in protein composition and gene expression. We found a significant increase in the levels of smooth muscle actin, transforming growth factor-beta, hypoxia-inducible factor 1 alpha, lysyl oxidase, lysyl oxidase-like 2, tenascin C, matrix metalloproteinase-2, matrix metalloproteinase-9, fibronectin, collagen types III and VI, hemoglobin subunit alpha and hemoglobin subunit beta, and an overexpression of ACTA2, FN1, TGFB1, HIF1A and MMP2 genes in the contracted medial side tissue of clubfoot. In the affected tissue, we have identified an increase in the level of hypoxia-related proteins, together with an overexpression of corresponding genes. Our results suggest that the hypoxia-associated pathway is potentially a factor contributing to the etiology of clubfoot relapses, as it stimulates both angioproliferation and fibroproliferation, which are considered to be key factors in the progression and development of relapses.

Minoxidil decreases collagen I deposition and tissue-like contraction in clubfoot-derived cells: a way to improve conservative treatment of relapsed clubfoot?

Jarmila Knitlova, Martina Doubkova, Martin Plencner, David Vondrasek, Adam Eckhardt, Martin Ostadal, Jana Musilkova, Lucie Bacakova, Tomas Novotny

Connective Tissue Research 2021, Volume 62, No. 5, Pages 554–569
DOI: https://doi.org/10.1080/03008207.2020.1816992

Published: 20 September 2020

Abstract

Aim: Clubfoot is a congenital deformity affecting the musculoskeletal system, resulting in contracted and stiff tissue in the medial part of the foot. Minoxidil (MXD) has an inhibitory effect on lysyl hydroxylase, which influences the quality of extracellular matrix crosslinking, and could therefore be used to reduce the stiffness and to improve the flexibility of the tissue. We assessed the in vitro antifibrotic effects of minoxidil on clubfoot-derived cells.

Methods: Cell viability and proliferation were quantified by xCELLigence, MTS, and LIVE/DEAD assays. The amount of collagen I deposited into the extracellular matrix was quantified using immunofluorescence with subsequent image segmentation analysis, hydroxyproline assay, and Second Harmonic Generation imaging. Extracellular matrix contraction was studied in a 3D model of cell-populated collagen gel lattices.

Results: MXD concentrations of 0.25, 0.5, and 0.75 mM inhibited the cell proliferation in a concentration-dependent manner without causing a cytotoxic effect. Exposure to ≥0.5 mM MXD resulted in a decrease in collagen type I accumulation after 8 and 21 days in culture. Changes in collagen fiber assembly were observed by immunofluorescence microscopy and nonlinear optical microscopy (second harmonic generation). MXD also inhibited the contraction of cell-populated collagen lattices (0.5 mM by 22%; 0.75 mM by 28%).

Conclusions: Minoxidil exerts an in vitro inhibitory effect on the cell proliferation, collagen accumulation, and extracellular matrix contraction processes that are associated with clubfoot fibrosis. This study provides important preliminary results

demonstrating the potential relevance of MXD for adjuvant pharmacological therapy in standard treatment of relapsed clubfoot.

Novel contribution to clubfoot pathogenesis: The possible role of extracellular matrix proteins

Adam Eckhardt, Tomas Novotny, Martina Doubkova, Lucia Hronkova, Ludek Vajner, Statis Pataridis, Daniel Hadraba, Lucie Kulhava, Martin Plencner, Jarmila Knitlova, Jana Liskova, Jiri Uhlik, Marie Zaloudikova, David Vondrasek, Ivan Miksik, Martin Ostadal

Journal of Orthopaedic Research, volume 37: 769-778
DOI: https://doi.org/10.1002/jor.24211

Published: 07 January 2019

Abstract: Idiopathic pes equinovarus (clubfoot) is a congenital deformity of the feet and lower legs. Clubfoot belongs to a group of fibro-proliferative disorders but its origin remains unknown. Our study aimed to achieve the first complex proteomic comparison of clubfoot contracted tissue of the foot (medial side; n = 16), with non-contracted tissue (lateral side; n = 13). We used label-free mass spectrometry quantification and immunohistochemistry. Seven proteins were observed to be significantly upregulated in the medial side (asporin, collagen type III, V, and VI, versican, tenascin-C, and transforming growth factor beta induced protein) and four in the lateral side (collagen types XII and XIV, fibromodulin, and cartilage intermediate layer protein 2) of the clubfoot. Comparison of control samples from cadavers brought only two different protein concentrations (collagen types I and VI). We also revealed pathological calcification and intracellular positivity of transforming growth factor beta only in the contracted tissue of clubfoot. Most of the 11 differently expressed proteins are strongly related to the extracellular matrix architecture and we assume that they may play specific roles in the pathogenesis of this deformity. These proteins seem to be promising targets for future investigations and treatment of this disease.

Human decellularized and crosslinked pericardium coated with bioactive molecular assemblies

Jana Musilkova, Elena Filova, Jan Pala, Roman Matejka, Daniel Hadraba, David Vondrasek, Ondrej Kaplan, Tomas Riedel, Eduard Brynda, Johanka Kucerova, Miroslav Konarik, Frantisek Lopot, Jan Pirk and Lucie Bacakova

Biomedical Materials, Volume 15, Number 1
DOI: https://doi.org/10.1088/1748-605X/ab52db

Published: 09 December 2019

Abstract: Decellularized human pericardium is under study as an allogenic material for cardiovascular applications. The effects of crosslinking on the mechanical properties of decellularized pericardium were determined with a uniaxial tensile test, and the effects of crosslinking on the collagen structure of decellularized pericardium were determined by multiphoton microscopy. The viability of human umbilical vein endothelial cells seeded on decellularized human pericardium and on pericardium strongly and weakly crosslinked with glutaraldehyde and with genipin was evaluated by means of an MTS assay. The viability of the cells, measured by their metabolic activity, decreased considerably when the pericardium was crosslinked with glutaraldehyde. Conversely, the cell viability increased when the pericardium was crosslinked with genipin. Coating both non-modified pericardium and crosslinked pericardium with a fibrin mesh or with a mesh containing attached heparin and/or fibronectin led to a significant increase in cell viability. The highest degree of viability was attained for samples that were weakly crosslinked with genipin and modified by means of a fibrin and fibronectin coating. The results indicate a method by which in vivo endothelialization of human cardiac allografts or xenografts could potentially be encouraged.

Uniaxial tensile testing device for measuring mechanical properties of biological tissue with stress-relaxation test under a confocal microscope

David Vondrášek, Daniel Hadraba, Roman Matějka, František Lopot, Martin Svoboda, Karel Jelen

Manufacturing Technology 2018, Volume 18, Issue 5, Pages 866 - 872
DOI: 10.21062/ujep/180.2018/a/1213-2489/MT/18/5/866

Published: 01 October 2018

Abstract: Biological soft tissue is a non-linear and viscoelastic material and its mechanical properties can greatly affect quality of life. Many external mechanical factors can alter the tissue, for example the tissue of talipes equinovarus congenitus, also known as clubfoot, which is the most frequent congenital deformity affecting lower extremities with pathological changes of connective tissue. In clubfoot, the presence of disc-like mass of fibrous tissue, resembling intervertebral disc tissue, is described to be between the medial malleolus and the medial side of the navicular bone. The clubfoot tissue is often referred to be stiffer or rigid by clinicians, or it is referred to as contracted and less contracted tissue, however relevant evidence about mechanical properties is missing. Therefore, the description "disc-like" is informing only about relative mechanical properties of clubfoot tissue. We aim to prepare methodical approach to quantify mechanical properties of biological tissue with uniaxial tensile stress-relaxation test, in order to help clinicians and scientist to identify precisely the mechanical properties of normal and pathological tissue and their structural behaviour during mechanical testing. In this study, we test and tune the uniaxial tensile stress-relaxation test on biological tissue with high content of connective tissue such as collagen. The model tissue is porcine pericardium. The tissue has clear collagen fibres aligning parallel to the force applied. Modulus of elasticity measured here is comparable to other studies.

Bibliography

ADAMIAK, K. & SIONKOWSKA, A. (2020). Current methods of collagen cross-linking: Review. *International Journal of Biological Macromolecules* **161**, 550–560.

AITKEN, P. G., BREESE, G. R., DUDEK, F. F., EDWARDS, F., ESPANOL, M. T., LARKMAN, P. M., LIPTON, P., NEWMAN, G. C., NOWAK, T. S., PANIZZON, K. L., RALEY-SUSMAN, K. M., REID, K. H., RICE, M. E., SARVEY, J. M., SCHOEPP, D. D., SEGAL, M., TAYLOR, C. P., TEYLER, T. J. & VOULALAS, P. J. (1995). Preparative methods for brain slices: a discussion. *Journal of Neuroscience Methods* **59**, 139–149.

AKHTAR, R., SHERRATT, M. J., CRUICKSHANK, J. K. & DERBY, B. (2011). Characterizing the elastic properties of tissues. *Materials Today* **14**, 96–105.

ANAND, A. & SALA, D. (2008). Clubfoot: Etiology and treatment. *Indian Journal of Orthopaedics* **42**, 22.

ANDERSON, G. S. (1999). Human morphology and temperature regulation. *International Journal of Biometeorology* **43**, 99–109.

ANDRIOTIS, O. G., DESISSAIRE, S. & THURNER, P. J. (2018). Collagen Fibrils: Nature's Highly Tunable Nonlinear Springs. *ACS nano* **12**, 3671–3680.

ARUN GOPINATHAN, P., KOKILA, G., JYOTHI, M., ANANJAN, C., PRADEEP, L. & HUMAIRA NAZIR, S. (2015). Study of Collagen Birefringence in Different Grades of Oral Squamous Cell Carcinoma Using Picrosirius Red and Polarized Light Microscopy. *Scientifica* **2015**, e802980.

AULT, H. K. & HOFFMAN, A. H. (1992a). A Composite Micromechanical Model for Connective Tissues: Part II—Application to Rat Tail Tendon and Joint Capsule. *Journal of Biomechanical Engineering* **114**, 142–146.

———— (1992b). A Composite Micromechanical Model for Connective Tissues: Part I—Theory. *Journal of Biomechanical Engineering* **114**, 137–141.

AZRIL, HUANG, K.-Y., HOBLEY, J., ROUHANI, M., LIU, W.-L. & JENG, Y.-R. (2023). A methodology to evaluate different histological preparations of soft tissues: Intervertebral disc tissues study. *Journal of Applied Biomaterials & Functional Materials* **21**, 22808000231155634.

BACHMANN, L. & SCHMITT, W. W. (1971). Improved Cryofixation Applicable to Freeze Etching. *Proceedings of the National Academy of Sciences* **68**, 2149–2152.

BALAUR, E., O' TOOLE, S., SPURLING, A. J., MANN, G. B., YEO, B., HARVEY, K., SADATNAJAFI, C., HANSSEN, E., ORIAN, J., NUGENT, K. A., PARKER, B. S. & ABBEY, B. (2021). Colorimetric histology using plasmonically active microscope slides. *Nature* **598**, 65–71.

BANCROFT, J. D. & LAYTON, C. (2019). The hematoxylins and eosin. In Bancroft's Theory and Practice of Histological Techniques, Suvarna, S. K., Layton, C. & Bancroft, J. D. (Eds.), pp. 126–138. Elsevier, 2019, https://doi.org/10.1016/B978-0-7020-6864-5.00010-4.

BAUMGART, F. (2000). Stiffness — an unknown world of mechanical science? *Injury* **31**, 14–84.

BEST, R. B., BROCKWELL, D. J., TOCA-HERRERA, J. L., BLAKE, A. W., SMITH, D. A., RADFORD, S. E. & CLARKE, J. (2003). Force mode atomic force microscopy as a tool for protein folding studies. *Analytica Chimica Acta* **479**, 87–105.

BINNIG, G., QUATE, C. F. & GERBER, CH. (1986). Atomic Force Microscope. *Physical Review Letters* **56**, 930–933.

BOZEC, L. & HORTON, M. (2005). Topography and Mechanical Properties of Single Molecules of Type I Collagen Using Atomic Force Microscopy. *Biophysical Journal* **88**, 4223–4231.

BRAAK, H. & BRAAK, E. (1991). Demonstration of Amyloid Deposits and Neurofibrillary Changes in Whole Brain Sections. *Brain Pathology* **1**, 213–216.

BRAMOWICZ, M., KULESZA, S., CZAJA, P. & MAZIARZ, W. (2014). Application of the Autocorrelation Function and Fractal Geometry Methods for Analysis of MFM Images. *Archives of Metallurgy and Materials* **59**, 451–457.

BRASSELET, SOPHIE, AÏT-BELKACEM, D., GASECKA, A., MUNHOZ, F., BRUSTLEIN, S. & BRASSELET, S. (2010). Influence of birefringence on polarization resolved nonlinear microscopy and collagen SHG structural imaging. *Optics Express* **18**, 14859.

BREEN, M., JOHNSON, R. L., SITTIG, R. A., WEINSTEIN, H. G. & VEIS, A. (1972). The Acidic Glycosaminoglycans in Human Fetal Development and Adult Life: Cornea, Sclera and Skin. *Connective Tissue Research* **1**, 291–303.

BRIDGENS, J. & KIELY, N. (2010). Current management of clubfoot (congenital talipes equinovarus). *BMJ* **340**, c355–c355.

BROWN, A. C., FIORE, V. F., SULCHEK, T. A. & BARKER, T. H. (2013). Physical and chemical microenvironmental cues orthogonally control the degree and duration of fibrosis-associated epithelial-to-mesenchymal transitions. *The Journal of pathology* **229**, 25–35.

BUCKLEY, M. R., SARVER, J. J., FREEDMAN, B. R. & SOSLOWSKY, L. J. (2013). The dynamics of collagen uncrimping and lateral contraction in tendon and the effect of ionic concentration. *Journal of Biomechanics* **46**, 2242–2249.

BURRY, R. W. (2011). Controls for Immunocytochemistry: An Update. *Journal of Histochemistry & Cytochemistry* **59**, 6–12.

CAPLAN, J., NIETHAMMER, M., TAYLOR, R. M. & CZYMMEK, K. J. (2011). The power of correlative microscopy: multi-modal, multi-scale, multi-dimensional. *Current Opinion in Structural Biology* **21**, 686–693.

CARNIEL, E. L., FONTANELLA, C. G., STEFANINI, C. & NATALI, A. N. (2013). A procedure for the computational investigation of stress-relaxation phenomena. *Mechanics of Time-Dependent Materials* **17**, 25–38.

CHAUDHURI, S., NGUYEN, H., RANGAYYAN, R. M., WALSH, S. & FRANK, C. B. (1987). A Fourier Domain Directional Filterng Method for Analysis of Collagen Alignment in Ligaments. *IEEE Transactions on Biomedical Engineering* **BME-34**, 509–518.

CHAURASIA, S. S., CHAMPAKALAKSHMI, R., LI, A., POH, R., TAN, X. W., LAKSHMINARAYANAN, R., LIM, C. T., TAN, D. T. & MEHTA, J. S. (2012). Effect of Fibrin Glue on the Biomechanical Properties of Human Descemet's Membrane. *PLOS ONE* **7**, e37456.

CHEN, D. T. N., WEN, Q., JANMEY, P. A., CROCKER, J. C. & YODH, A. G. (2010). Rheology of Soft Materials. *Annual Review of Condensed Matter Physics* **1**, 301–322.

CHOTEL, F., PAROT, R., SERINGE, R., BERARD, J. & WICART, P. (2011). Comparative Study: Ponseti Method Versus French Physiotherapy for Initial Treatment of Idiopathic Clubfoot Deformity. *Journal of Pediatric Orthopaedics* **31**, 320–325.

CICCHI, R., VOGLER, N., KAPSOKALYVAS, D., DIETZEK, B., POPP, J. & PAVONE, F. S. (2013). From molecular structure to tissue architecture: collagen organization probed by SHG microscopy. *Journal of Biophotonics* **6**, 129–142.

COMLEY, K. & FLECK, N. A. (2010). A micromechanical model for the Young's modulus of adipose tissue. *International Journal of Solids and Structures* **47**, 2982–2990.

COOKE, S. J., BALAIN, B., KERIN, C. C. & KIELY, N. T. (2008). Clubfoot. *Current Orthopaedics* **22**, 139–149.

COONS, A. H., CREECH, H. J. & JONES, R. N. (1941). Immunological Properties of an Antibody Containing a Fluorescent Group. *Experimental Biology and Medicine* **47**, 200–202.

COSMA, D. & VASILESCU, D. E. (2015). A Clinical Evaluation of the Pirani and Dimeglio Idiopathic Clubfoot Classifications. *The Journal of Foot and Ankle Surgery* **54**, 582–585.

COUPPÉ, C., SVENSSON, R. B., GROSSET, J.-F., KOVANEN, V., NIELSEN, R. H., OLSEN, M. R., LARSEN, J. O., PRAET, S. F. E., SKOVGAARD, D., HANSEN, M., AAGAARD, P., KJAER, M. & MAGNUSSON, S. P. (2014). Life-long endurance running is associated with reduced glycation and mechanical stress in connective tissue. *Age* **36**, 9665.

CROCE, A. C., FERRIGNO, A., VAIRETTI, M., BERTONE, R., FREITAS, I. & BOTTIROLI, G. (2005). Autofluorescence spectroscopy of rat liver during experimental transplantation procedure. An approach for hepatic metabolism assessment. *Photochemical & Photobiological Sciences* **4**, 583–590.

CUI, J. Z., CHIU, A., MABERLEY, D., MA, P., SAMAD, A. & MATSUBARA, J. A. (2007). Stage specificity of novel growth factor expression during development of proliferative vitreoretinopathy. *Eye* **21**, 200–208.

DAPSON, R. (2005). Dye–tissue interactions: mechanisms, quantification and bonding parameters for dyes used in biological staining. *Biotechnic & Histochemistry* **80**, 49–72.

DARVELL, B. W. (2018). Mechanical Testing. In Materials Science for Dentistry, Darvell, B.W. (Ed.), pp. 1–39. Woodhead Publishing, 2009, https://doi.org/10.1533/9781845696672.1.

DASTJERDI, M. M. & MAHLOOJIFAR, A. (2008). Towards Realistic Modeling of Breast Elasticity Modulus Alterations in Medical Simulation. In 2008 IEEE International Symposium on Knowledge Acquisition and Modeling Workshop, pp. 1148–1151. Wuhan, China, 2008, doi: 10.1109/KAMW.2008.4810712.

DÉBARRE, D., SUPATTO, W., PENA, A.-M., FABRE, A., TORDJMANN, T., COMBETTES, L., SCHANNE-KLEIN, M.-C. & BEAUREPAIRE, E. (2006). Imaging lipid bodies in cells and tissues using third-harmonic generation microscopy. *Nature Methods* **3**, 47–53.

DIAMANT, J., KELLER, A., BAER, E., LITT, M. & ARRIDGE, R. G. (1972). Collagen; ultrastructure and its relation to mechanical properties as a function of ageing. *Proceedings of the Royal Society of London. Series B, Biological Sciences* **180**, 293–315.

DIBELLO, D., TORELLI, L., DI CARLO, V., D'ADAMO, A. P., FALETRA, F., MANGOGNA, A. & COLIN, G. (2022). Incidence of Congenital Clubfoot: Preliminary Data from Italian CeDAP Registry. *International Journal of Environmental Research and Public Health* **19**, 5406.

DIMEGLIO, A. & CANAVESE, F. (2012). The French functional physical therapy method for the treatment of congenital clubfoot. *Journal of Pediatric Orthopaedics B* **21**, 28–39.

DONNELLY, E., BAKER, S. P., BOSKEY, A. L. & VAN DER MEULEN, M. C. H. (2006). Effects of surface roughness and maximum load on the mechanical properties of cancellous bone measured by nanoindentation. *Journal of biomedical materials research. Part A* **77**, 426–435.

DUCE, S. L., D'ALESSANDRO, M., DU, Y., JAGPAL, B., GILBERT, F. J., CRICHTON, L., BARKER, S., COLLINSON, J. M. & MIEDZYBRODZKA, Z. (2013). 3D MRI Analysis of the Lower Legs of Treated Idiopathic Congenital Talipes Equinovarus (Clubfoot). *PLOS ONE* **8**, e54100.

DUCLOS, S. E. & MICHALEK, A. J. (2017). Residual strains in the intervertebral disc annulus fibrosus suggest complex tissue remodeling in response to in-vivo loading. *Journal of the Mechanical Behavior of Biomedical Materials* **68**, 232–238.

ECKHARDT, A., NOVOTNY, T., DOUBKOVÁ, M., HRONKOVA, L., VAJNER, L., PATARIDIS, S., HADRABA, D., KULHAVA, L., PLENCNER, M., KNITLOVÁ, J., LISKOVA, J., UHLÍK, J., ZALOUDIKOVA, M., VONDRÁŠEK, D., MIKSÍK, I. & OŠŤÁDAL, M. (2019). Novel contribution to clubfoot pathogenesis: The possible role of extracellular matrix proteins. *Journal of Orthopaedic Research*.

EDWARDS, A. M. & SILVA, E. (2001). Effect of visible light on selected enzymes, vitamins and amino acids. *Journal of Photochemistry and Photobiology B: Biology* **63**, 126–131.

EGBO, M. K. (2021). A fundamental review on composite materials and some of their applications in biomedical engineering. *Journal of King Saud University - Engineering Sciences* **33**, 557–568.

ELESWARAPU, S. V., RESPONTE, D. J. & ATHANASIOU, K. A. (2011). Tensile Properties, Collagen Content, and Crosslinks in Connective Tissues of the Immature Knee Joint. *PLOS ONE* **6**, e26178.

ELMASRY, G., NAGAI, H., MORIA, K., NAKAZAWA, N., TSUTA, M., SUGIYAMA, J., OKAZAKI, E. & NAKAUCHI, S. (2015). Freshness estimation of intact frozen fish using fluorescence spectroscopy and chemometrics of excitation–emission matrix. *Talanta* **143**, 145–156.

FALDINI, C., TRAINA, F., DI MARTINO, A., NANNI, M. & ACRI, F. (2013). Can Selective Soft Tissue Release and Cuboid Osteotomy Correct Neglected Clubfoot? *Clinical Orthopaedics & Related Research* **471**, 2658–2665.

FEHER, J. (2017). Osmosis and Osmotic Pressure. In Quantitative Human Physiology (Second Edition), Feher, J. (Ed.), pp. 182–198. Boston: Academic Press, 2017, https://doi.org/10.1016/B978-0-12-800883-6.00017-3.

FERNANDES, R. M. P., MENDES, M. D. DOS S., AMORIM, R., PRETI, M. A., STERNICK, M. B. & GAIARSA, G. P. (2016). Surgical treatment of neglected clubfoot using external fixator. *Revista Brasileira de Ortopedia (English Edition)* **51**, 501–508.

FESSEL, G. & SNEDEKER, J. G. (2011). Equivalent stiffness after glycosaminoglycan depletion in tendon — an ultra-structural finite element model and corresponding experiments. *Journal of Theoretical Biology* **268**, 77–83.

FRIEDMAN, L. M. (2005). Clinical Significance versus Statistical Significance. In Encyclopedia of Biostatistics, Armitage, P. & Colton, T. (Eds.). Wiley, 2005, https://doi.org/10.1002/0470011815.b2a01006.

FULTON, Z., BRIGGS, D., SILVA, S. & SZALAY, E. A. (2015). Calf Circumference Discrepancies in Patients With Unilateral Clubfoot: Ponseti Versus Surgical Release. *Journal of Pediatric Orthopaedics* **35**, 403–406.

FUNG, D. T., SEREYSKY, J. B., BASTA-PLJAKIC, J., LAUDIER, D. M., HUQ, R., JEPSEN, K. J., SCHAFFLER, M. B. & FLATOW, E. L. (2010). Second Harmonic Generation Imaging and Fourier Transform Spectral Analysis Reveal Damage in Fatigue-Loaded Tendons. *Annals of Biomedical Engineering* **38**, 1741–1751.

GARCÍA, R. (2002). Dynamic atomic force microscopy methods. *Surface Science Reports* **47**, 197–301.

GATTO, R. & JAMMALAMADAKA, S. R. (2007). The generalized von Mises distribution. *Statistical Methodology* **4**, 341–353.

GAVARA, N. (2017). A beginner's guide to atomic force microscopy probing for cell mechanics. *Microscopy Research and Technique* **80**, 75–84.

GIESSIBL, F. J. (2003). Advances in atomic force microscopy. *Rev. Mod. Phys.* **75**, 35.

GOLDSTEIN, D. J. (1969). The fluorescence of elastic fibres stained with Eosin and excited by visible light. *The Histochemical Journal* **1**, 187–198.

GÓRECKI, J., MALUJDA, I. & TALAŚKA, K. (2016). Investigation of Internal Friction of Agglomerated Dry Ice. *Procedia Engineering* **136**, 275–279.

GORIAINOV, V., JUDD, J. & UGLOW, M. (2010). Does the Pirani score predict relapse in clubfoot? *Journal of Children's Orthopaedics* **4**, 439–444.

GRALKA, M. & KROY, K. (2015). Inelastic mechanics: A unifying principle in biomechanics. *Biochimica et Biophysica Acta (BBA) - Molecular Cell Research* **1853**, 3025–3037.

GRANT, C. A., BROCKWELL, D. J., RADFORD, S. E. & THOMSON, N. H. (2008). Effects of hydration on the mechanical response of individual collagen fibrils. *Applied Physics Letters* **92**, 233902.

———— (2009). Tuning the Elastic Modulus of Hydrated Collagen Fibrils. *Biophysical Journal* **97**, 2985–2992.

GRANT, C. A. & TWIGG, P. C. (2013). Pseudostatic and Dynamic Nanomechanics of the Tunica Adventitia in Elastic Arteries Using Atomic Force Microscopy. *ACS Nano* **7**, 456–464.

GUOSONG, H., ANTARIS, A. L. & HONGJIE, D. (2017). Near-infrared fluorophores for biomedical imaging. Nature Biomedical Engineering 1.

HADRABA, D., JANACEK, J., FILOVA, E., LOPOT, F., PAESEN, R., FANTA, O., JARMAN, A., NECAS, A., AMELOOT, M. & JELEN, K. (2017). Calcaneal Tendon Collagen Fiber Morphometry and Aging. *Microscopy and Microanalysis* **23**, 1–8.

HALPER, J. & KJAER, M. (2014). Basic Components of Connective Tissues and Extracellular Matrix: Elastin, Fibrillin, Fibulins, Fibrinogen, Fibronectin, Laminin, Tenascins and Thrombospondins. In Progress in Heritable Soft Connective Tissue Diseasesvol. 802, Advances in Experimental Medicine and Biology, Halper, J. (Ed.), pp. 31–47. Dordrecht: Springer Netherlands, https://doi.org/10.1007/978-3-030-80614-9_4.

HAMILTON, K., CHRZAN, A. & MICHALEK, A. (2021). Reflected cross-polarized light microscopy as a method for measuring collagen fiber crimp in musculoskeletal tissues. *Journal of the Mechanical Behavior of Biomedical Materials* **125**, 104953.

HANDELSMAN, J. E. & BADALAMENTE, M. A. (2008). Club Foot: a Neuromuscular Disease. *Developmental Medicine & Child Neurology* **24**, 3–12.

HANSEN, K. A., WEISS, J. A. & BARTON, J. K. (2002). Recruitment of Tendon Crimp With Applied Tensile Strain. *Journal of Biomechanical Engineering* **124**, 72–77.

HAYS, A. G., HIRSCH, G. A., KELLE, S., GERSTENBLITH, G., WEISS, R. G. & STUBER, M. (2010). Noninvasive Visualization of Coronary Artery Endothelial Function in Healthy Subjects and in Patients With Coronary Artery Disease. *Journal of the American College of Cardiology* **56**, 1657–1665.

HEIM, A. J., MATTHEWS, W. G. & KOOB, T. J. (2006). Determination of the elastic modulus of native collagen fibrils via radial indentation. *Applied Physics Letters* **89**, 181902.

HERMANOWICZ, P., SARNA, M., BURDA, K. & GABRYŚ, H. (2014). AtomicJ: An open source software for analysis of force curves. *Review of Scientific Instruments* **85**, 063703.

HERSH, A. (1967). The Role of Surgery in the Treatment of Club Feet. *JBJS* **49**, 1684.

HIESINGER, W., BRUKMAN, M. J., MCCORMICK, R. C., FITZPATRICK, J. R., FREDERICK, J. R., YANG, E. C., MUENZER, J. R., MAROTTA, N. A., BERRY, M. F., ATLURI, P. & WOO, Y. J. (2012). Myocardial tissue elastic properties determined by atomic force microscopy after stromal cell–derived factor 1α angiogenic therapy for acute myocardial infarction in a murine model. *The Journal of Thoracic and Cardiovascular Surgery* **143**, 962–966.

HIRAOKA, Y., SEDAT, J. W. & AGARD, D. A. (1990). Determination of three-dimensional imaging properties of a light microscope system. Partial confocal behavior in epifluorescence microscopy. *Biophysical Journal* **57**, 325–333.

HOFFMAN, A. S., GRANDE, L. A. & PARK, J. B. (1977). Sequential enzymolysis of human aorta and resultant stress-strain behavior. *Biomaterials, medical devices, and artificial organs* **5**, 121–145.

HOROBIN, R. (2002). Biological staining: mechanisms and theory. *Biotechnic & Histochemistry* **77**, 3–13.

HUBBARD, R. P. & SOUTAS-LITTLE, R. W. (1984). Mechanical Properties of Human Tendon and Their Age Dependence. *Journal of Biomechanical Engineering* **106**, 144–150.

HUMPHREY, J. D. (2003). Review Paper: Continuum biomechanics of soft biological tissues. *Proceedings of the Royal Society of London. Series A: Mathematical, Physical and Engineering Sciences* **459**, 3–46.

HUTSON, H., KUJAWA, C., ELICEIRI, K., CAMPAGNOLA, P. & MASTERS, K. (2019). Impact of tissue preservation on collagen fiber architecture. *Biotechnic & histochemistry : official publication of the Biological Stain Commission* **94**, 134–144.

IPPOLITO, E., DE MAIO, F., MANCINI, F., BELLINI, D. & OREFICE, A. (2009). Leg muscle atrophy in idiopathic congenital clubfoot: Is it primitive or acquired? *Journal of Children's Orthopaedics* **3**, 171–178.

JAN, N.-J., GRIMM, J. L., TRAN, H., LATHROP, K. L., WOLLSTEIN, G., BILONICK, R. A., ISHIKAWA, H., KAGEMANN, L., SCHUMAN, J. S. & SIGAL, I. A. (2015). Polarization microscopy for characterizing fiber orientation of ocular tissues. *Biomedical Optics Express* **6**, 4705–4718.

JASTRZEBSKA, M., WRZALIK, R., KOCOT, A., ZALEWSKA-REJDAK, J. & CWALINA, B. (2003). Raman spectroscopic study of glutaraldehyde-stabilized collagen and pericardium tissue. *Journal of Biomaterials Science, Polymer Edition* **14**, 185–197.

JOHNSEN, S. (2001). Hidden in plain sight: The ecology and physiology of organismal transparency. *The Biological Bulletin* **201**, 301–318.

JOHNSON, K. L., KENDALL, K., ROBERTS, A. D. & TABOR, D. (1997). Surface energy and the contact of elastic solids. *Proceedings of the Royal Society of London. A. Mathematical and Physical Sciences* **324**, 301–313.

JORBA, I., URIARTE, J. J., CAMPILLO, N., FARRÉ, R. & NAVAJAS, D. (2017). Probing Micromechanical Properties of the Extracellular Matrix of Soft Tissues by Atomic Force Microscopy: ECM MICROMECHANICS BY AFM. *Journal of Cellular Physiology* **232**, 19–26.

KADHUM, M., LEE, M.-H., CZERNUSZKA, J. & LAVY, C. (2019). An Analysis of the Mechanical Properties of the Ponseti Method in Clubfoot Treatment. *Applied Bionics and Biomechanics* 4308462.

KANNUS, P. (2000). Structure of the tendon connective tissue: Tendon connective tissue structure. *Scandinavian Journal of Medicine & Science in Sports* **10**, 312–320.

KANNUS, P., JOZSA, L., JÄRVINEN, T. A. H., JÄRVINEN, T. L. N., KVIST, M., NATRI, A. & JÄRVINEN, M. (1998). Location and Distribution of Non-collagenous Matrix Proteins in Musculoskeletal Tissues of Rat. *The Histochemical Journal* **30**, 799–810.

KASAS, S., THOMSON, N. H., SMITH, B. L., HANSMA, P. K., MIKLOSSY, J. & HANSMA, H. G. (1997). Biological applications of the AFM: From single molecules to organs. *International Journal of Imaging Systems and Technology* **8**, 151–161.

KASTEN, F. H. (2002). Introduction to dyes and stains. In Conn's Biological Stains, Horobin, R. & Kiernan, J. (Eds.). Taylor & Francis, London, 2002, https://doi.org/10.1201/9781003076841.

KERLING, A., STOLTENBURG-DIDINGER, G., GRAMS, L., TEGTBUR, U., HORSTMANN, H., KÜCK, M. & MELLEROWICZ, H. (2018). The congenital clubfoot – immunohistological analysis of the extracellular matrix. *Orthopedic Research and Reviews* **Volume 10**, 55–62.

KINGSLEY, K., CARROLL, K., HUFF, J. L. & PLOPPER, G. E. (2001). Photobleaching of Arterial Autofluorescence for Immunofluorescence Applications. *BioTechniques* **30**, 794–797.

KNITLOVA, J., DOUBKOVA, M., ECKHARDT, A., OSTADAL, M., MUSILKOVA, J., BACAKOVA, L. & NOVOTNY, T. (2021). Increased Collagen Crosslinking in Stiff Clubfoot Tissue: Implications for the Improvement of Therapeutic Strategies. *International Journal of Molecular Sciences* **22**, 11903.

KNITLOVA, J., DOUBKOVÁ, M., PLENCNER, M., VONDRÁŠEK, D., ECKHARDT, A., OŠŤÁDAL, M., MUSÍLKOVÁ, J., BACAKOVA, L. & NOVOTNY, T. (2020). Minoxidil decreases collagen I deposition and tissue-like contraction in clubfoot-derived cells: a way to improve conservative treatment of relapsed clubfoot? *Connective Tissue Research*.

KOENDERS, M. M. J. F., YANG, L., WISMANS, R. G., VAN DER WERF, K. O., REINHARDT, D. P., DAAMEN, W., BENNINK, M. L., DIJKSTRA, P. J., VAN KUPPEVELT, T. H. & FEIJEN, J. (2009). Microscale mechanical properties of single elastic fibers: The role of fibrillin–microfibrils. *Biomaterials* **30**, 2425–2432.

KYZER, S. P. & STARK, S. L. (1995). Congenital Idiopathic Clubfoot Deformities. *AORN Journal* **61**, 491–506.

LAYTON, C., BANCROFT, J. D. & SUVARNA, S. K. (2019). Fixation of tissues. In Bancroft's Theory and Practice of Histological Techniques, Suvarna, S. K., Layton, C. & Bancroft, J. D. (Eds.), pp. 40–63. Elsevier, 2019, https://doi.org/10.1016/B978-0-7020-6864-5.00004-9.

LEE, S.-H., SHIN, S., ROH, Y., OH, S. J., LEE, S. H., SONG, H. S., RYU, Y.-S., KIM, Y. K. & SEO, M. (2020). Label-free brain tissue imaging using large-area terahertz metamaterials. *Biosensors and Bioelectronics* **170**, 112663.

LEFÈVRE, E., GUIVIER-CURIEN, C., PITHIOUX, M. & CHARRIER, A. (2013). Determination of mechanical properties of cortical bone using AFM under dry and immersed conditions. *Computer Methods in Biomechanics and Biomedical Engineering* **16**, 337–339.

LEGERLOTZ, K., RILEY, G. P. & SCREEN, H. R. C. (2013). GAG depletion increases the stress-relaxation response of tendon fascicles, but does not influence recovery. *Acta Biomaterialia* **9**, 6860–6866.

LEVILLAIN, A., ORHANT, M., TURQUIER, F. & HOC, T. (2016). Contribution of collagen and elastin fibers to the mechanical behavior of an abdominal connective tissue. *Journal of the Mechanical Behavior of Biomedical Materials* **61**, 308–317.

LEWIS, N. T., HUSSAIN, M. A. & MAO, J. J. (2008). Investigation of nano-mechanical properties of annulus fibrosus using atomic force microscopy. *Micron* **39**, 1008–1019.

LI, C., NGUYEN, Q., COLE, W. G. & ALMAN, B. A. (2001). Potential treatment for clubfeet based on growth factor blockade. *Journal of Pediatric Orthopedics* **21**, 372–377.

LI, H., YAN, M., YU, J., XU, Q., XIA, X., LIAO, J. & ZHENG, W. (2020). In vivo identification of arteries and veins using two-photon excitation elastin autofluorescence. *Journal of Anatomy* **236**, 171–179.

LI, L. P., HERZOG, W., KORHONEN, R. K. & JURVELIN, J. S. (2005). The role of viscoelasticity of collagen fibers in articular cartilage: axial tension versus compression. *Medical Engineering & Physics* **27**, 51–57.

LIM, H. W., KOHLI, I., RUVOLO, E., KOLBE, L. & HAMZAVI, I. H. (2022). Impact of visible light on skin health: The role of antioxidants and free radical quenchers in skin protection. *Journal of the American Academy of Dermatology* **86**, S27–S37.

LIN, L. (2020). Revealing The Potential Pathogenic Mechanism Of Clubfoot By Silencing The Gene Pitx1. *Acta Medica Mediterranea* 1699–1705.

LIU, B., ZHANG, L. & GAO, H. (2006). Poisson ratio can play a crucial role in mechanical properties of biocomposites. *Mechanics of Materials* **38**, 1128–1142.

LIU, X., WANG, L., JI, J., YAO, W., WEI, W., FAN, J., JOSHI, S., LI, D. & FAN, Y. (2014). A Mechanical Model of the Cornea Considering the Crimping Morphology of Collagen Fibrils. *Investigative Ophthalmology & Visual Science* **55**, 2739–2746.

LO, W., CHEN, W.-L., HSUEH, C.-M., GHAZARYAN, A. A., CHEN, S.-J., MA, D. H.-K., DONG, C.-Y. & TAN, H.-Y. (2012). Fast Fourier Transform–Based Analysis of Second-Harmonic Generation Image in Keratoconic Cornea. *Investigative Ophthalmology & Visual Science* **53**, 3501–3507.

LOMBARDO, M., LOMBARDO, G., CARBONE, G., DE SANTO, M. P., BARBERI, R. & SERRAO, S. (2012). Biomechanics of the Anterior Human Corneal Tissue Investigated with Atomic Force Microscopy. *Investigative Ophthalmology & Visual Science* **53**, 1050–1057.

LOPARIC, M., WIRZ, D., DANIELS, A. U., RAITERI, R., VANLANDINGHAM, M. R., GUEX, G., MARTIN, I., AEBI, U. & STOLZ, M. (2010). Micro- and Nanomechanical Analysis of Articular Cartilage by Indentation-Type Atomic Force Microscopy: Validation with a Gel-Microfiber Composite. *Biophysical Journal* **98**, 2731–2740.

LUJAN, T. J., UNDERWOOD, C. J., HENNINGER, H. B., THOMPSON, B. M. & WEISS, J. A. (2007). Effect of dermatan sulfate glycosaminoglycans on the quasi-static material properties of the human medial collateral ligament. *Journal of Orthopaedic Research* **25**, 894–903.

MAGERLE, R., DEHNERT, M., VOIGT, D. & BERNSTEIN, A. (2020). Nanomechanical 3D Depth Profiling of Collagen Fibrils in Native Tendon. *Analytical Chemistry* **92**, 8741–8749.

MALACRIDA, L., HEDDE, P. N., RANJIT, S., CARDARELLI, F. & GRATTON, E. (2017). Visualization of barriers and obstacles to molecular diffusion in live cells by spatial pair-cross-correlation in two dimensions. *Biomedical Optics Express* **9**, 303–321.

MALICK, L. E., WILSON, R. B. & STETSON, D. (1975). Modified Thiocarbohydrazide Procedure for Scanning Electron Microscopy: Routine use for Normal, Pathological, or Experimental Tissues. *Stain Technology* **50**, 265–269.

MATERA, D. L., WANG, W. Y. & BAKER, B. M. (2021). New directions and dimensions for bioengineered models of fibrosis. *Nature Reviews Materials* **6**, 192–195.

MATHIAS, R. G., LULE, J. K., WAISWA, G., NADDUMBA, E. K., PIRANI, S., & UGANDA SUSTAINABLE CLUBFOOT CARE PROJECT (2010). Incidence of Clubfoot in Uganda. *Canadian Journal of Public Health* **101**, 341–344.

MATYKA, K., MATYKA, M., MRÓZ, I., ZALEWSKA-REJDAK, J. & CISZEWSKI, A. (2007). An AFM study on mechanical properties of native and dimethyl suberimidate cross-linked pericardium tissue. *Journal of Molecular Recognition* **20**, 524–530.

MAUGIS, D. (1995). Extension of the Johnson-Kendall-Roberts Theory of the Elastic Contact of Spheres to Large Contact Radii. *Langmuir* **11**, 679–682.

MCDONALD, L. S., VAN DER LIST, J. P., JONES, K. J., ZUIDERBAAN, H. A., NGUYEN, J. T., POTTER, H. G. & PEARLE, A. D. (2017). Passive Anterior Tibial Subluxation in the Setting of Anterior Cruciate Ligament Injuries: A Comparative Analysis of Ligament-Deficient States. *The American Journal of Sports Medicine* **45**, 1537–1546.

MCKEE, C. T., LAST, J. A., RUSSELL, P. & MURPHY, C. J. (2011). Indentation Versus Tensile Measurements of Young's Modulus for Soft Biological Tissues. *Tissue Engineering. Part B, Reviews* **17**, 155–164.

MERRILL, L. J., GURNETT, C. A., SIEGEL, M., SONAVANE, S. & DOBBS, M. B. (2011). Vascular Abnormalities Correlate with Decreased Soft Tissue Volumes in Idiopathic Clubfoot. *Clinical Orthopaedics and Related Research* **469**, 1442–1449.

MILLER, T., LIN, J.-M., PIROLLI, L., COQUILLEAU, L., LUHARUKA, R. & TEPLYAKOV, A. V. (2012). Investigation of thin titanium carbonitride coatings deposited onto stainless steel. *Thin Solid Films* **522**, 193–198.

MINNS, R. J., SODEN, P. D. & JACKSON, D. S. (1973). The role of the fibrous components and ground substance in the mechanical properties of biological tissues: A preliminary investigation. *Journal of Biomechanics* **6**, 153–165.

MKANDAWIRE, N. C. & KAUNDA, E. (2004). Incidence and patterns of congenital talipes equinovarus (Clubfoot) deformity at Queen Elizabeth Central Hospital, Banter, Malawi. *East and Central African Journal of Surgery* **9**, 28–31.

MORGAN, J. T., RAGHUNATHAN, V. K., THOMASY, S. M., MURPHY, C. J. & RUSSELL, P. (2014). Robust and artifact-free mounting of tissue samples for atomic force microscopy. BioTechniques 56. 40–42.

MORRISS, L., WITTEK, A. & MILLER, K. (2008). Compression testing of very soft biological tissues using semi-confined configuration—A word of caution. *Journal of Biomechanics* **41**, 235–238.

MUNDER, M. C., MIDTVEDT, D., FRANZMANN, T., NÜSKE, E., OTTO, O., HERBIG, M., ULBRICHT, E., MÜLLER, P., TAUBENBERGER, A., MAHARANA, S., MALINOVSKA, L., RICHTER, D., GUCK, J., ZABURDAEV, V. & ALBERTI, S. (2016). A pH-driven transition of the cytoplasm from a fluid- to a solid-like state promotes entry into dormancy. *eLife* **5**, e09347.

MURIENNE, B. J., CHEN, M. L., QUIGLEY, H. A. & NGUYEN, T. D. (2016). The contribution of glycosaminoglycans to the mechanical behaviour of the posterior human sclera. *Journal of The Royal Society Interface* **13**, 20160367.

MUSILKOVA, J., FILOVA, E., PALA, J., MATEJKA, R., HADRABA, D., VONDRASEK, D., KAPLAN, O., RIEDEL, T., BRYNDA, E., KUCEROVA, J., KONARIK, M., LOPOT, F., PIRK, J. & BACAKOVA, L. (2019). Human decellularized and crosslinked pericardium coated with bioactive molecular assemblies. Biomedical Materials. 15(1), 015008.

NAMOCO JR., C. S. (2010). Improving the Rigidity of Sheet Metal by Embossing and Restoration Technique. **8**, 10.

NEUMANN, T. (2008). Determining the elastic modulus of biological samples using atomic force microscopy. *JPK Instruments Application Report* 1–9. https://www.jpk.com/app-technotes-img/AFM/pdf/jpk-app-elastic -modulus. 14-1.pdf

NELSON, C. M. & BISSELL, M. J. (2006). Of Extracellular Matrix, Scaffolds, and Signaling: Tissue Architecture Regulates Development, Homeostasis, and Cancer. *Annual Review of Cell and Developmental Biology* **22**, 287–309.

NICOLLE, S., VEZIN, P. & PALIERNE, J.-F. (2010). A strain-hardening bi-power law for the nonlinear behaviour of biological soft tissues. *Journal of Biomechanics* **43**, 927–932.

NOVOTNY, T., ECKHARDT, A., DOUBKOVA, M., KNITLOVA, J., VONDRASEK, D., VANASKOVA, E., OSTADAL, M., UHLIK, J., BACAKOVA, L. & MUSILKOVA, J. (2022). The possible role of hypoxia in the affected tissue of relapsed clubfoot. *Scientific Reports* **12**, 4462.

NOVOTNY, T., ECKHARDT, A., KNITLOVA, J., DOUBKOVA, M., OSTADAL, M., UHLIK, J. & MUSILKOVA, J. (2020). Increased Microvessel and Arteriole Density in the Contracted Side of the Relapsed Clubfoot. *Journal of Pediatric Orthopaedics* **40**, 592–596.

ODERMATT, P. D., SHIVANANDAN, A., DESCHOUT, H., JANKELE, R., NIEVERGELT, A. P., FELETTI, L., DAVIDSON, M. W., RADENOVIC, A. & FANTNER, G. E. (2015). High-Resolution Correlative Microscopy: Bridging the Gap between Single Molecule Localization Microscopy and Atomic Force Microscopy. *Nano Letters* **15**, 4896–4904.

OŠT'ÁDAL, M., ECKHARDT, A., HERGET, J., MIKŠÍK, I., DUNGL, P., CHOMIAK, J., FRYDRYCHOVÁ, M. & BURIAN, M. (2015). Proteomic analysis of the extracellular matrix in idiopathic pes equinovarus. *Molecular and Cellular Biochemistry* **401**, 133–139.

OŠŤÁDAL, M., LIŠKOVÁ, J., HADRABA, D. & ECKHARDT, A. (2017). Possible Pathogenetic Mechanisms and New Therapeutic Approaches of Pes Equinovarus. *Physiological Research* 403–410.

OTTANI, V., RASPANTI, M. & RUGGERI, A. (2001). Collagen structure and functional implications. *Micron* **32**, 251–260.

OWEN, R. M., CAPPER, B. & LAVY, C. (2018). Clubfoot treatment in 2015: a global perspective. *BMJ Global Health* **3**, e000852.

PAL, S. (2014). Mechanical Properties of Biological Materials. In Design of Artificial Human Joints & Organs, pp. 23–40. Springer, Boston, MA, https://doi.org/10.1007/978-1-4614-6255-2_2.

PANDEY, S. & PANDEY, A. K. (2003). The classification of clubfoot a practical approach. *The Foot* **13**, 61–65.

PATEL, D. P., CHRISTENSEN, M. B., HOTALING, J. M. & PASTUSZAK, A. W. (2020). Inflammation and Fibrosis: Implications for the Pathogenesis of Peyronie's Disease. *World journal of urology* **38**, 253–261.

PAVONE, V., CHISARI, E., VESCIO, A., LUCENTI, L., SESSA, G. & TESTA, G. (2018). The etiology of idiopathic congenital talipes equinovarus: a systematic review. *Journal of Orthopaedic Surgery and Research* **13**.

PEARSE, A. D. & GARDNER, D. L. (1972). Preparation of unfixed undemineralized bone sections: the Bright bone cryostat. *Journal of Clinical Pathology* **25**, 26–29.

PELLICER, A. & BRAVO, M. DEL C. (2011). Near-infrared spectroscopy: A methodology-focused review. *Seminars in Fetal and Neonatal Medicine* **16**, 42–49.

POGREL, M. A., YEN, C.-K. & HANSEN, L. S. (1990). A comparison of carbon dioxide laser, liquid nitrogen cryosurgery, and scalpel wounds in healing. *Oral Surgery, Oral Medicine, Oral Pathology* **69**, 269–273.

PONSETI, I. V. (2002). Relapsing Clubfoot: Causes, Prevention, and Treatment. *The Iowa Orthopaedic Journal* **22**, 55–56.

POON, R., LI, C. & ALMAN, B. A. (2009). Beta-catenin Mediates Soft Tissue Contracture in Clubfoot. *Clinical Orthopaedics and Related Research* **467**, 1180–1185.

QUIGGLE, A., CHARNG, W.-L., ANTUNES, L., NIKOLOV, M., BLEDSOE, X., HECHT, J. T., DOBBS, M. B. & GURNETT, C. A. (2022). Whole Exome Sequencing in Individuals with Idiopathic Clubfoot Reveals a Recurrent Filamin B (FLNB) Deletion. *Clinical Orthopaedics and Related Research* **480**, 421–430.

RADER, A. J., HESPENHEIDE, B. M., KUHN, L. A. & THORPE, M. F. (2002). Protein unfolding: Rigidity lost. *Proceedings of the National Academy of Sciences* **99**, 3540–3545.

RADMACHER, M. (1997). Measuring the elastic properties of biological samples with the AFM. *IEEE engineering in medicine and biology magazine: the quarterly magazine of the Engineering in Medicine & Biology Society* **16**, 47–57.

RANGANATHAN, P., PRAMESH, C. S. & BUYSE, M. (2015). Common pitfalls in statistical analysis: Clinical versus statistical significance. *Perspectives in Clinical Research* **6**, 169–170.

RANJIT, S., DOBRINSKIKH, E., MONTFORD, J., DVORNIKOV, A., LEHMAN, A., ORLICKY, D. J., NEMENOFF, R., GRATTON, E., LEVI, M. & FURGESON, S. (2016). Label-free fluorescence lifetime and second harmonic generation imaging microscopy improves quantification of experimental renal fibrosis. *Kidney International* **90**, 1123–1128.

RICHOZ, O., HAMMER, A., TABIBIAN, D., GATZIOUFAS, Z. & HAFEZI, F. (2013). The Biomechanical Effect of Corneal Collagen Cross-Linking (CXL) With Riboflavin and UV-A is Oxygen Dependent. *Translational Vision Science & Technology* **2**, 6.

VAN DER RIJT, J. A. J., VAN DER WERF, K. O., BENNINK, M. L., DIJKSTRA, P. J. & FEIJEN, J. (2006). Micromechanical Testing of Individual Collagen Fibrils. *Macromolecular Bioscience* **6**, 697–702.

ROARK, R. J., YOUNG, W. C. & BUDYNAS, R. G. (2002). *Roark's formulas for stress and strain*. 7th ed. New York: McGraw-Hill.

ROBINSON, P. S., LIN, T. W., REYNOLDS, P. R., DERWIN, K. A., IOZZO, R. V. & SOSLOWSKY, L. J. (2004). Strain-Rate Sensitive Mechanical Properties of Tendon Fascicles From Mice With Genetically Engineered Alterations in Collagen and Decorin. *Journal of Biomechanical Engineering* **126**, 252–257.

RODUIT, C., SEKATSKI, S., DIETLER, G., CATSICAS, S., LAFONT, F. & KASAS, S. (2009). Stiffness Tomography by Atomic Force Microscopy. *Biophysical Journal* **97**, 674–677.

ROSALIA, L., HALLOU, A., COCHRANE, L. & SAVIN, T. (2023). A magnetically actuated, optically sensed tensile testing method for mechanical characterization of soft biological tissues. *Science Advances* **9**, eade2522.

SAGE, E., GIRARD, P.-M. & FRANCESCONI, S. (2012). Unravelling UVA-induced mutagenesis. *Photochemical & Photobiological Sciences* **11**, 74–80.

SANDELL, J. L. & ZHU, T. C. (2011). A review of *in-vivo* optical properties of human tissues and its impact on PDT. *Journal of Biophotonics* **4**, 773–787.

SANDERSON, T., WILD, G., CULL, A. M., MARSTON, J. & ZARDIN, G. (2019). Immunohistochemical and immunofluorescent techniques. In *Bancroft's Theory and Practice of Histological Techniques*, pp. 337–394. Elsevier, 2019, https://doi.org/10.1016/B978-0-7020-6864-5.00019-0.

SANO, H., UHTHOFF, H. K., JARVIS, J. G., MANSINGH, A. & WENCKEBACH, G. F. C. (1998). Pathogenesis of soft-tissue contracture in club foot. *The Journal of Bone and Joint Surgery* **80**, 4.

SANTOS, N. C. & CASTANHO, M. A. R. B. (2004). An overview of the biophysical applications of atomic force microscopy. *Biophysical Chemistry* **107**, 133–149.

SAPER, C. B. (2009). A Guide to the Perplexed on the Specificity of Antibodies. *Journal of Histochemistry & Cytochemistry* **57**, 1–5.

SCHEGA, Y., FLINNER, N. & HANSMANN, M.-L. (2020). Quantitative assessment of optical clearing methods on formalin-fixed human lymphoid tissue. *Pathology - Research and Practice* **216**, 153136.

SCHMIDT, M. B., MOW, V. C., CHUN, L. E. & EYRE, D. R. (1990). Effects of proteoglycan extraction on the tensile behavior of articular cartilage. *Journal of Orthopaedic Research* **8**, 353–363.

SEIFERT, J., HAMMER, C. M., RHEINLAENDER, J., SEL, S., SCHOLZ, M., PAULSEN, F. & SCHÄFFER, T. E. (2014). Distribution of Young's Modulus in Porcine Corneas after Riboflavin/UVA-Induced Collagen Cross-Linking as Measured by Atomic Force Microscopy. *PLOS ONE* **9**, e88186.

SHAH, R. G., PIERCE, M. C. & SILVER, F. H. (2017). Morphomechanics of dermis -A method for non-destructive testing of collagenous tissues. *Skin Research and Technology* **23**, 399–406.

SHARMA, P. & MAFFULLI, N. (2006). Biology of tendon injury: healing, modeling and remodeling. *Journal of Musculoskeletal & Neuronal Interactions* **6**, 181–190.

SHERMAN, V. R., YANG, W. & MEYERS, M. A. (2015). The materials science of collagen. *Journal of the Mechanical Behavior of Biomedical Materials* **52**, 22–50.

SHIRMOHAMMADI, M., YARLAGADDA, P. K. D. V., GUDIMETLA, P. & KOSSE, V. (2011). Mechanical Behaviours of Pumpkin Peel under Compression Test. *Advanced Materials Research* **337**, 3–9.

SIAPKARA, A. & DUNCAN, R. (2007). Congenital talipes equinovarus. *Bone & Joint Journal* **89**, 995–1000.

SIMON, M. C. & GOTTSCHALK, K. V. (2007). Waves and rays in uniaxial birefringent crystals. *Optik* **118**, 457–470.

SLATTERY, A. D., BLANCH, A. J., QUINTON, J. S. & GIBSON, C. T. (2013). Accurate measurement of Atomic Force Microscope cantilever deflection excluding

tip-surface contact with application to force calibration. *Ultramicroscopy* **131**, 46–55.

SOSINSKY, G. E., CRUM, J., JONES, Y. Z., LANMAN, J., SMARR, B., TERADA, M., MARTONE, M. E., DEERINCK, T. J., JOHNSON, J. E. & ELLISMAN, M. H. (2008). The combination of chemical fixation procedures with high pressure freezing and freeze substitution preserves highly labile tissue ultrastructure for electron tomography applications. *Journal of Structural Biology* **161**, 359–371.

STEU, S., BAUCAMP, M., VON DACH, G., BAWOHL, M., DETTWILER, S., STORZ, M., MOCH, H. & SCHRAML, P. (2008). A procedure for tissue freezing and processing applicable to both intra-operative frozen section diagnosis and tissue banking in surgical pathology. *Virchows Archiv* **452**, 305–312.

STOCHERT, J. C. (2002). Reactive staining reagents and fluorescent labels. In *Conn's Biological Stains, Horobin, R. & Kiernan, J. (Eds.). Taylor & Francis, London, 2002, https://doi.org/10.1201/9781003076841*

STOLLER, P., REISER, K. M., CELLIERS, P. M. & RUBENCHIK, A. M. (2002). Polarization-Modulated Second Harmonic Generation in Collagen. *Biophysical Journal* **82**, 3330–3342.

STOLZ, M., RAITERI, R., DANIELS, A. U., VANLANDINGHAM, M. R., BASCHONG, W. & AEBI, U. (2004). Dynamic Elastic Modulus of Porcine Articular Cartilage Determined at Two Different Levels of Tissue Organization by Indentation -Type Atomic Force Microscopy. *Biophysical Journal* **86**, 3269–3283.

STRASSER, S., ZINK, A., JANKO, M., HECKL, W. M. & THALHAMMER, S. (2007). Structural investigations on native collagen type I fibrils using AFM. *Biochemical and Biophysical Research Communications* **354**, 27–32.

STRUPLER, M., PENA, A.-M., HERNEST, M., THARAUX, P.-L., MARTIN, J.-L., BEAUREPAIRE, E. & SCHANNE-KLEIN, M.-C. (2007). Second harmonic imaging and scoring of collagen in fibrotic tissues. *Optics Express* **15**, 4054.

SUNDARARAGHAVAN, H. G., MONTEIRO, G. A., LAPIN, N. A., CHABAL, Y. J., MIKSAN, J. R. & SHREIBER, D. I. (2008). Genipin-induced changes in collagen gels: Correlation of mechanical properties to fluorescence. *Journal of Biomedical Materials Research Part A* **87A**, 308–320.

SUTCLIFFE, J. E. S., THRASIVOULOU, C., SERENA, T. E., MADDEN, L., RICHARDS, T., PHILLIPS, A. R. J. & BECKER, D. L. (2017). Changes in the extracellular matrix surrounding human chronic wounds revealed by 2-photon imaging. *International Wound Journal* **14**, 1225–1236.

SVENSSON, R. B., HEINEMEIER, K. M., COUPPÉ, C., KJAER, M. & MAGNUSSON, S. P. (2016). Effect of aging and exercise on the tendon. *Journal of Applied Physiology* **121**, 1353–1362.

TAKAZA, M., MOERMAN, K. M., GINDRE, J., LYONS, G. & SIMMS, C. K. (2013). The anisotropic mechanical behaviour of passive skeletal muscle tissue subjected to large tensile strain. *Journal of the Mechanical Behavior of Biomedical Materials* **17**, 209–220.

TAO, N. J., LINDSAY, S. M. & LEES, S. (1992). Measuring the microelastic properties of biological material. *Biophysical Journal* **63**, 1165–1169.

TAQI, S. A., SAMI, S. A., SAMI, L. B. & ZAKI, S. A. (2018). A review of artifacts in histopathology. *Journal of Oral and Maxillofacial Pathology : JOMFP* **22**, 279.

THOMAS, G., BURNHAM, N. A., CAMESANO, T. A. & WEN, Q. (2013). Measuring the Mechanical Properties of Living Cells Using Atomic Force Microscopy. *JoVE (Journal of Visualized Experiments)* e50497.

THOMASY, S. M., KRISHNA RAGHUNATHAN, V., WINKLER, M., REILLY, C. M., SADELI, A. R., RUSSELL, P., JESTER, J. V. & MURPHY, C. J. (2014). Elastic modulus and collagen organization of the rabbit cornea: epithelium to endothelium. *Acta biomaterialia* **10**, 785–791.

VIDAL, B. (2010). Form birefringence as applied to biopolymer and inorganic material supraorganization. *Biotechnic & Histochemistry* **85**, 365–378.

VINCKIER, A. & SEMENZA, G. (1998). Measuring elasticity of biological materials by atomic force microscopy. *FEBS Letters* **430**, 12–16.

WALKER, G. E., VERTI, B., MARZULLO, P., SAVIA, G., MENCARELLI, M., ZURLENI, F., LIUZZI, A. & DI BLASIO, A. M. (2007). Deep Subcutaneous Adipose Tissue: A Distinct Abdominal Adipose Depot. *Obesity* **15**, 1933–1943.

WALLANDER, H., HOVELIUS, L. & MICHAELSSON, K. (2006). Incidence of congenital clubfoot in Sweden. *Acta Orthopaedica* **77**, 847–852.

WEIGELIN, B., BAKKER, G.-J. & FRIEDL, P. (2016). Third harmonic generation microscopy of cells and tissue organization. *Journal of Cell Science* **129**, 245–255.

WEISENHORN, A. L., KHORSANDI, M., KASAS, S., GOTZOS, V. & BUTT, H.-J. (1993). Deformation and height anomaly of soft surfaces studied with an AFM. *Nanotechnology* **4**, 106.

WELCH, A. J., TORRES, J. H. & CHEONG, W.-F. (1989). Laser Physics and Laser -Tissue Interaction. *Texas Heart Institute Journal* **16**, 141–149.

WELLER, T. H. & COONS, A. H. (1954). Fluorescent Antibody Studies with Agents of Varicella and Herpes Zoster Propagated in vitro. *Proceedings of the Society for Experimental Biology and Medicine* **86**, 789–794.

WELLS, R. G. (2013). Tissue mechanics and fibrosis. *Biochimica et Biophysica Acta (BBA) - Molecular Basis of Disease* **1832**, 884–890.

WENDEROTT, J. K., FLESHER, C. G., BAKER, N. A., NEELEY, C. K., VARBAN, O. A., LUMENG, C. N., MUHAMMAD, L. N., YEH, C., GREEN, P. F. & O'ROURKE, R. W. (2020). Elucidating nanoscale mechanical properties of diabetic human adipose tissue using atomic force microscopy. *Scientific Reports* **10**.

WENGER, M. P. E., BOZEC, L., HORTON, M. A. & MESQUIDA, P. (2007). Mechanical Properties of Collagen Fibrils. *Biophysical Journal* **93**, 1255–1263.

WILKE, H.-J., KRISCHAK, S. & CLAES, L. E. (1996). Formalin fixation strongly influences biomechanical properties of the spine. *Journal of Biomechanics* **29**, 1629–1631.

WILLIAMS, L. M., MCCANN, F. E., CABRITA, M. A., LAYTON, T., CRIBBS, A., KNEZEVIC, B., FANG, H., KNIGHT, J., ZHANG, M., FISCHER, R., BONHAM, S., STEENBEEK, L. M., YANG, N., SOOD, M., BAINBRIDGE, C., WARWICK, D., HARRY, L., DAVIDSON, D., XIE, W., SUNDSTRÖM, M., FELDMANN, M. & NANCHAHAL, J. (2020). Identifying collagen VI as a target of fibrotic diseases regulated by CREBBP/EP300. *Proceedings of the National Academy of Sciences* **117**, 20753–20763.

WILLIAMS, R. M., ZIPFEL, W. R. & WEBB, W. W. (2005). Interpreting Second-Harmonic Generation Images of Collagen I Fibrils. *Biophysical Journal* **88**, 1377–1386.

WILLINGHAM, M. C. (1999). Conditional Epitopes: Is Your Antibody Always Specific? *Journal of Histochemistry & Cytochemistry* **47**, 1233–1235.

WORCESTER, D. L., MILLER, R. G. & BRYANT, P. J. (1988). Atomic force microscopy of purple membranes. *Journal of Microscopy* **152**, 817–821.

WU, J., YUAN, H., LI, L., FAN, K., QIAN, S. & LI, B. (2018). Viscoelastic shear lag model to predict the micromechanical behavior of tendon under dynamic tensile loading. *Journal of Theoretical Biology* **437**, 202–213.

YOO, L., REED, J., SHIN, A. & DEMER, J. L. (2014). Atomic force microscopy determination of Young′s modulus of bovine extra-ocular tendon fiber bundles. *Journal of Biomechanics* **47**, 1899–1903.

YUE, S., SLIPCHENKO, M. N. & CHENG, J.-X. (2011). Multimodal Nonlinear Optical Microscopy. *Laser & photonics reviews* **5**, 496-512..

ZAITSEV, V. Y., MATVEYEV, A. L., MATVEEV, L. A., GUBARKOVA, E. V., SOVETSKY, A. A., SIROTKINA, M. A., GELIKONOV, G. V., ZAGAYNOVA, E. V., GLADKOVA, N. D. & VITKIN, A. (2017). Practical obstacles and their mitigation strategies in compressional optical coherence elastography

of biological tissues. *Journal of Innovative Optical Health Sciences* **10**, 1742006.

ZHU, G.-G., KAUPPILA, A., RISTELI, L., MÄKINEN, M., STENBÄCK, F. & RISTELI, J. (1995). Immunohistochemical study of type I collagen and type I pN-collagen in benign and malignant ovarian neoplasms. *Cancer* **75**, 1010–1017.